ABSTRACT

MCDIFFETT, DANA. Thermodynamic Modeling of Binary and Ternary Systems of Interest to Gas Antisolvent Precipitation. (Under the direction of Dr. Peter K. Kilpatrick and Dr. Ruben G. Carbonell.)

CO_2 is a poor solvent for polar and complex molecules. The batch process known as GAS precipitation exploits the ability of CO_2 to function as an antisolvent. CO_2 is dissolved at low temperatures and moderate pressures into an organic solvent into which a solute has been dissolved. The liquid phase is expanded, reducing the solvent power, and causing precipitation of the solute. In this way, thermally-labile pharmaceutical compounds can be purified from organic solutions as very fine, uniform particles.

In a simple (1) antisolvent – (2) solvent – (3) solute GAS system, solid-vapor-liquid equilibrium (SVLE) exists at the point of precipitation. The solubilities of acetaminophen in CO_2-expanded ethanol, x_3, and of acetaminophen in the equilibrium vapor phase, y_3, were predicted using a three-component, ternary-phase Mathcad code. The Peng-Robinson equation of state was used to represent the fluid phases and a simple fugacity expression was used to represent the solid phase. Binary interaction parameters for the CO_2-ethanol and ethanol-acetaminophen pairs, k_{12}=0.0890 and k_{23}=0.0099, were regressed from literature solubility data. The binary interaction parameter for the CO_2-acetaminophen pair, k_{13}=0.2614, was regressed using solubility data taken using a static equilibrium apparatus.

The vapor phase mole fraction of acetaminophen in CO_2 at 323K ranges from 10^{-6} to 10^{-4} over the pressure range 1500 psi to 4000 psi. The Peng-Robinson equation of

state model is unable to capture the solubility behavior, but the data are adequately fit using a non-predictive density-based correlation. A sensitivity analysis conducted on the SVLE model to determine the effect of the binary interaction parameters on the prediction of x_3 indicates that a poor fit for k_{13} does not prevent making an adequate prediction for the change in x_3 with increasing pressure.

At a given temperature, the solubility of acetaminophen in CO_2-expanded ethanol decreases with pressure, indicating that GAS precipitation could be a viable means of forming acetaminophen particles. At a given pressure, the liquid phase acetaminophen solubility increases with temperature, indicating that higher operating temperatures will require higher operating pressures to achieve maximum solute product yields. In the future, experimental x_3 data can be used to fit the k_{13} parameter in order to improve and validate the thermodynamic model.

THERMODYNAMIC MODELING OF BINARY AND TERNARY SYSTEMS OF INTEREST TO GAS ANTISOLVENT PRECIPITATION

by

Dana McDiffett

A thesis submitted to the Graduate Faculty of
North Carolina State University
in partial fulfillment of the requirements
for the Degree of Masters of Science

Department of Chemical Engineering

Raleigh, North Carolina
August 2004

Approved by:

Dr. George W. Roberts
Chemical Engineering
Committee Member

Dr. Peter K. Kilpatrick
Chemical Engineering
Chair of Advisory Committee

Dr. Ruben G. Carbonell
Chemical Engineering
Co-chair of Advisory Committee

BIOGRAPHY

Dana McDiffett was born in Anchorage, Alaska on August 24, 1980. She is the oldest of ten daughters born to Tim and Mary McDiffett. Dana attended East Anchorage High School, and graduated valedictorian of her class in June of 1998.

After high school, Dana began her studies in chemical engineering at the University of Notre Dame in South Bend, Indiana. During her junior year at Notre Dame, she spent a semester doing undergraduate research under the direction of Dr. Arvind Varma. Dana spent five summers interning with energy companies in Anchorage, Alaska during undergraduate school and after graduation. In May of 2002, she graduated Magna Cum Laude from Notre Dame with her Bachelors of Science.

Dana began her graduate studies in chemical engineering at North Carolina State University in August of 2002, where she was awarded both the Dean's Fellowship and the Andrews Fellowship during her first year. Her thesis research is in the area of thermodynamic modeling, and was conducted under the direction of Dr. Peter K. Kilpatrick and Dr. Ruben G. Carbonell.

In the fall of 2004 Dana will begin work with Shell Exploration and Production Company in Houston, Texas.

ACKNOWLEDGEMENTS

I would like to thank my advisors, Dr. Kilpatrick and Dr. Carbonell, for their direction and advice throughout my thesis project. I would also like to acknowledge the National Science Foundation for funding my work.

Thank you to Alan Chang for his endless help with the static equilibrium experiments. I really appreciate the time you always took to show me how to put something together, tell me what to order, or to answer my questions, even more than once. I'm glad that we've become friends. A big thank you goes to Bryan Tracy for helping Alan and me with the static equilibrium apparatus. You certainly kept things interesting in the lab. Thank you also to Bryan Kirkman who took the initial resveratrol ester solubility measurements.

A special thank you goes to Coray Colina and Erik Santiso for their help with the thermodynamic modeling. Coray, thank you for putting up with my speaking English far too quickly. Erik, you have a magic touch when it comes to Mathcad. Thank you for always being so willing to help me with my codes, and for starting me off with your fugacity functions. You always know just what to fix when something doesn't work, and you offer your help so selflessly to so many people, even on Friday afternoons when no one else wants to be working.

Thank you to Angelica Sanchez, my most fashionable friend, for help with the DSC measurements. Thank you also for being so sweet, and for getting just as excited as I do (if not more excited) about SATC.

To April (Morris) Kloxin, I will always be so glad that I met you. Thank you for always being such a great listener and for offering good advice. You truly are an endless source of information. I always look forward to meeting at 5:00 to go running – such fun and such ridiculousness. It's the best part of the day. To Alison Julson, thanks for always checking up on me. It is always so nice to get your phone call when you're just calling to see how things are going. Always remember, "slow and steady wins the race"…except when you blow by us at the end and win.

Thank you to my family, especially my parents Tim and Mary McDiffett, for always being so supportive. You always have infinitely more faith in me than I have in myself. Your love and encouragement mean more than you will ever know.

Last, yet most of all, thank you to my boyfriend, Tom Nelson. Even with all of the stress of graduate school, you've always kept me laughing…really hard. I can't figure out if that is because you are funny or just because you make ridiculous faces. North Carolina was our first big adventure together. Thank you for making it fun. I couldn't have done this without you, and I wouldn't have wanted to do it with anyone else.

TABLE OF CONTENTS

LIST OF TABLES

LIST OF FIGURES

1.0 INTRODUCTION

1.1 Motivation for Research

In the year 2000 nutrition industry sales in the U.S. approached $50 billion. Functional foods accounted for $17.3 billion, and dietary supplements accounted for $17.0 billion (Burrill, 2002). These health items are the delivery media for nutraceuticals, small molecule substances extracted from plants that have associated health benefits. Because of this fast-growing market we are interested in designing an efficient extraction and separation process to recover these high value products.

Alkyl aryl esters are promising extraction solvents for the removal of nutraceuticals from plant tissue. These esters enjoy GRAS (Generally Recognized As Safe) status from the Food and Drug Administration (FDA), and their substituent groups can be chosen to achieve a desired polarity and hydrophobicity, allowing specific nutraceuticals to be targeted. Following filtration to remove the insoluble plant tissue, pressurized CO_2 can be dissolved into the extract solution, reducing the power of the solvent to solvate the nutraceutical molecules, and causing precipitation of the solid nutraceutical product. This batch process was first developed by Gallagher et al., and is known as gas antisolvent (GAS) precipitation (Gallagher et al., 1989).

GAS precipitation is carried out at low temperatures and moderate pressures, making it an especially attractive option for the processing of thermally-labile compounds. The pressure in GAS precipitation can be carefully controlled to allow for fractionation of the extract solution by exploiting the difference in solubility of the various fractions in the gas-expanded liquid phase (Catchpole et al., 1996). In contrast to RESS (Rapid Expansion of

Supercritical Solutions), another process that uses CO_2 for particle formation, it is not necessary for the solute to be soluble in the volatile antisolvent for GAS precipitation. This is advantageous, as many polar and complex molecules, including many pharmaceuticals and nutraceuticals, are only sparingly soluble in CO_2. GAS precipitation has been successfully used to precipitate organics (Dixon and Johnston, 1991; Liu et al., 2000; Ke and Tan, 2002), polymers (Benedetti et al., 1997; Li et al., 2000), and proteins (Yeo et al., 1993; Thiering et al., 2000; Muhrer and Mazzotti, 2003).

In order to optimize such a separation scheme, fundamental thermodynamic studies are required to better understand the equilibrium phase behavior of the ternary antisolvent-solvent-nutraceutical solute system and the three binary systems that it comprises. As Bristow et al. note, "the equilibrium solution concentration (solubility) is the most important thermodynamic parameter which defines both extraction and precipitation processes" (Bristow et al., 2001). In the extraction process, it is important for the nutraceutical of interest to be appreciably soluble in the extraction solvent; in fact, for the process to be economical, one would like the solvent selected to have the highest possible solvency for the desired solute. In the precipitation process, the driving force is the degree of solute supersaturation induced using a compressed gas as an antisolvent, where supersaturation is the ratio of the concentration to the equilibrium solubility. GAS precipitation will only be an effective means of purifying the nutraceutical product if a significant change in the equilibrium solubility can be effected through the addition of pressurized CO_2 as an antisolvent. In this work we use the Peng-Robinson equation of state (Peng and Robinson, 1976) to represent the fluid phases and a fugacity expression to represent the pure solid

solute phase. Mathcad codes were developed to be used in conjunction with binary experimental solubility data to predict the solubility of a nutraceutical product in a gas-expanded ester solvent as a function of temperature and pressure.

We initially chose trans-resveratrol, an antioxidant with proven chemopreventive properties (Jang et al., 1997) and found in the skins of red grapes, as our model nutraceutical. Analysis of this compound proved difficult, as in the presence of heat or UV light trans-resveratrol can isomerize to the cis conformation (Trela and Waterhouse, 1996). Preliminary findings related to our resveratrol work are detailed in Appendix A. Time constraints mandated that we look to a substitute model system, and fortunately, the phase equilibria Mathcad models we have developed are applicable to a wide range of systems.

Our laboratory is currently doing work on solvent enhanced dispersion by supercritical fluids (SEDS), an antisolvent precipitation process that employs a coaxial design (Hanna and York, 1994). In SEDS precipitation, a solution of a solute dissolved in a solvent is injected through the inner tube, and the antisolvent flows through the outer tube. At the nozzle exit the two fluids are mixed, causing supersaturation of the solute solution and precipitation of solute particles. Our group is studying the effect of SEDS process parameters on particle size and morphology, with a focus on the ternary system carbon dioxide-ethanol-acetaminophen. In order to design an efficient particle formation process, it is important to have an understanding of the phase behavior of the model ternary system; accordingly, we have shifted the focus of the present study to the thermodynamic modeling of the solubility of acetaminophen in CO_2-expanded ethanol, as a supplement to our group's SEDS work.

1.2 Research Objectives

The aim of the current study is to examine the phase behavior of our model system (1) carbon dioxide + (2) ethanol + (3) acetaminophen as it pertains to GAS precipitation. To that end, we have developed a Mathcad computer code capable of representing the behavior of this three-component, ternary-phase system using the Peng-Robinson equation of state to represent the fluid phases and a simple fugacity expression to represent the pure, precipitated solid phase. This Mathcad code requires as inputs all three sets of binary interaction parameters. We developed Mathcad codes capable of representing vapor-liquid equilibrium, solid-liquid equilibrium, and solid-vapor equilibrium in order to regress the binary interaction parameters from experimental data. Solubility data are available in the literature for CO_2 in ethanol at 298K from 200-900 psi and for acetaminophen in ethanol at 1 atm from 265-305 K, which allowed us to regress the (1)-(2) and (2)-(3) binary interaction parameters, respectively. We measured the solubility of acetaminophen in carbon dioxide at 323K from 1500 psi to 4000 psi using a static equilibrium apparatus, and regressed the (1)-(3) binary interaction parameter. We assume that the binary interaction parameters are temperature-independent. Finally, we used our ternary Mathcad code to make predictions for the solubility of acetaminophen in CO_2-expanded ethanol as a function of temperature and pressure and examined the sensitivity of the ternary model to the binary interaction parameters.

1.3 Outline of Thesis

This thesis contains five chapters and two appendices. The first chapter is an introduction that includes an explanation of the motivation for the present study, a brief description of the GAS process, and an explanation for the shift in focus of our work. The second chapter is a literature review in which background pertinent to the project is presented. A more detailed explanation of both particle formation processes and thermodynamic modeling of GAS precipitation can be found here. The third chapter includes a description of the experimental methods for the static equilibrium experiments performed to determine the solubility of acetaminophen in supercritical CO_2. The fourth chapter provides details of the thermodynamic modeling completed in the present study, including explanations for the structures of the Mathcad codes developed and a description of the parametric sensitivity analysis performed. The fifth chapter includes results and discussion for the static equilibrium experiments, the thermodynamic modeling, and the parametric sensitivity analysis. Conclusions drawn from the results and suggestions for future work are also included in the fifth chapter. Appendix A includes background on the possibility of GAS processing of nutraceuticals using alkyl aryl ester solvents and provides details of some initial resveratrol experiments performed. Appendix B is a complete listing of the four Mathcad codes developed in the present study.

1.4 References

Benedetti, L., A. Bertucco and P. Pallado (1997). "Production of micronic particles of biocompatible polymer using supercritical carbon dioxide." Biotechnology and Bioengineering **53**(2): 232-237.

Bristow, S., B. Y. Shekunov and P. York (2001). "Solubility analysis of drug compounds in supercritical carbon dioxide using static and dynamic extraction systems." Industrial & Engineering Chemistry Research **40**(7): 1732-1739.

Burrill, G. S. (2002). "Nutraceuticals - An overview." Agro Food Industry Hi-Tech **13**(4): 12-17.

Catchpole, O. J., S. Hochmann and S. R. J. Anderson (1996). Gas Anti-solvent Fractionation of Natural Products. High Pressure Chemical Engineering, Industrial Research Ltd.

Dixon, D. J. and K. P. Johnston (1991). "Molecular Thermodynamics of Solubilities in Gas Antisolvent Crystallization." Aiche Journal **37**(10): 1441-1449.

Gallagher, P. M., M. P. Coffey, V. J. Krukonis and N. Klasutis (1989). "Gas Antisolvent Recrystallization - New Process to Recrystallize Compounds Insoluble in Supercritical Fluids." Acs Symposium Series **406**: 334-354.

Hanna, M. and P. York (1994). "Method and Apparatus for the Formation of Particles." World Intellectual Property Organization: Patent WO95/01121.

Jang, M. S., E. N. Cai, G. O. Udeani, K. V. Slowing, C. F. Thomas, C. W. W. Beecher, H. H. S. Fong, N. R. Farnsworth, A. D. Kinghorn, R. G. Mehta, R. C. Moon and J. M. Pezzuto (1997). "Cancer chemopreventive activity of resveratrol, a natural product derived from grapes." Science **275**(5297): 218-220.

Ke, J. H. and C. S. Tan (2002). "Solvent selection for gas antisolvent precipitation process." Journal of the Chinese Institute of Chemical Engineers **33**(5): 491-497.

Li, D., Z. M. Liu, G. Y. Yang, B. X. Han and H. K. Yan (2000). "Phase equilibria of CO2-PET-phenol system and generation of PET powders by supercritical CO2 anti-solvent." Polymer **41**(15): 5707-5712.

Liu, Z. M., D. Li, G. Y. Yang and B. X. Han (2000). "Solubility of organic acids in ethyl acetate expanded with CO2." Fluid Phase Equilibria **167**(1): 123-130.

Muhrer, G. and M. Mazzotti (2003). "Precipitation of lysozyme nanoparticles from dimethyl sulfoxide using carbon dioxide as antisolvent." Biotechnology Progress **19**(2): 549-556.

Peng, D. and D. B. Robinson (1976). "New 2-Constant Equation of State." Industrial & Engineering Chemistry Fundamentals **15**(1): 59-64.

Thiering, R., F. Dehghani, A. Dillow and N. R. Foster (2000). "The influence of operating conditions on the dense gas precipitation of model proteins." Journal of Chemical Technology and Biotechnology **75**(1): 29-41.

Trela, B. C. and A. L. Waterhouse (1996). "Resveratrol: Isomeric molar absorptivities and stability." Journal of Agricultural and Food Chemistry **44**(5): 1253-1257.

Yeo, S. D., G. B. Lim, P. G. Debenedetti and H. Bernstein (1993). "Formation of Microparticulate Protein Powders Using a Supercritical Fluid Antisolvent." Biotechnology and Bioengineering **41**(3): 341-346.

2.0 LITERATURE REVIEW

2.1 Particle Formation

2.1.1 Current Particle Processing Methods

In pharmaceutical preparation, it is desirable to obtain very small, very pure drug particles with a narrow size distribution. Fine particles are better suited for drug delivery applications since micronized particles have increased efficacy, reducing the required dosage. Used with aerosol inhalers, they allow the primary dosage to bypass the liver, increasing the drug bioavailability (Shariati and Peters, 2002; Rasenack and Muller, 2004). Traditional micronization techniques include jet-milling and spray drying, each of which can pose problems for pharmaceutical and nutraceutical materials.

Jet-milling is used to produce particles in the 1 to 5 μm size range, making them respirable. The technique involves breaking up the drug material into smaller pieces through particle-particle interactions and particle-wall interactions using jets of compressed air (Louey et al., 2004). This common practice is energy-intensive and does not allow for definitive control of particle size and morphology (Beckman, 2004). The high temperatures encountered in jet-milling due to friction can damage thermally-labile pharmaceutical compounds. Additionally, the mechanical break-up process has the potential to alter the properties of the substance (Rasenack and Muller, 2004).

Spray-drying of particles consists of dissolving the pharmaceutical in water or an organic solvent, atomizing the solution into a hot gas, and drying the droplets to remove the solvent from the pharmaceutical of interest (Beckman, 2004). Like jet-milling, spray-drying

can also degrade pharmaceutical compounds due to the high drying temperatures required to remove residual solvent and yield a pure product (Rogers et al., 2001).

2.1.2 Use of Supercritical CO_2 for Particle Formation

Recently, much attention has been paid to the use of supercritical CO_2 for processing pharmaceutical particles. CO_2, acting as either a solvent or an antisolvent, represents a promising alternative to conventional techniques that can damage thermally-labile compounds. This has been the subject of several recent review articles (Reverchon, 1999; Jung and Perrut, 2001; Rogers et al., 2001; Foster et al., 2003; Shariati and Peters, 2003).

2.1.2.1 *Supercritical Fluid Extraction*

CO_2 is a non-toxic, non-flammable gas with an easily-attainable critical temperature of 31°C (Rowley et al., 2002). The molecular structure of CO_2 is shown in Figure 4.1. Supercritical CO_2 displays a liquid-like density that is tunable with pressure, a vapor-like diffusivity, and a viscosity that is quite low: 1/10 that of water (Beckman, 2004). These properties make supercritical CO_2 an attractive option to replace traditional organic solvents and antisolvents that are often volatile organic compounds (VOCs). Figure 2.1 is a typical pure component phase diagram showing the location of the supercritical regime.

Supercritical fluid extraction exploits the dramatic increase in density – and thus solvent strength – of CO_2 at pressures above the critical pressure. High solute loading can be achieved for non-polar substances, while polar and complex molecules are often only sparingly soluble in supercritical CO_2, even at very high pressures. These differences in solute solubilities can facilitate the implementation of an efficient separation scheme. Supercritical CO_2 can be used to selectively extract a molecule of interest, as has been done

commercially with the decaffeination of coffee (McHugh and Krukonis, 1994), or conversely, CO_2 can be used to dissolve and remove impurities, leaving behind the desired product. In one example, Almodovar and coworkers selectively purified acetaminophen from a non-polar matrix by dissolving the waxy support material in supercritical CO_2 at moderate pressures, leaving behind the polar acetaminophen (Almodovar et al., 1998).

The possibilities of extracting polar pharmaceuticals and nutraceuticals using supercritical CO_2 are often quite limited, as these substances typically exhibit very low CO_2-solubility (Dean and Khundker, 1997). For instance, coumaric acid isomers found in the extracts from many natural products exhibit solubilities in supercritical CO_2 in the range of 10^{-8} to 10^{-7} mole fraction (Choi et al., 1998). Solute loadings of polar compounds in supercritical CO_2 may be increased through the addition of polar modifiers, which are commonly short chain alcohols (Clifford, 1999).

2.1.2.2 *RESS Process*

If a pharmaceutical compound can be dissolved into supercritical CO_2, solvent-free particles can be formed by the expansion of the supercritical fluid solution through a nozzle. The high pressure is drastically decreased almost instantaneously, reducing the solvating power of the CO_2 and causing a high supersaturation ratio. The resulting supersaturation is the driving force for precipitation. This process, shown schematically in Figure 2.2, is known as rapid expansion of supercritical solutions (RESS), and has been successfully used to form particles of polymers, dyes, pharmaceuticals, and inorganic substances (Bertucco and Vetter, 2001).

The RESS process has the advantages of a solvent-free system and the possibility of obtaining particle size diameters on the order of nanometers. However, the low solubilities of many substances in supercritical CO_2 require large gas/solute loading ratios (Bertucco and Vetter, 2001). In many cases the solubilities of some pharmaceuticals of interest may be too low to permit a commercially viable process (Reverchon and Perrut, 2000).

2.1.2.3 *GAS Process*

Gas antisolvent (GAS) precipitation is a batch process, complementary to RESS, that exploits the low solubilities of polar compounds and polymers in CO_2. First, a solution is made of the solute in an organic solvent. The solution is then pressurized with CO_2. Unlike oxygen and hydrogen, pressurized CO_2 is very soluble in many liquid organic solvents (Beckman, 2004). The dissolved CO_2 expands the liquid phase, reducing the density and reducing the solvent strength of the solution. Due to the resulting supersaturation, pure solute particles precipitate out of solution (Subramaniam et al., 1997). The particle size and morphology can be controlled by the rate and method of CO_2 addition (Gallagher et al., 1989). Solid solute particles are separated from the expanded liquid phase through filtration at high pressure. The filtered liquid phase can be easily separated by depressurization, and both the solvent and CO_2 can be recycled. GAS precipitation, shown schematically in Figure 2.3, was first developed by Gallagher and coworkers (Gallagher et al., 1989) who used GAS to process sensitive explosives.

GAS precipitation is carried out at low temperatures and moderate pressures, making it an especially attractive option for the processing of thermally-labile compounds, including proteins. Yeo and coworkers used a GAS process to precipitate insulin powders from

dimethyl sulfoxide (DMSO). Instead of introducing the CO_2 flow to a stagnant solution, Yeo et al. continuously fed the insulin solution and supercritical CO_2 into the precipitator simultaneously in order to dissolve the CO_2 into the DMSO and evaporate the DMSO into the CO_2-rich phase, reducing the particle drying time (Yeo et al., 1993). Thiering and coworkers examined the effect of operating conditions on the precipitation of lysozyme, insulin, and myoglobin powders from DMSO solutions and ethanol solutions, including operating temperature, anti-solvent addition rate and initial solute concentration (Thiering et al., 2000). They reported that the proteins typically precipitated at similar liquid phase concentrations of the antisolvent. Muhrer and Mazzotti examined the effect of those same three process variables on particle size and distribution for the system lysozyme precipitated from CO_2-expanded DMSO (Muhrer and Mazzotti, 2003). They found that CO_2 addition rate, initial solute concentration, and operating temperature had a negligible effect on particle size and size distribution.

Using GAS to precipitate polymeric particles for drug delivery and materials processing applications is currently of great interest, as many polymers have low CO_2-solubilities. Benedetti and coworkers formed particles of benzylic ester, a biocompatible polymer, from CO_2-expanded DMSO with mean diameters of 0.5 μm using a semi-batch GAS process (Benedetti et al., 1997). Elvassore and coworkers used a semi-continuous GAS process to precipitate insulin-loaded polyethylene glycol and polylactide nanoparticles from DMSO solutions and dichloromethane solutions (Elvassore et al., 2001). Li and coworkers examined the phase behavior of the ternary GAS system CO_2-phenol-

polyethylene terephthalate (PET) (Li et al., 2000). PET powders are typically used for forming films and fibers.

The GAS process has been successfully used to precipitate several organic substances, including naphthalene and phenanthrene from CO_2-expanded toluene (Dixon and Johnston, 1991; Berends et al., 1996), salicylic acid from CO_2-expanded propanol (Shariati and Peters, 2002) and from CO_2-expanded ethyl acetate (Liu et al., 2000), and tetradecanoic acid, stearic acid, and behenic acid from CO_2-expanded ethyl acetate (Liu et al., 2000). GAS precipitation has also been used to process natural products. Chang and Randolph precipitated β-carotene from CO_2-expanded toluene (Chang and Randolph, 1990); Cocero and Ferrero later precipitated β-carotene from CO_2-expanded ethyl acetate and CO_2-expanded dichloromethane (Cocero and Ferrero, 2002). Liu and coworkers explored the ternary phase behavior of cholesterol precipitated from CO_2-expanded acetone (Liu et al., 2002).

The pressure in GAS precipitation can be carefully controlled to allow fractionation of a solution of mixed solutes by exploiting the difference in solubility of the various fractions in the gas-expanded liquid phase. Catchpole and co-workers used GAS precipitation to separate lectin and Soya oil mixtures in toluene (Catchpole et al., 1996). They found that at a given temperature, the pressure that a solute precipitates from a solution that has a mixture of solutes does not correspond to the pressure that the solute precipitates from the pure solvent. The difference in precipitation pressures is much lower for solutes when they are in the mixture. This result is consistent with the findings of Bertucco and coworkers, who selectively precipitated phenanthrene from a mixture of naphthalene and

phenanthrene in toluene (Bertucco et al., 1998). Bertucco et al. were able to achieve a phenanthrene product that was 98.5% pure. They point out that a higher pressure is required to precipitate solutes that are more soluble in the antisolvent: at low pressures the CO_2 acts as a cosolvent, and as an antisolvent at higher pressures. Shishikura and coworkers successfully separated citric acid from other organic acids in a CO_2-expanded acetone solution (Shishikura et al., 1994), indicating that GAS precipitation may be a promising method of separating fermentation broths. Winters and coworkers used GAS precipitation to separate protein mixtures, achieving fractional crystallization of mixtures of lysozyme and ribonuclease, alkaline phosphase and insulin, and trypsin and catalase from CO_2-expanded DMSO (Winters et al., 1999). Chang and coworkers used GAS precipitation to separate β-carotene from oxides (Chang et al., 1991); they further separated the cis and trans-β-carotene isomers, indicating the potential for using GAS fractionation to separate subtly-different molecules.

Mazzotti and coworkers have completed several studies on GAS precipitation, developing mathematical models to examine mass transfer effects and determine the effect of GAS process parameters (Muller et al., 2000; Muhrer et al., 2002; Lin et al., 2003). Elvassore and coworkers have examined the kinetics of particle formation in GAS precipitation (Elvassore et al., 2003). Almost all of the published work on GAS precipitation has been done on a laboratory scale, very little scale-up work has been done. Reverchon and coworkers reported results for pilot scale GAS precipitation of amoxicillin from CO_2-expanded N-methylpyrrolidone (Reverchon et al., 2003), and Muhrer and

coworkers reported results for the scaling up of a process involving the precipitation of a proprietary pharmaceutical compound from CO_2-expanded ethanol (Muhrer et al., 2003).

2.1.2.4 *SEDS Process*

Solution enhanced dispersion by supercritical fluids (SEDS) represents a specific implementation of the GAS process. SEDS and GAS precipitation share the same thermodynamic system: a saturated liquid solution in equilibrium with both a CO_2-rich vapor phase and a pure precipitated solid solute phase. In the SEDS process, shown schematically in Figure 2.4, both the solute solution and the antisolvent are fed into the precipitation chamber through a coaxial nozzle. The solute dissolved in an organic solvent flows through the center tube, and the antisolvent, typically CO_2, flows through the outer tube. This allows for rapid mixing of the streams in the nozzle, where the CO_2 dissolves into the solution droplets and the solvent is dissolved into the CO_2-rich phase. The SEDS design was patented by Hanna and York (Hanna and York, 1994).

2.2 Thermodynamic Modeling of Binary and Ternary Systems of Interest to GAS Precipitation

2.2.1 Importance of Phase Behavior Studies for GAS Process

A simple GAS precipitation system includes three components: (1) a compressed gas antisolvent, typically CO_2, (2) a liquid organic solvent, and (3) a solid solute of interest. Following crystallization, three phases are present: a solvent-rich CO_2-expanded liquid phase saturated with the solute, a CO_2-rich vapor phase with extracted solvent and a small amount of solute, and a pure, solid solute phase. The lack of extensive experimental solubility data for ternary GAS precipitation systems makes it especially important to

conduct fundamental thermodynamic studies in order to develop robust predictive phase behavior models (Reverchon, 1999).

Reverchon and coworkers have shown that knowledge of the ternary phase behavior for the system CO_2-DMSO-yttrium acetate is very important for achieving specific particle sizes and morphologies. They report that sub-micron particles are formed, independent of the injector size, when the operating temperature and pressure are above the mixture critical point. They further report that knowledge of the phase behavior of the binary antisolvent-organic solvent system, assuming that the solute behaves as an ideal solute, can be used to explain particle morphologies obtained from operating at certain temperatures and pressures. In particular, operating in the vicinity of the CO_2-rich side of the P-x-y phase envelope can have dramatic effects on particle dimensions (Reverchon et al., 2003). A typical binary P-x-y diagram is shown in Figure 2.5. Reverchon et al. suggest conducting fundamental phase behavior studies of GAS systems considering all three components, as some solutes may significantly change the shape of the P-x-y phase envelopes.

At a given temperature, small changes in the system pressure may cause a dramatic change in the equilibrium solubility of the solute in the CO_2-expanded liquid phase, causing solutes to precipitate out of solution (Shariati and Peters, 2002). This behavior is shown in Figure 2.6 for the system CO_2-propanol-salicylic acid (Shariati and Peters, 2002). Shariati and Peters note that at 288 K, 70% of the salicylic acid can be precipitated out of solution with a change in pressure of only 100 psi. A robust thermodynamic model can be used to predict this solubility behavior, and to determine the appropriate operating conditions

necessary to effect a significant change in the solute solubility and ensure adequate product yields.

2.2.2 Thermodynamic Modeling of GAS Precipitation

Various thermodynamic models have been proposed to represent the GAS process, in particular to predict the solubility of the solute of interest in the CO_2-expanded liquid phase. Several researchers have focused their attention on determining the optimum GAS precipitation operating conditions, including temperature and pressure, which has sparked some debate about the proper selection criteria. Most of the work in this area has focused on the relationship between the volume expansion of the liquid phase upon pressurization with CO_2 and the precipitation pressure. Gallagher and coworkers defined the volume expansion, $\Delta V/V$, as the change in the volume of the liquid phase with the addition of CO_2, divided by the initial volume, $V_2(T,P_o)$, of the pure solvent (Gallagher et al., 1989),

$$\frac{\Delta V}{V} = \frac{V_L(T,P,x_1) - V_2(T,P_o)}{V_2(T,P_o)} \qquad 2\text{-}1$$

Equation 2-1 can also be rearranged into a form explicit in the mole fraction of CO_2 in the liquid phase, x_1, the molar volume of the liquid solution, $v_L(T,P,x_1)$, and the molar volume of the solvent, $v_2(T,P_o)$,

$$\frac{\Delta V}{V} = \frac{1}{1-x_1} \cdot \frac{v_L(T,P,x_1)}{v_2(T,P_o)} - 1 \qquad 2\text{-}2$$

At low pressure, the volume expansion follows a linear Henry's Law trend. At pressures near the critical pressure of CO_2 the liquid phase expansion is dramatically increased with a small increase in pressure, eventually leveling off. This behavior is depicted in Figure 2.7.

Kordikowski and coworkers report the experimental liquid phase volume expansions for several CO_2-organic solvent pairs (Kordikowski et al., 1995).

Badilla and coworkers assert that the original definition of the relative volume expansion (Equation 2-1) is inadequate for determining the proper operating conditions for GAS precipitation, because for a given antisolvent, this definition does not distinguish the behavior of various organic solvents (Badilla et al., 2000). The relative volume expansion behavior for CO_2 and various organic solvents, calculated using Equation 2-1, is shown in Figure 2.8. Instead, Badilla et al. present an alternative definition for the relative volume expansion, using only the relative change in the *molar* volume of the liquid phase as the criteria for choosing an operating pressure (Equation 2-3), where the Peng-Robinson equation of state (presented in Section 2.2.3) is used to calculate the molar volume of the liquid phase.

$$\frac{\Delta v}{v} = \frac{v_L(T, P, x_1)}{v_2(T, P_o)} - 1 \qquad \text{2-3}$$

The behavior of the same CO_2-solvent systems displayed in Figure 2.8 is shown in Figure 2.9 using the new definition of the volume expansion. The behavior of the various solvent systems can now be differentiated. Using this definition, the relative molar volume expansion as a function of CO_2 mole fraction in the liquid phase goes through a minimum. For the system CO_2-toluene-naphthalene, Badilla and coworkers found that this minimum corresponds to the largest drop in the solubility of naphthalene in the CO_2-expanded liquid phase. In a subsequent work, this group reported that the same holds true for the ternary systems CO_2-propanol-salicylic acid and CO_2-acetone-benzoic acid (Badilla et al., 2004).

Mukhopadhyay presents Equation 2-4, the relative partial molar volume reduction (RPMVR), as the criteria for determining a proper operating pressure for the GAS process – an alternative to both the relative volume expansion and the relative molar volume expansion (Mukhopadhyay, 2003). Mukhopadhyay explains that the relative partial molar volume of the solvent, $\bar{v}_2$, is much more sensitive to the mole fraction of CO_2 in the liquid phase than is the liquid phase molar volume. This is shown in Figure 2.10 for the system CO_2-hexane.

$$-\frac{\Delta\bar{v}}{v} = 1 - \frac{\bar{v}_2}{v_2} \qquad 2\text{-}4$$

The RPMVR is, by definition, always positive. For comparison, the inverse of the molar volume expansion presented in Equation 2-3, the relative molar volume reduction (RMVR), is shown with the RPMVR in Figure 2.11 for the system CO_2-hexane. The abrupt increase in the RPMVR at high CO_2 mole fractions is much easier to discern than the maximum in the RMVR that occurs at this same point.

Chang and Randolph first predicted that the expansion behavior of the liquid phase, the solubility of the solute in the CO_2-expanded liquid phase, $x_3(T,P)$, and the supersaturation in the three component GAS system can all be explained by considering only the (1) antisolvent – (2) organic solvent pair (Chang and Randolph, 1990). They hypothesized that in a dilute system the drop in solute solubility with pressure is due to a decrease in the partial molar volume of the organic solvent. Chang and Randolph correlated the solubility of β-carotene in CO_2-expanded toluene and acetaminophen in CO_2-expanded n-butanol using Equation 2-5, where $x_3(T,1)$ is the solubility of the solute in the pure solvent

at atmospheric pressure, $\bar{v}_2(T,P,x_1)$ is the partial molar volume of the solvent in the solution, and $\bar{v}_2(T,1,0)$ is the partial molar volume of the pure solvent at atmospheric pressure. This same equation was used by Mukhopadhyay to model the solubility of β-carotene in CO_2-expanded ethyl acetate. Mukhopadhyay attributes the model's poor predictions at higher pressures to experimental uncertainties in the solubility data due to nucleation (Mukhopadhyay, 2003).

$$x_3(T,P) = \frac{\bar{v}_2(T,P,x_1)}{\bar{v}_2(T,1,0)} \cdot x_3(T,1) \qquad 2\text{-}5$$

The Peng-Robinson equation of state (Peng and Robinson, 1976) was used to calculate the solvent partial molar volumes in Equation 2-5, considering only the CO_2-solvent pair. This model assumes an interaction between the solute and the solvent, but only through the solute solubility at atmospheric pressure, $x_3(T,1)$; the model assumes no interaction between the solute and the antisolvent. As Bertucco and coworkers discovered later, this second assumption cannot be correct, as the precipitation pressure increases for compounds that are more soluble in CO_2 (Bertucco et al., 1998).

Dixon and Johnston proposed an expanded liquid equation of state model to predict the solute solubility in the liquid phase over the whole pressure range of interest (Dixon and Johnston, 1991). Their model uses regular solution theory to represent the fugacity of the solute in the liquid phase at low pressures and the Peng-Robinson equation of state to represent the fugacity of the solute in the liquid phase at high pressures. Using this model, their solubility predictions for naphthalene and phenanthrene in CO_2-expanded toluene were much better than the results they obtained using only regular solution theory to calculate the

fugacity of the solute in the liquid phase. Dixon and Johnston make the assumption that no solute is present in the equilibrium vapor phase, but they acknowledge that this assumption becomes poor for high temperature and supercritical pressure operating conditions.

Kikic et al., Shariati and Peters, and Badilla et al. used the basic approach outlined below in Section 2.2.3 for determining the equilibrium compositions of the vapor and liquid phases in a GAS process (Kikic et al., 1997; Shariati and Peters, 2002; Badilla et al., 2004). This model takes into account antisolvent-solvent, antisolvent-solute, and solvent-solute molecular interactions. While many other models consider only the calculation of the liquid phase composition, using this model the composition of the vapor phase is necessarily predicted simultaneously.

2.2.3 Phase Equilibrium Calculations Using an Equation of State

The Gibbs Phase Rule states that for an equilibrium system the number of degrees of freedom, F, or independent intensive variables which must be set to completely specify an equilibrium system with C components and π phases, is given by:

$$F = C - \pi + 2 \qquad \text{2-6}$$

Thus, for a two-component vapor-liquid equilibrium (VLE), solid-liquid equilibrium (SLE), or solid-vapor equilibrium (SVE) system, or a three-component solid-vapor-liquid equilibrium (SVLE) system, only the temperature and pressure need be specified for the compositions of the fluid phase(s) to be set in each case (Sandler, 1999).

By definition, at equilibrium the temperature and pressure are constant in all phases, and the chemical potential, μ_i, of each component is equal in all phases that the component appears,

$$T^1 = T^2 = ... = T^\pi \qquad \text{2-7}$$

$$P^1 = P^2 = ... = P^\pi \qquad \text{2-8}$$

$$\begin{aligned} &\mu_1^1 = \mu_1^2 = ... = \mu_1^\pi \\ &\vdots \\ &\mu_1^1 = \mu_C^2 = ... = \mu_C^\pi \end{aligned} \qquad \text{2-9}$$

It is convenient to use iso-fugacity relationships to represent this chemical equilibrium for mixtures, where $\hat{f}_i^\alpha$ is the fugacity of component *i* in phase α at the equilibrium temperature, *T*, and pressure, *P*,

$$\hat{f}_i^\alpha(T, P, x) = \hat{f}_i^\beta(T, P, x) \qquad \text{2-10}$$

For VLE at very low pressures, iso-fugacity can be represented using Raoult's Law (Equation 2-11), which assumes an ideal liquid, where $P_i^{sat}(T)$ is the vapor pressure of component *i* at the equilibrium temperature. Raoult's law is often used to generate initial guesses for the vapor and liquid compositions in phase equilibria calculations.

$$x_i \cdot P_i^{sat}(T) = y_i \cdot P \qquad \text{2-11}$$

For real fluid mixtures, an equation of state is used to calculate the fugacity of components in the vapor phase. The fugacity of components in the liquid phase may be calculated using an equation of state or an activity coefficient relationship. The former method, known as the φ-φ approach, uses an ideal gas as the reference state for both phase (Equations 2-12 and 2-13). The latter method, known as the φ-γ approach, uses an ideal gas as the reference state for the vapor phase and an ideal solution as the reference state for the liquid phase (Equations 2-12 and 2-14), where $f_i^L(T, P)$ in Equation 2-14 is the fugacity of pure component *i* in the liquid phase.

$$\hat{f}_i^V(T,P,y) = P \cdot y_i \cdot \hat{\phi}_i^V(T,P,y) \qquad 2\text{-}12$$

$$\hat{f}_i^L(T,P,x) = P \cdot x_i \cdot \hat{\phi}_i^L(T,P,x) \qquad 2\text{-}13$$

$$\hat{f}_i^L(T,P,x) = f_i^L(T,P) \cdot x_i \cdot \hat{\gamma}_i^L(T,P,x) \qquad 2\text{-}14$$

A φ-γ approach may provide better predictions for the liquid phase density at low pressure, but using the two different relationships means that convergence near the critical point is not possible (Orbey and Sandler, 1998); accordingly, only the φ-φ approach is considered below.

The ideal gas equation assumes no interaction between molecules and treats each molecule as a point, with no physical size. In the φ-φ approach, an equation of state is used to solve for a fugacity coefficient for each of the fluid phases to try and represent their non-ideality. The pressure-explicit Peng-Robinson equation of state (PREOS), given in Equation 2-15, is considered here (Peng and Robinson, 1976). The PREOS is semi-empirical with two parameters: *a*, a temperature-dependent energy parameter which provides a measure of the intermolecular attractive force, and *b*, a volume parameter related to the size of the molecules. The expressions for the fugacity coefficients using the PREOS are given in Equations 2-16 and 2-17.

$$P = \frac{RT}{v-b} - \frac{a(T)}{v(v+b)+b(v-b)} \qquad 2\text{-}15$$

$$\ln(\phi_i) = \frac{b_m}{b}\left(Z^V - 1\right) - \ln\left(Z^V - B\right) - \frac{A}{2\sqrt{2}B}\left[\frac{2\sum_{k=1}^{N} x_k a_{ki}}{a} - \frac{b_i}{b}\right]\ln\left[\frac{Z^V + 2.414B}{Z^V - 0.414B}\right] \qquad 2\text{-}16$$

$$\ln(\phi_i) = \frac{b_m}{b}\left(Z^L - 1\right) - \ln\left(Z^L - B\right) - \frac{A}{2\sqrt{2}B}\left[\frac{2\sum_{k=1}^{N} x_k a_{ki}}{a} - \frac{b_i}{b}\right]\ln\left[\frac{Z^L + 2.414B}{Z^L - 0.414B}\right] \qquad 2\text{-}17$$

First, the pure component parameters can be calculated using the critical temperatures, T_{ci}, the critical pressures, P_{ci}, and the acentric factors, ω_i, for each component in the mixture. R represents the ideal gas constant.

$$a_i(T) = 0.45724\frac{R^2\left(T_{ci}\right)^2}{P_{ci}}\left[1 + \left(0.37464 + 1.54226\omega_i - 0.26992\omega_i^2\right)\cdot\left(1 - \sqrt{\frac{T}{T_{ci}}}\right)\right]^2 \qquad 2\text{-}18$$

$$b_i = 0.07780\frac{RT_{ci}}{P_{ci}} \qquad 2\text{-}19$$

Traditionally, quadratic mixing rules are employed to solve for the mixture parameters in terms of the equilibrium composition of the mixture. Two binary interaction parameters, k_{ij} and l_{ij}, are fit from binary *i-j* data, and can allow for much better predictions of equilibrium compositions. Often l_{ij} is set to zero and only a single binary interaction parameter is used (Orbey and Sandler, 1998).

$$a = \sum_{i=1}^{N}\sum_{j=1}^{N} x_i x_j \cdot \sqrt{a_i(T)\cdot a_j(T)}\cdot(1 - k_{ij}) \qquad 2\text{-}20$$

$$b = \sum_{i=1}^{N}\sum_{j=1}^{N} x_i x_j \cdot \left(\frac{b_i + b_j}{2}\right)\cdot\left(1 - l_{ij}\right) \qquad 2\text{-}21$$

Then, A and B are calculated,

$$A = \frac{aP}{RT} \qquad 2\text{-}22$$

$$B = \frac{bP}{RT} \qquad 2\text{-}23$$

It is necessary to solve the cubic Equations 2-24 and 2-25 for the compressibility factor for both the vapor phase, Z^V, and the liquid phase, Z^L,

$$\left(Z^V\right)^3 - (1-B)\left(Z^V\right)^2 + (A - 3B^2 - 2B)Z^V - (AB - B^2 - B^3) = 0 \qquad 2\text{-}24$$

$$\left(Z^L\right)^3 - (1-B)\left(Z^L\right)^2 + (A - 3B^2 - 2B)Z^L - (AB - B^2 - B^3) = 0 \qquad 2\text{-}25$$

The largest root of Equation 2-24 represents the correct solution for the vapor phase, and the smallest root of Equation 2-25 represents the correct solution for the liquid phase, as the compressibility factor is proportional to the molar volume of each phase,

$$Z^\alpha = \frac{Pv^\alpha}{RT} \qquad 2\text{-}26$$

The compressibility factors can be substituted back into Equations 2-16 and 2-17 to solve for the fugacity coefficients.

Equations 2-12 and 2-13 are used along with the necessary conditions that the equilibrium composition values sum to unity for each phase to solve for the mole fractions of each component in the vapor and liquid phases. Because calculation of the fugacity coefficients requires knowing the compositions of each phase, an iterative process must be employed using an appropriate initial guess for the equilibrium mole fractions.

When a solid phase is present, as in the case of SLE, SVE, or SVLE, the fugacity of the fluid phases can be represented using an equation of state, but a separate relationship is required for the pure solid. Equation 2-27 represents the pure solid phase fugacity (Prausnitz et al., 1999), where $f_3^L\left(T, P_{tp}\right)$ is the fugacity of the pure, subcooled liquid solute

at the equilibrium temperature and a reference pressure, ΔH_{fus} is the heat of fusion of the solute at the melting temperature, T_{tp} is the triple point temperature, P_{tp} is the triple point pressure, ΔC_p is the differential heat capacity, and v_3^S is the molar volume of the solid. The PREOS can be used to calculate $f_3^L(T, P_{tp})$.

$$f_3^S = f_3^L(T, P_{tp})\exp\left[\frac{\Delta H_{fus}}{R}\left(\frac{1}{T_{tp}} - \frac{1}{T}\right) + \frac{v_3^S(P - P_{tp})}{RT} - \frac{\Delta C_P}{R}\left(\ln\left(\frac{T_{tp}}{T}\right) - \frac{T_{tp}}{T} + 1\right)\right] \quad \text{2-27}$$

The differential heat capacity is the difference between the heat capacity of the liquid and the solid solute at the melting temperature. Often this last term in the exponential is neglected, since at high pressure the first and second terms dominate. The triple point temperature is usually approximated as the melting temperature.

For the simple case of binary VLE for an (1) antisolvent - (2) solvent pair, Equations 2-28 and 2-29 must be solved simultaneously for the equilibrium compositions of the vapor and liquid phases.

$$P \cdot y_1 \cdot \hat{\phi}_1^V(T, P, y) = P \cdot x_1 \cdot \hat{\phi}_1^L(T, P, x) \quad \text{2-28}$$

$$P \cdot y_2 \cdot \hat{\phi}_2^V(T, P, y) = P \cdot x_2 \cdot \hat{\phi}_2^L(T, P, x) \quad \text{2-29}$$

For the case of binary SLE for a (2) solvent - (3) solute pair, only Equation 2-30 must be solved, using Equation 2-27 to calculate the solid phase fugacity. The solid phase is assumed to be pure, and so only component (3) is present in both phases.

$$P \cdot x_3 \cdot \hat{\phi}_3^L(T, P, x) = f_3^S \quad \text{2-30}$$

For the case of binary SVE for a (1) antisolvent – (3) solute pair, only Equation 2-31 must be solved, again, using Equation 2-27 to calculate the solid phase fugacity.

$$P \cdot y_3 \cdot \hat{\phi}_3^V(T,P,y) = f_3^S \qquad 2\text{-}31$$

For the case of SVLE for a (1) antisolvent – (2) solvent – (3) solute system, as is encounter in GAS precipitation, Equations 2-28, 2-29, 2-30, and 2-32 must be solved simultaneously, as the solute component is present in all three phases.

$$P \cdot y_3 \cdot \hat{\phi}_3^V(T,P,y) = P \cdot x_3 \cdot \hat{\phi}_3^L(T,P,x) \qquad 2\text{-}32$$

This approach to thermodynamic modeling employed by Kikic et al., Shariati and Peters, and Badilla et al. for the ternary GAS system was used in the present study. Predictions for the equilibrium fluid phase composition for the GAS system (1) CO_2 – (2) ethanol – (3) acetaminophen as a function of temperature and pressure are provided in Section 5.3. The k_{13} parameter for the (1) CO_2 – (3) acetaminophen pair was regressed from solubility data measured in the present study, and the experimental procedure for the collection of these data is outlined next in Chapter 3.

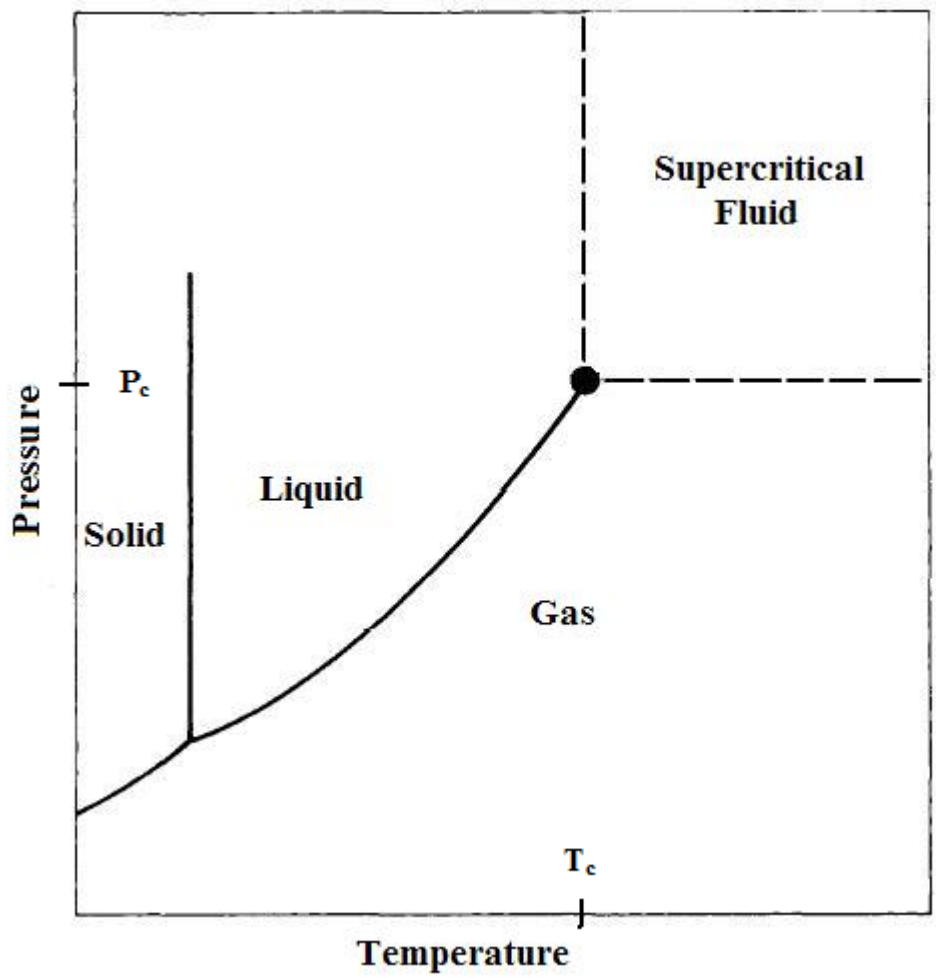

Figure 2.1 A pure component phase diagram. The vapor pressure line representing the coexistence of liquid and vapor phases ends at the critical point where the two phases merge into one.

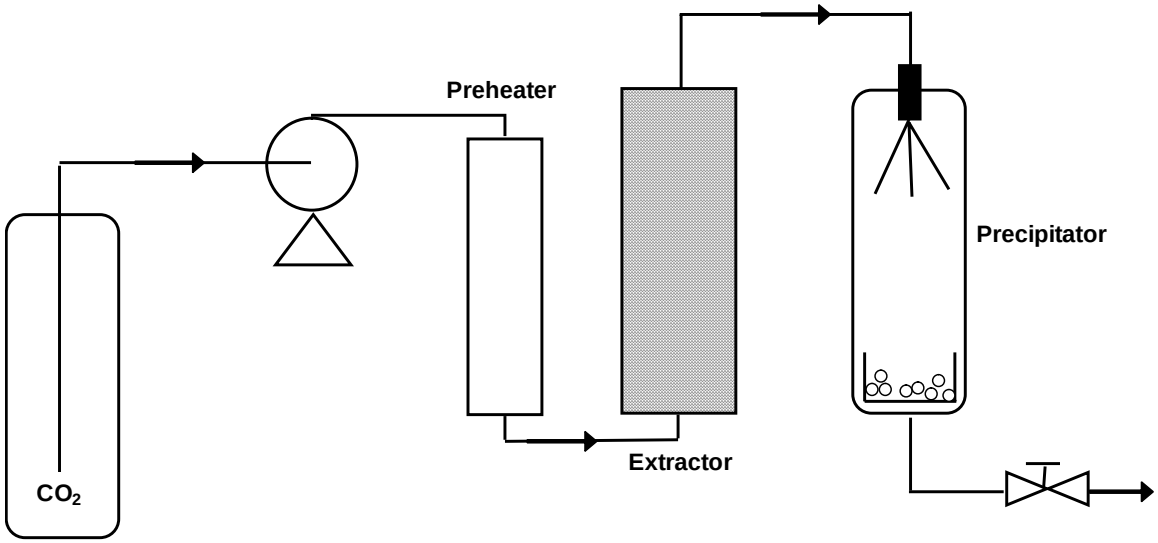

Figure 2.2 A schematic of the rapid expansion of supercritical solutions (RESS) process (Subramaniam et al., 1997).

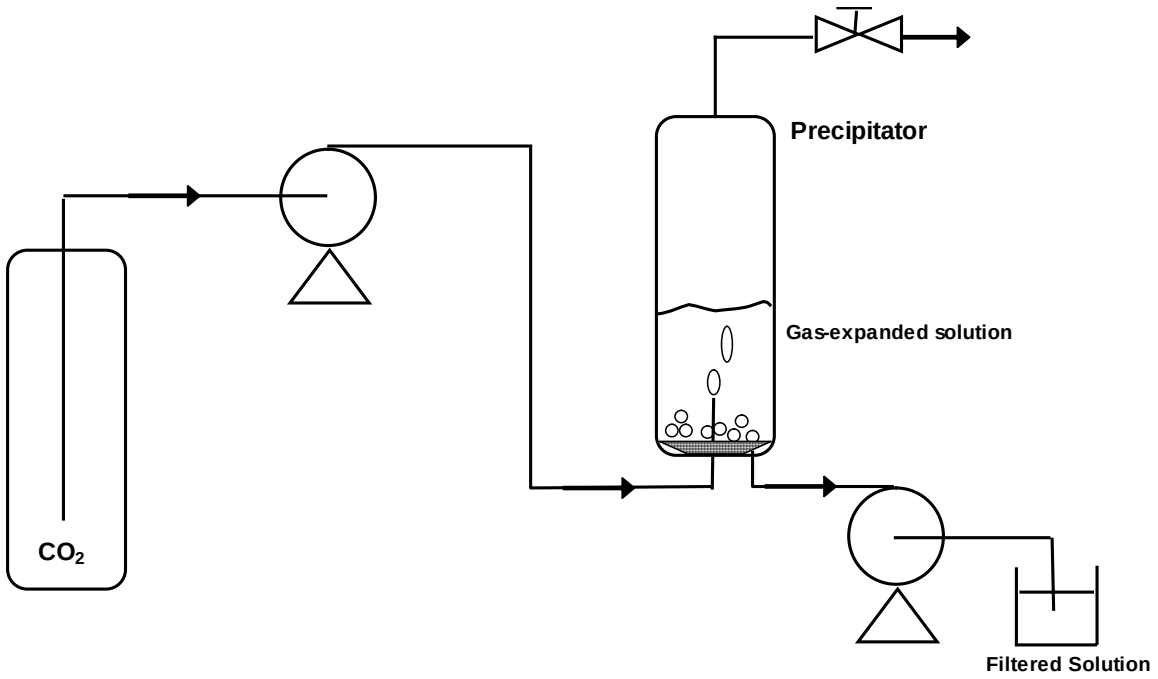

Figure 2.3 A schematic of the gas antisolvent (GAS) precipitation process (Subramaniam et al., 1997).

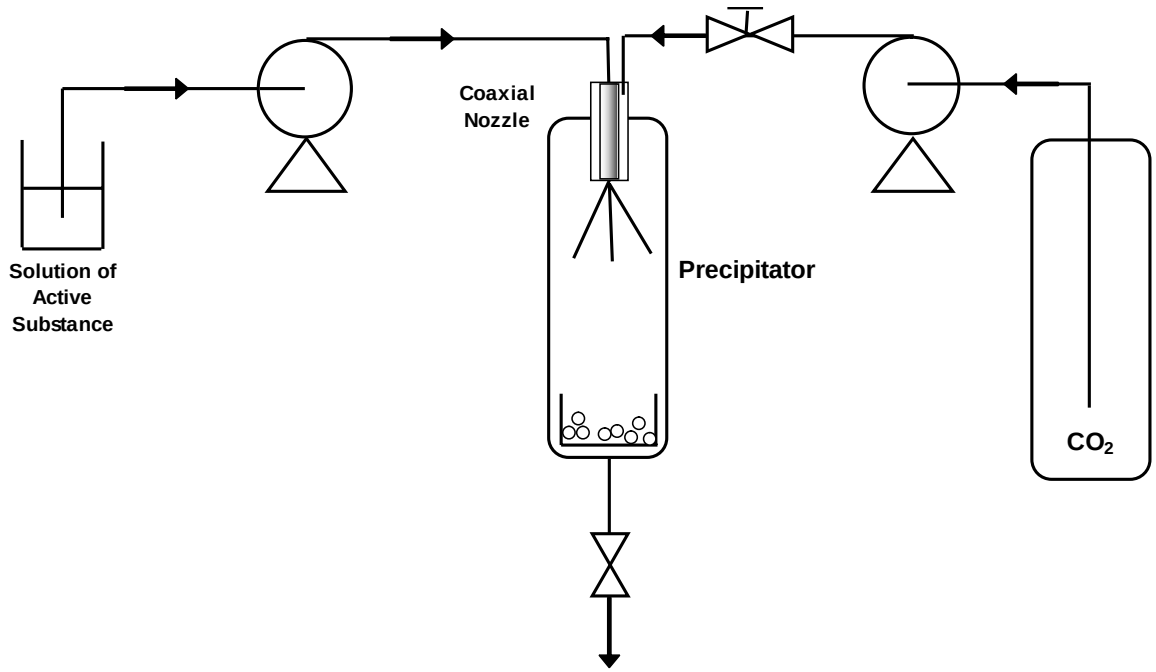

Figure 2.4 A schematic of the solvent enhanced dispersion by supercritical fluids (SEDS) process.

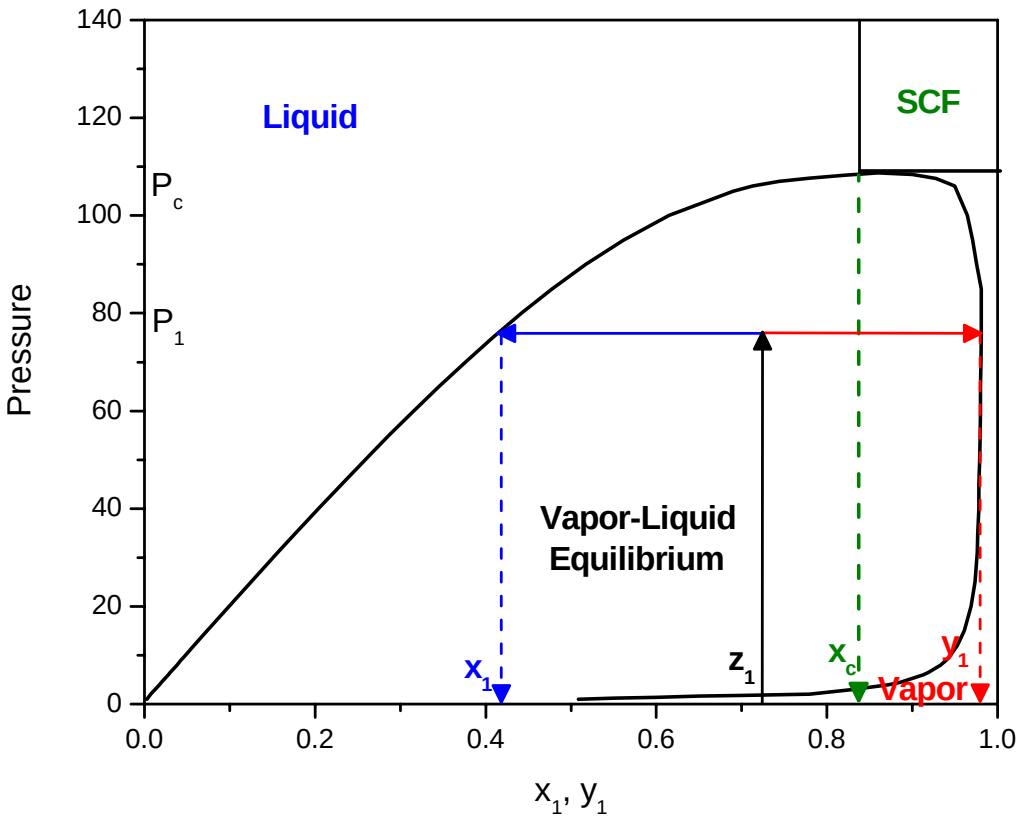

Figure 2.5 A typical binary VLE P-x-y phase envelope. Within the phase envelope a vapor phase and a liquid phase coexist. At pressure P_1 a mixture with overall composition z_1 will split into a liquid phase with composition x_1 and a vapor phase with composition y_1. Above the mixture critical pressure, P_c, a supercritical fluid exists above the critical composition, x_c, and a liquid phase exists for compositions below the critical composition.

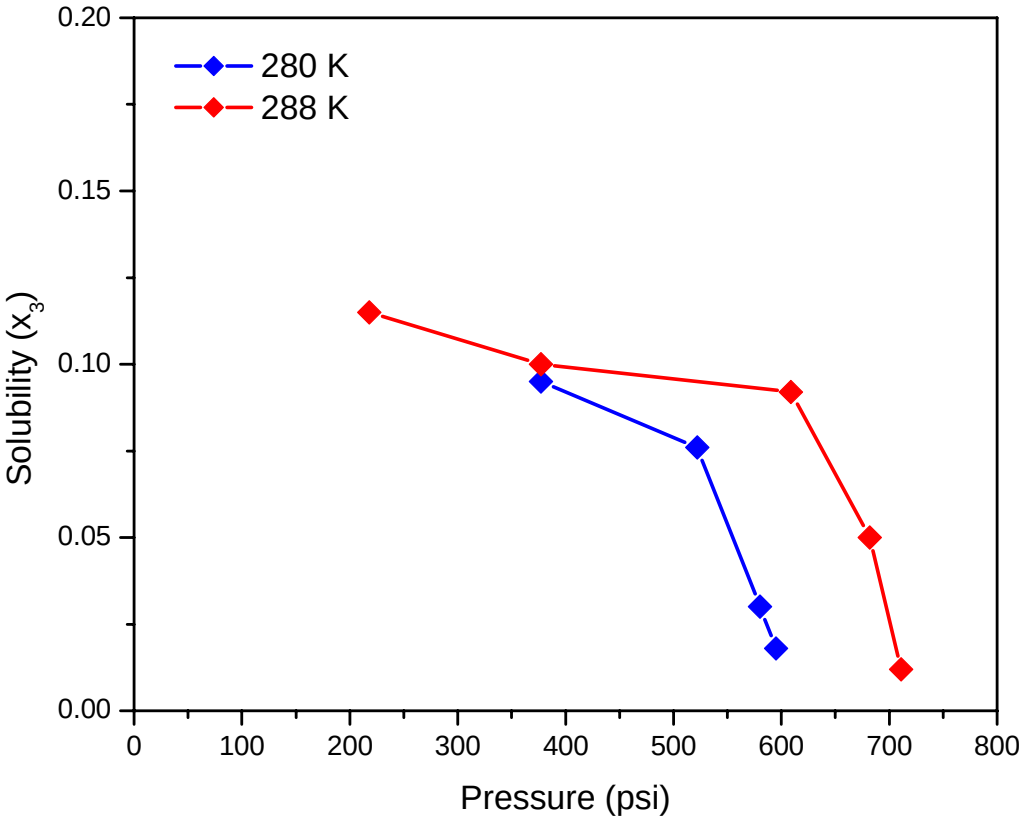

Figure 2.6 The solubility of (3) salicylic acid in (1) CO_2-expanded (2) propanol at 280K and 288 K (Shariati and Peters, 2002).

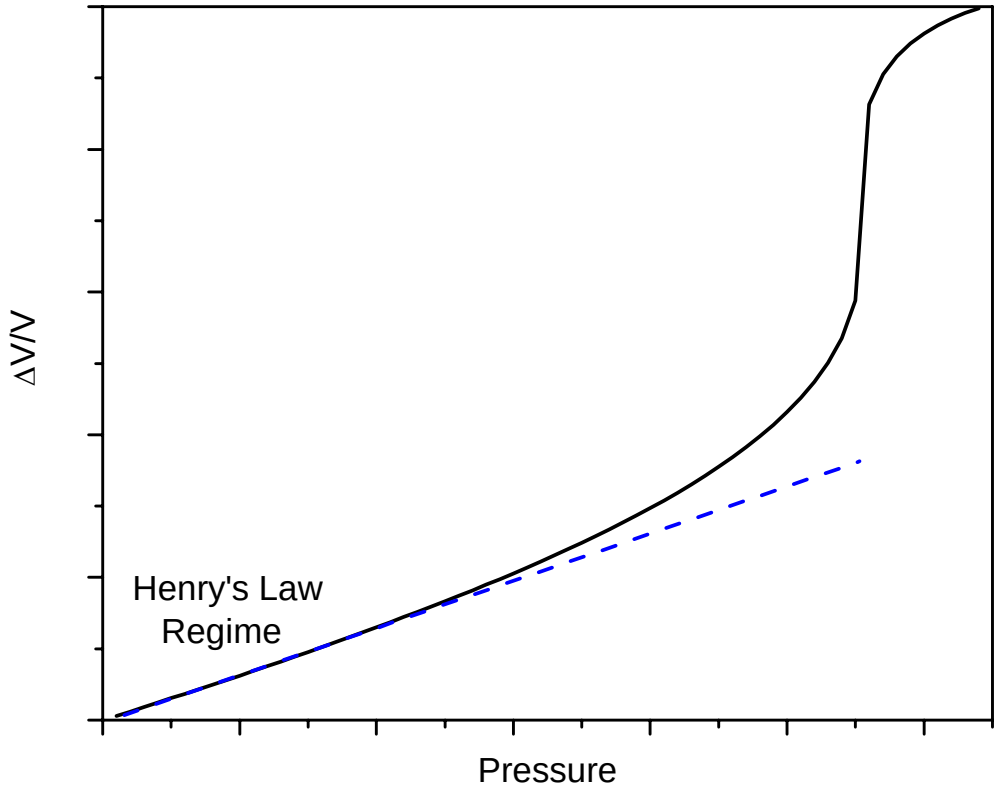

Figure 2.7 The relative volume expansion of the liquid phase in GAS precipitation as a function of pressure. In the low-pressure limit the expansion is linear, following Henry's Law; a sharp increase in the anti-solvent solubility in the liquid phase results in a spike in the volume expansion. Eventually, the volume expansion levels off at high pressures.

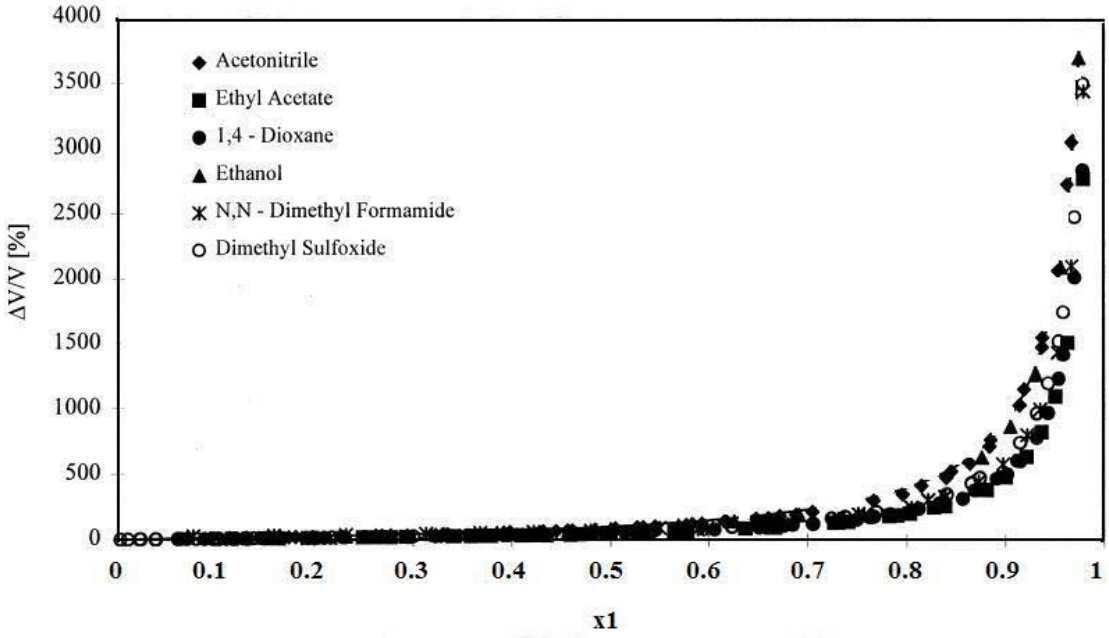

Figure 2.8 The relative volume expansion of the liquid phase for (1) CO_2 + (2) organic solvent at 298 K, 303K and 313 K, calculated using Equation 2-1. Plot taken from (Badilla et al., 2000).

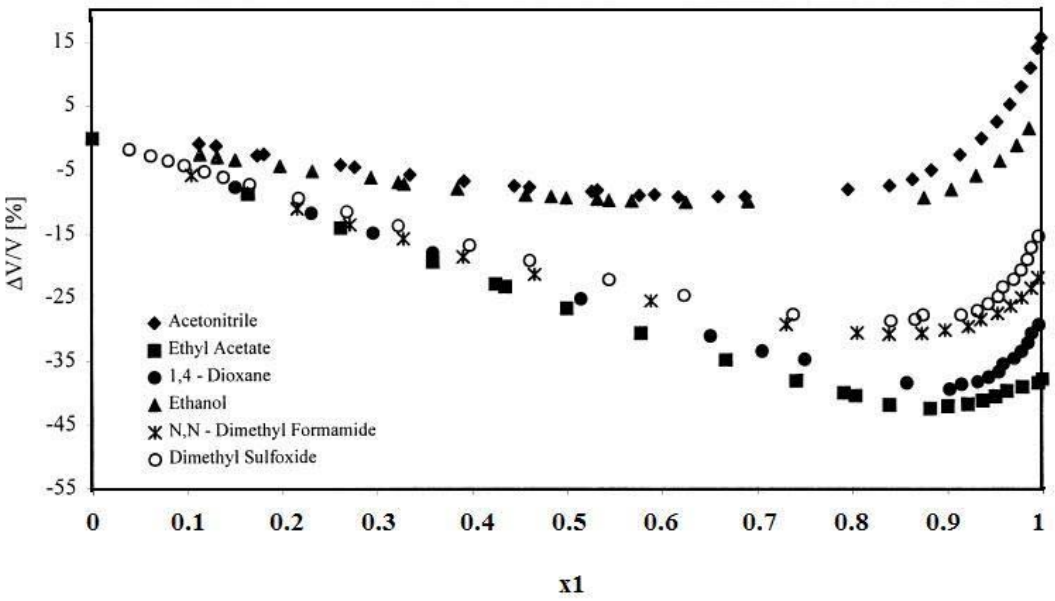

Figure 2.9 The relative volume expansion of the liquid phase for (1) CO_2 + (2) organic solvent at 298 K, calculated using Equation 2-3. Plot taken from (Badilla et al., 2000).

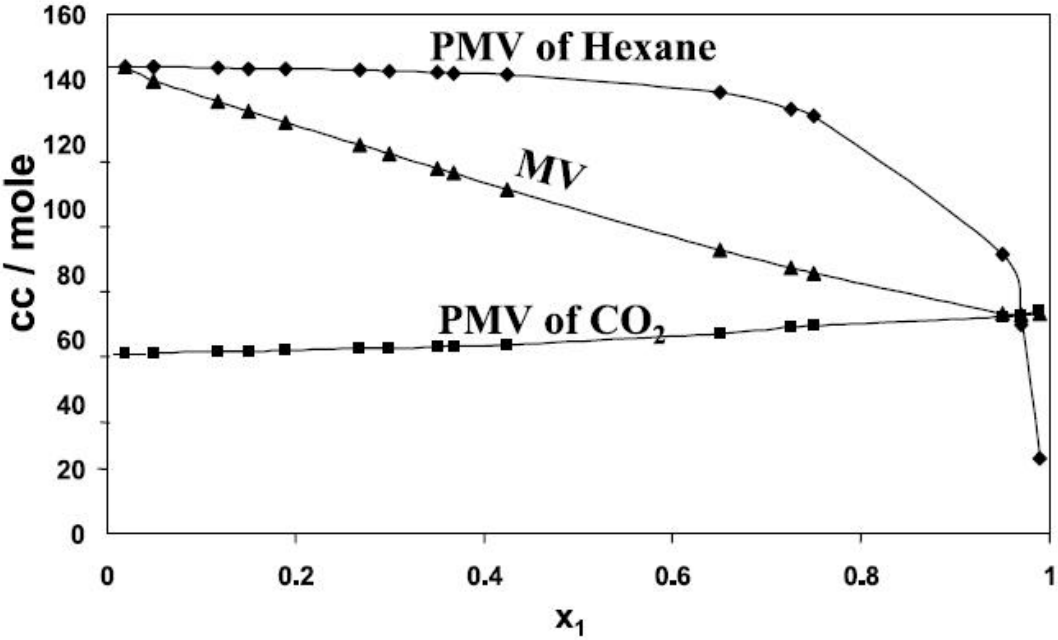

Figure 2.10 The effect of increasing antisolvent mole fraction in the liquid phase on the partial molar volume of the solvent, the molar volume of the liquid, and the partial molar volume of the antisolvent for the system (1) CO_2 + (2) hexane at 298 K. Plot taken from (Mukhopadhyay, 2003).

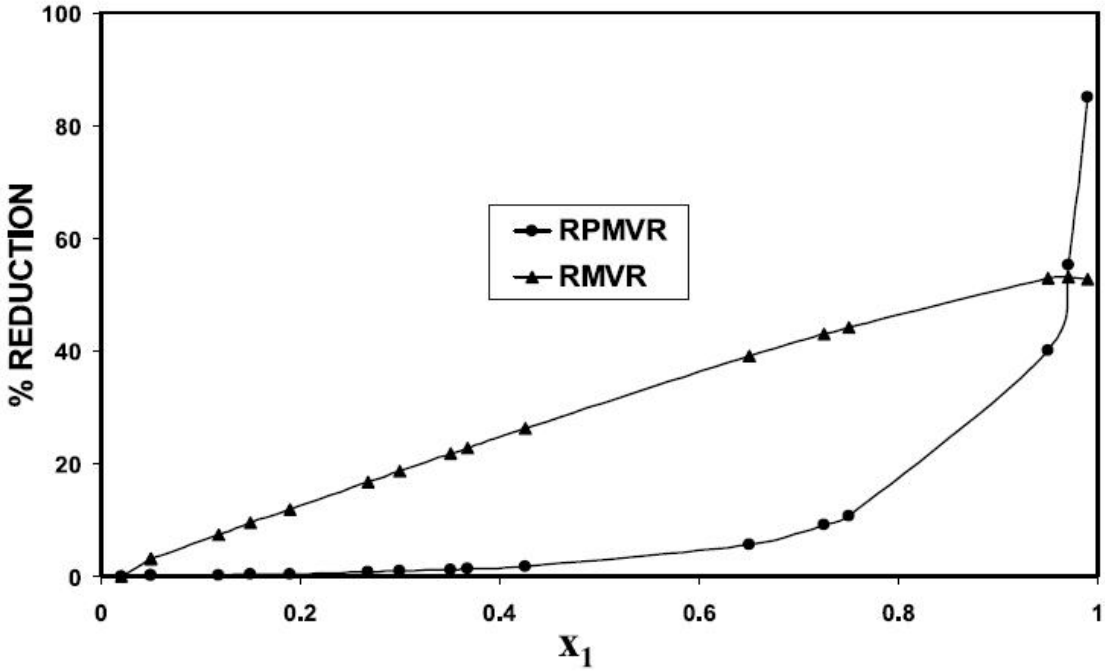

Figure 2.11 A comparison of the RMVR and RPMVR versus liquid phase mole fraction of the antisolvent for the system (1) CO_2 + (2) hexane at 298 K. Plot taken from (Mukhopadhyay, 2003).

2.5 References

Almodovar, R. A., R. A. Rodriguez and O. Rosario (1998). "Inverse supercritical extraction of acetaminophen from suppositories." Journal of Pharmaceutical and Biomedical Analysis **17**(1): 89-93.

Badilla, J., C. J. Peters and J. D. Arons (2000). "Volume expansion in relation to the gas-antisolvent process." Journal of Supercritical Fluids **17**(1): 13-23.

Badilla, J., A. Shariati and C. J. Peters (2004). "On the selection of optimum thermodynamic conditins for the GAS process." Journal of Supercritical Fluids **In Press**.

Beckman, E. J. (2004). "Supercritical and near-critical CO2 in green chemical synthesis and processing." Journal of Supercritical Fluids **28**(2-3): 121-191.

Benedetti, L., A. Bertucco and P. Pallado (1997). "Production of micronic particles of biocompatible polymer using supercritical carbon dioxide." Biotechnology and Bioengineering **53**(2): 232-237.

Berends, E. M., O. S. L. Bruinsma, J. deGraauw and G. M. vanRosmalen (1996). "Crystallization of phenanthrene from toluene with carbon dioxide by the GAS process." Aiche Journal **42**(2): 431-439.

Bertucco, A., M. Lora and I. Kikic (1998). "Fraction Crystallization by Gas Antisolvent Technique: Theory and Experiments." Aiche Journal **44**(10): 2149-2158.

Bertucco, A. and G. Vetter (2001). High Pressure Process Technology: Fundamentals and Applications. Amsterdam, Elsevier Science B. V.

Catchpole, O. J., S. Hochmann and S. R. J. Anderson (1996). Gas Anti-solvent Fractionation of Natural Products. High Pressure Chemical Engineering, Industrial Research Ltd.

Chang, C. J. and A. D. Randolph (1990). "Solvent Expansion and Solute Solubility Predictions in Gas-Expanded Liquids." Aiche Journal **36**(6): 939-942.

Chang, C. J., A. D. Randolph and N. E. Craft (1991). "Separation of beta-Carotene Mixtures Precipitated from Liquid Solvents with High-Pressure CO2." Biotechnology Progress **7**: 275-278.

Choi, E. S., M. J. Noh and K. P. Yoo (1998). "Solubilities of o-, m- and p-coumaric acid isomers in carbon dioxide at 308.15-323.15 K and 8.5-25 MPa." Journal of Chemical and Engineering Data **43**(1): 6-8.

Clifford, T. (1999). Fundamentals of Supercritical Fluids. New York, Oxford University Press, Inc.

Cocero, M. J. and S. Ferrero (2002). "Crystallization of beta-carotene by a GAS process in batch: Effect of operating conditions." Journal of Supercritical Fluids **22**: 237-245.

Dean, J. R. and S. Khundker (1997). "Extraction of pharmaceuticals using pressurised carbon dioxide." Journal of Pharmaceutical and Biomedical Analysis **15**(7): 875-886.

Dixon, D. J. and K. P. Johnston (1991). "Molecular Thermodynamics of Solubilities in Gas Antisolvent Crystallization." Aiche Journal **37**(10): 1441-1449.

Elvassore, N., A. Bertucco and P. Caliceti (2001). "Production of insulin-loaded poly(ethylene glycol)/poly(l-lactide) (PEG/PLA) nanoparticles by gas antisolvent techniques." Journal of Pharmaceutical Sciences **90**(10): 1628-1636.

Elvassore, N., T. Parton, A. Bertucco and V. Di Noto (2003). "Kinetics of particle formation in the gas antisolvent precipitation process." Aiche Journal **49**(4): 859-868.

Foster, N., R. Mammucari, F. Dehghani, A. Barrett, K. Bezanehtak, E. Coen, G. Combes, L. Meure, A. Ng, H. L. Regtop and A. Tandya (2003). "Processing pharmaceutical compounds using dense gas technology." Industrial & Engineering Chemistry Research **42**(25): 6476-6493.

Gallagher, P. M., M. P. Coffey, V. J. Krukonis and N. Klasutis (1989). "Gas Antisolvent Recrystallization - New Process to Recrystallize Compounds Insoluble in Supercritical Fluids." Acs Symposium Series **406**: 334-354.

Hanna, M. and P. York (1994). "Method and Apparatus for the Formation of Particles." World Intellectual Property Organization: Patent WO95/01121.

Jung, J. and M. Perrut (2001). "Particle design using supercritical fluids: Literature and patent survey." Journal of Supercritical Fluids **20**(3): 179-219.

Kikic, I., M. Lora and A. Bertucco (1997). "A thermodynamic analysis of three-phase equilibria in binary and ternary systems for applications in rapid expansion of a supercritical solution (RESS), particles from gas-saturated solutions (PGSS), and supercritical antisolvent (SAS)." Industrial & Engineering Chemistry Research **36**(12): 5507-5515.

Kordikowski, A., A. P. Schenk, R. M. VanNielen and C. J. Peters (1995). "Volume expansions and vapor-liquid equilibria of binary mixtures of a variety of polar solvents and certain near-critical solvents." Journal of Supercritical Fluids **8**(3): 205-216.

Li, D., Z. M. Liu, G. Y. Yang, B. X. Han and H. K. Yan (2000). "Phase equilibria of CO2-PET-phenol system and generation of PET powders by supercritical CO2 anti-solvent." Polymer **41**(15): 5707-5712.

Lin, C., G. Muhrer, M. Mazzotti and B. Subramaniam (2003). "Vapor-Liquid Mass Transfer during Gas Antisolvent Recrystallization: Modeling and Experiments." Industrial & Engineering Chemistry Research **42**: 2171-2182.

Liu, Z., D. Li, G. Yang and B. Han (2000). "Solubility of hydroxybenzoic acid isomers in ethyl acetate expanded with CO2." Journal of Supercritical Fluids **18**: 111-119.

Liu, Z., J. Wang, L. Song, G. Yang and B. Han (2002). "Study on the phase behavior of cholesterol-acetone-CO2 system and recrystallization of cholesterol by antisolvent CO2." Journal of Supercritical Fluids **24**: 1-6.

Liu, Z. M., D. Li, G. Y. Yang and B. X. Han (2000). "Solubility of organic acids in ethyl acetate expanded with CO2." Fluid Phase Equilibria **167**(1): 123-130.

Louey, M. D., M. Van Oort and A. J. Hickey (2004). "Aerosol dispersion of respirable particles in narrow size distributions produced by jet-milling and spray-drying techniques." Pharmaceutical Research **21**(7): 1200-1206.

McHugh, M. A. and V. J. Krukonis (1994). Supercritical Fluid Extraction: Principles and Practice. Boston, Butterworth-Heinemann.

Muhrer, G., C. Lin and M. Mazzotti (2002). "Modeling the Gas Antisolvent Recrystallization Process." Industrial & Engineering Chemistry Research **41**: 3566-3579.

Muhrer, G. and M. Mazzotti (2003). "Precipitation of lysozyme nanoparticles from dimethyl sulfoxide using carbon dioxide as antisolvent." Biotechnology Progress **19**(2): 549-556.

Muhrer, G., M. Mazzotti and M. Muller (2003). "Gas antisolvent recrystallization of an organic compound: Tailoring product PSD and scaling-up." Journal of Supercritical Fluids **27**: 195-203.

Mukhopadhyay, M. (2003). "Partial molar volume reduction of solvent for solute crystallization using carbon dioxide as antisolvent." Journal of Supercritical Fluids **25**(3): 213-223.

Muller, M., U. Meier, A. Kessler and M. Mazzotti (2000). "Experimental Study of the Effect of Process Parameters in the Recrystallization of an Organic Compound Using Compressed Carbon Dioxide as Antisolvent." Industrial & Engineering Chemistry Research **39**: 2260-2268.

Orbey, H. and S. Sandler (1998). Modeling Vapor-Liquid Equilibria: Cubic Equations of State and Their Mixing Rules. Cambridge, MA, Cambridge University Press.

Peng, D. and D. B. Robinson (1976). "New 2-Constant Equation of State." Industrial & Engineering Chemistry Fundamentals **15**(1): 59-64.

Prausnitz, J. M., R. N. Lichtenthaler and E. G. d. Azevedo (1999). Molecular Thermodynamics of Fluid Phase Equilibria. Upper Saddle River, NJ, Prentice Hall.

Rasenack, N. and B. W. Muller (2004). "Micron-size drug particles: Common and novel micronization techniques." Pharmaceutical Development and Technology **9**(1): 1-13.

Reverchon, E. (1999). "Supercritical antisolvent precipitation of micro- and nano-particles." Journal of Supercritical Fluids **15**(1): 1-21.

Reverchon, E., G. Caputo and I. De Marco (2003). "Role of phase behavior and atomization in the supercritical antisolvent precipitation." Industrial & Engineering Chemistry Research **42**(25): 6406-6414.

Reverchon, E., I. De Marco, G. Caputo and G. Della Porta (2003). "Pilot scale micronization of amoxicillin by supercritical antisolvent precipitation." Journal of Supercritical Fluids **26**: 1-7.

Reverchon, E. and M. Perrut (2000). Particle Design Using Supercritical Fluids: Reviews and Examples. 7th Meeting on Supercritical Fluids: Particle Design, Materials and Natural Products Processing, France, International Society for the Advancement of Supercritical Fluids.

Rogers, T. L., K. P. Johnston and R. O. Williams (2001). "Solution-based particle formation of pharmaceutical powders by supercritical or compressed fluid CO2 and cryogenic spray-freezing technologies." Drug Development and Industrial Pharmacy **27**(10): 1003-1015.

Rowley, R. L., W. V. Wilding, J. L. Oscarson, N. A. Zundel, T. L. Marshall, T. E. Daubert and R. P. Danner (2002). DIPPR Data Compilation of Pure Component Properties. New York, Design Institute for Physical Properties, AIChE.

Sandler, S. (1999). Chemical and Engineering Thermodynamics. New York, John Wiley and Sons, Inc.

Shariati, A. and C. J. Peters (2002). "Measurements and modeling of the phase behavior of ternary systems of interest for the GAS process: I. The system carbon dioxide plus 1-propanol plus salicylic acid." Journal of Supercritical Fluids **23**(3): 195-208.

Shariati, A. and C. J. Peters (2003). "Recent developments in particle design using supercritical fluids." Current Opinion in Solid State & Materials Science **7**(4-5): 371-383.

Shishikura, A., K. Kanamori, H. Takahashi and H. Kinbara (1994). "Separation and Purification of Organic Acids by Gas Antisolvent Crystallization." Journal of Agricultural and Food Chemistry **42**: 1993-1997.

Subramaniam, B., R. A. Rajewski and K. Snavely (1997). "Pharmaceutical processing with supercritical carbon dioxide." Journal of Pharmaceutical Sciences **86**(8): 885-890.

Thiering, R., F. Dehghani, A. Dillow and N. R. Foster (2000). "The influence of operating conditions on the dense gas precipitation of model proteins." Journal of Chemical Technology and Biotechnology **75**(1): 29-41.

Winters, M. A., D. Z. Frankel, P. G. Debenedetti, J. Carey, M. Devaney and T. M. Przybycien (1999). "Protein Purification with Vapor-Phase Carbon Dioxide." Biotechnology and Bioengineering **62**(3): 247-258.

Yeo, S. D., G. B. Lim, P. G. Debenedetti and H. Bernstein (1993). "Formation of Microparticulate Protein Powders Using a Supercritical Fluid Antisolvent." Biotechnology and Bioengineering **41**(3): 341-346.

3.0 EXPERIMENTAL SECTION

3.1 Materials

Acetaminophen, CAS [103-90-2](99% purity) from Sigma-Aldrich, carbon dioxide, CAS [124-38-9](>99.99% purity) from National Welders, and ethanol, CAS [64-17-5] (HPLC grade) from Sigma-Aldrich, were used for all solubility experiments. Prior to each experiment, the solid acetaminophen powder was coated onto 200μm glass beads from Alltech Associated, Inc., in a 20:1 mass ratio of beads to pharmaceutical. All substances were used without further purification.

3.2 Static Equilibrium Apparatus

A static equilibrium cell with off-line UV/Vis spectroscopic analysis was used to measure the solubility of acetaminophen in supercritical CO_2 (Figure 3.1). CO_2 was pressurized in an ISCO 260D high-pressure syringe pump [B], and then injected into the system at the desired pressure (± 1%) via one of two three-way valves [V4] that saddle the magnetic circulation pump (Micropump) [C]. Half-inch heating tape (Fisher Scientific) enveloped all tubing not housed within the convection oven (Precision) [F] to ensure a constant and uniform system temperature. From the second three-way valve [V5], the supercritical fluid flowed through a 5 mL volume capacity high-pressure view cell placed in a UV-Visible Spectrophotometer (Jasco V-550) [D]. A second 5 mL capacity high-pressure view cell was filled with pure CO_2 from the ISCO pump [B], and held at the same temperature and pressure as the extraction system to serve as the reference cell. The acetaminophen sample was placed into a 2 mL stainless steel extraction vessel (Valco) [E]

fit with 0.5μm filters at both ends. An Omega pressure transducer (±30 psi) [V5] measured the system pressure, and three temperature controllers (Barnant Company, R/S) maintained a constant system temperature (±0.1°C). [TC1] controlled the oven temperature, [TC2] controlled the temperature of the lines flowing in and out of the convection oven, and [TC3] controlled the temperature of the view cells.

3.3 Experimental Methods

3.3.1 Equilibrium Runs

To begin each experiment, the extraction vessel was filled with acetaminophen-coated glass beads. The system was flushed with low-pressure CO_2 to remove any trapped air, and then heated to 323K. When the system temperature equilibrated, the reference view cell was charged with CO_2 from the ISCO pump at the desired pressure. The valves on both sides of the extraction vessel ([V4] and [V8]) were initially closed to prevent through-flow. The remainder of the system was pressurized by adding a known volume of CO_2 from the ISCO pump into the system through valve [V4]. Valve [V4] was then closed, and the system was checked for leaks. Once the pressure and temperature stabilized in the system, valves [V8] and [V4] were opened to allow the CO_2 to flow through the extraction vessel, and the circulation pump [C] was turned on.

The spectrophotometer was not used to provide on-line quantitative analysis of the fluid-phase composition, but rather to provide a qualitative indication of whether equilibrium had been achieved. An absorbance reading was taken every thirty minutes until the peak height remained constant; typically this took 4-5 hours.

3.3.2 Sampling

Once the system reached equilibrium, the circulation pump was stopped, and the extracted acetaminophen was collected in two steps, resulting in two samples: the "bubble sample" and the "flush sample". First, the line running from the ISCO pump into [V4] was removed and replaced with a short piece of tubing. The supercritical solution was bubbled very slowly through approximately 7 mL of ethanol in a sampling vial, via the added piece of tubing, to collect the extracted acetaminophen. A large amount of the acetaminophen precipitated in the collection tubing during this process. In the second step, the extraction vessel was removed from the system and the system loop was flushed with a known amount of ethanol for approximately 5 minutes to recover the remaining acetaminophen. Care was taken to minimize the volatilized ethanol while trying to capture all of the extracted acetaminophen; however, the sample phase transfer steps can be a source of experimental error. The bubble and flush samples were analyzed as described below in the Analytical Methods section.

3.4 Analytical Methods

3.4.1 Beer's Law Calibration

Prior to the acetaminophen solubility experiments, Alan Chang, a doctoral student in our lab, constructed a calibration curve of absorbance at λ_{max}=250nm versus concentration for acetaminophen in ethanol (Figure 3.2). Using this curve, the concentrations of acetaminophen in the bubble and flush samples were calculated based on their absorbance readings.

3.4.2 Calculation of Equilibrium Solubility

The number of moles of acetaminophen in each of the samples, n_{bubble} and n_{flush}, is the product of the volume and the concentration of the sample. The total number of moles of acetaminophen extracted into the supercritical CO_2 is the sum of these values (Equation 3-1). The number of moles of CO_2 in the system is the product of the CO_2 density , ρ_1, and the volume of CO_2 added, V_1 (Equation 3-2). The density of CO_2 at room temperature and at the ISCO pump pressure was taken from the NIST WebBook (Lemmon, 2003). Using the number of moles of each of the two components, the equilibrium solubility, y_3, was calculated (Equation 3-3).

$$n_2 = n_{bubble} + n_{flush} \qquad 3\text{-}1$$

$$n_1 = \rho_1 \cdot V_1 \qquad 3\text{-}2$$

$$y_3 = \frac{n_3}{n_1 + n_3} \qquad 3\text{-}3$$

The solubility data obtained at 323 K ranged from 10^{-6}–10^{-4} mole fraction over the pressure range 1500 psi to 4000 psi. The results are listed in Table 3.1 and plotted in Figure 3.3. These data are correlated using the Peng-Robinson equation of state and an empirical density-based model in Section 5.2.2.

Table 3.1 The solubility of (3) acetaminophen in (1) supercritical CO_2 at 323 K.

P (psi)	y_3
1450	1.538E-6
1830	1.326E-6
2195	1.837E-6
2675	2.805E-6
2760	3.630E-6
3030	7.939E-6
3515	1.715E-5
3580	2.279E-5
3605	2.339E-5
3910	7.867E-5
4055	6.150E-5

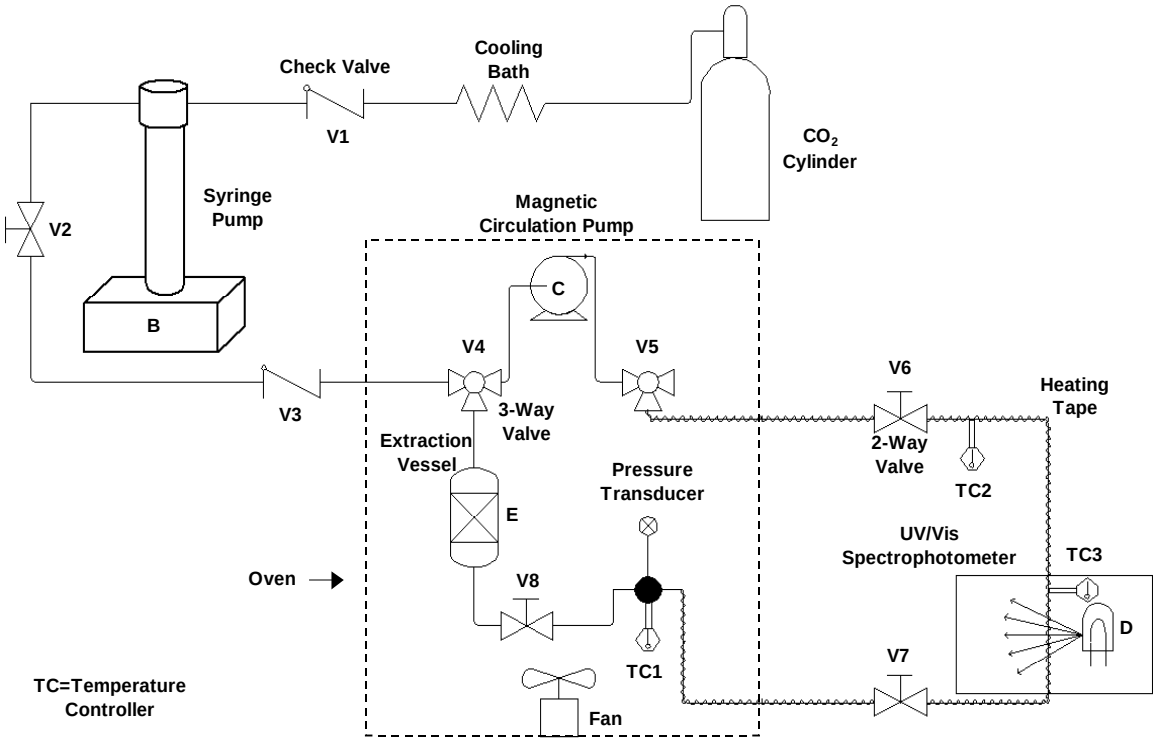

Figure 3.1 The static equilibrium apparatus used to determine the solubility of acetaminophen in supercritical CO_2.

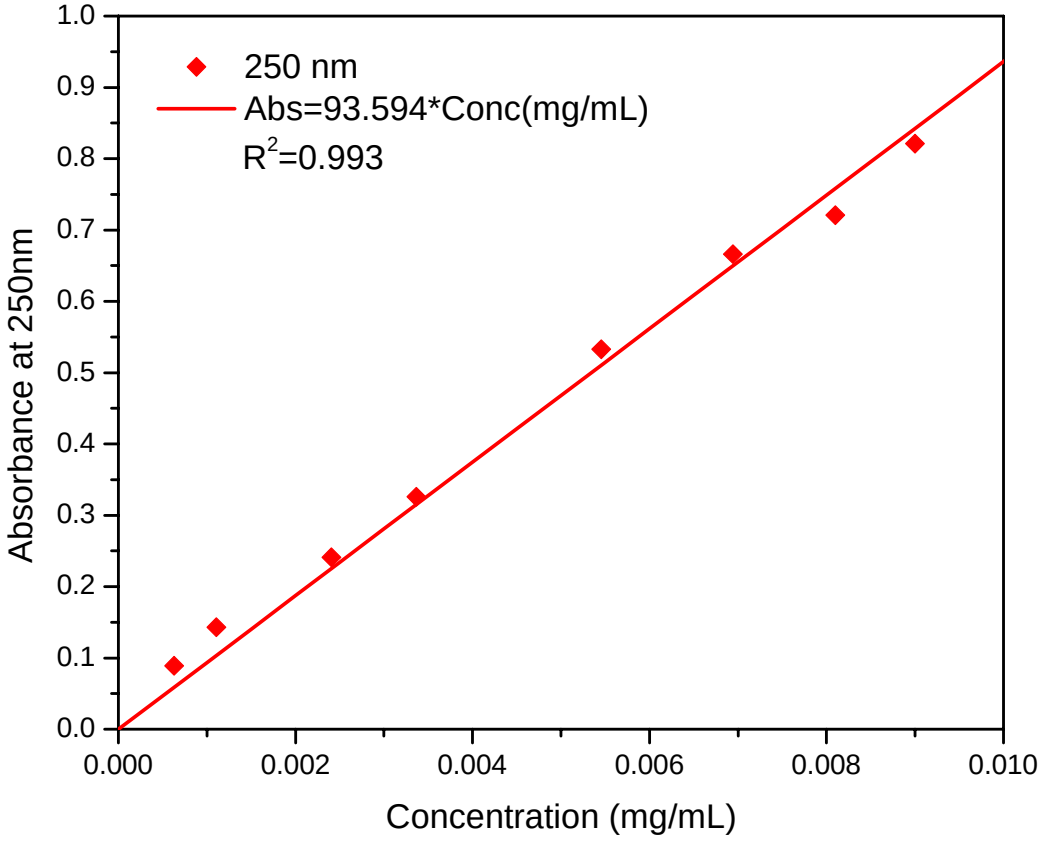

Figure 3.2 The Beers Law calibration curve for the acetaminophen in ethanol.

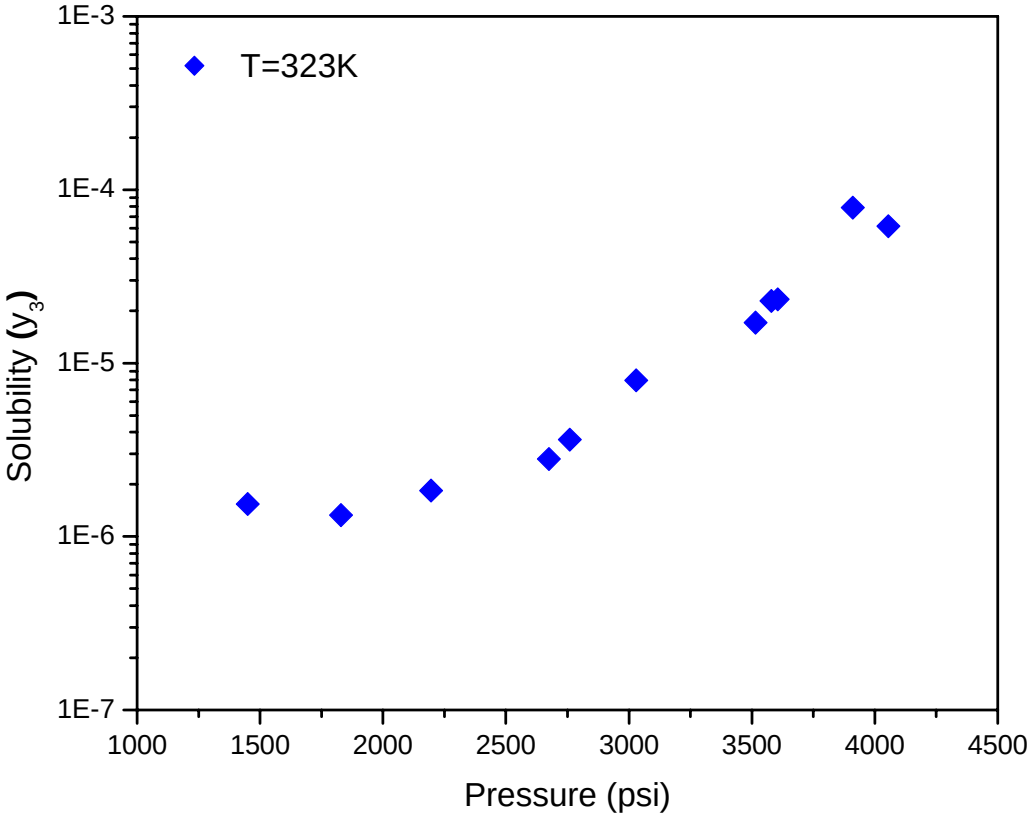

Figure 3.3 The solubility of (3) acetaminophen in (1) supercritical CO_2 at 323 K.

3.5 References

Lemmon, E. W., M.O. McLinden and D.G. Friend (2003). Thermophysical Properties of Fluid Systems" in NIST Chemistry WebBook, NIST Standard Reference Database Number 69, Eds. P.J. Linstrom and W.G. Mallard, National Institute of Standards and Technology, Gaithersburg MD, 20899 (http://webbook.nist.gov).

4.0 THERMODYNAMIC MODELING

4.1 Mathcad Phase Equilibrium Codes

4.1.1 Structure of Phase Equilibrium Codes and Required Inputs

To gain insight into the thermodynamics of GAS precipitation, a Mathcad code was developed to calculate the fluid phase compositions for solid-vapor-liquid equilibrium (SVLE). The Peng-Robinson equation of state (PREOS) is used to calculate the fugacity coefficients for the fluid phases, and an independent relationship is used to calculate the fugacity of the solid phase.

The PREOS, presented in detail in Section 2.2.3, has two parameters: a, a temperature dependent energy parameter, and b, a volume parameter. Calculation of the pure component parameters, a_i and b_i, requires the input of the critical temperature, T_{ci}, critical pressure, P_{ci}, and acentric factor, ω_i, for each component, i, all of which can be found in the DIPPR database (Rowley et al., 2002) for many common compounds. The physical property parameter values for components included in this study are listed in Table 4.1. Calculation of the mixture parameters, a and b, is done using quadratic mixing rules with binary interaction parameters, k_{ij} and l_{ij}, which must be regressed from experimental i-j data. The second binary interaction parameter, l_{ij}, was set to zero in this study to test the hypothesis that the solubility behavior of the binary systems can be adequately captured using only one interaction parameter.

Vapor-liquid equilibrium (VLE), solid-liquid equilibrium (SLE), and solid-vapor equilibrium (SVE) Mathcad codes were developed to regress the binary interaction parameters from solubility data for each of the three pairs that the ternary (1) CO_2 – (2)

ethanol – (3) acetaminophen system comprises. The k_{12} and k_{23} parameters for the pairs (1) CO_2 – (2) ethanol and (2) ethanol – (3) acetaminophen were regressed using solubility data from the literature (Sections 5.1.1 and 5.1.2), and the k_{13} parameter for the pair (1) CO_2 – (3) acetaminophen was regressed using solubility data measured in the present study (Section 5.2.2). The VLE, SLE, SVE, and SVLE Mathcad codes are provided in Appendix B.

4.1.1.1 *Vapor-Liquid Equilibrium Code*

As described in Section 2.2.3, for two-component binary phase equilibrium and three-component ternary phase equilibrium the entire system is specified when T and P are set. The simplest case to consider is (1) antisolvent – (2) solvent VLE, which has four unknowns: the equilibrium mole fractions of each component in the fluid phases. Equations 2-28, 2-29, 4-1, and 4-2 are the constraints. The structure of the VLE code is represented in a flowchart in Figure 4.2.

$$P \cdot y_1 \cdot \hat{\phi}_1^V(T,P,y) = P \cdot x_1 \cdot \hat{\phi}_1^L(T,P,x) \qquad \text{2-28}$$

$$P \cdot y_2 \cdot \hat{\phi}_2^V(T,P,y) = P \cdot x_2 \cdot \hat{\phi}_2^L(T,P,x) \qquad \text{2-29}$$

$$\sum_i x_i = 1 \qquad \text{4-1}$$

$$\sum_i y_i = 1 \qquad \text{4-2}$$

Equations 2-28, and 2-29 are non-linear in the equilibrium mole fractions, and an iterative process is employed to solve them.

In each of the four Mathcad codes the equilibrium fluid phase compositions are computed using a “while loop” function. For the VLE code, guesses must be input for the pure component vapor pressures at the equilibrium temperature, $P^{sat}(T)_i^{guess}$. Next, the pure

component form of the PREOS is used to calculate the vapor pressure of each component, $P_{sat}(T)_i$, using the input initial guesses as a starting point for the calculation. Recall that in the low pressure limit for simple systems iso-fugacity can be represented by Raoult's Law using Equation 2-11, where x_i is the mole fraction of component i in the liquid phase and y_i is the mole fraction of component i in the vapor phase.

$$x_i \cdot P_i^{sat}(T) = y_i \cdot P \qquad \text{2-11}$$

The partition coefficient, or volatility, K_i, is defined as the ratio of y_i to x_i, and is a measure of how each component "partitions" itself between the fluid phases at equilibrium,

$$K_i = \frac{y_i}{x_i} \qquad \text{4-1}$$

K values can be approximated from a rearrangement of Raoult's Law,

$$K_i = \frac{y_i}{x_i} = \frac{P_i^{sat}(T)}{P} \qquad \text{4-2}$$

Next, guesses for the equilibrium fluid phase mole fractions are calculated in terms of K values,

$$x_1 = \frac{K_2 - 1}{K_2 - K_1} \qquad \text{4-3}$$

$$y_1 = K_i \cdot x_1 \qquad \text{4-4}$$

$$x_2 = 1 - x_1 \qquad \text{4-5}$$

$$y_2 = 1 - y_1 \qquad \text{4-6}$$

Using the guesses for x_i and y_i, the fugacity coefficients for each component in both the vapor and liquid phases, $\hat{\phi}_i^V(T,P,y)$ and $\hat{\phi}_i^L(T,P,x)$, are calculated using the cubic roots of Equations 2-24 and 2-25 plugged into Equations 2-16 and 2-17,

$$\ln(\phi_i) = \frac{b_m}{b}\left(Z^V - 1\right) - \ln\left(Z^V - B\right) - \frac{A}{2\sqrt{2}B}\left[\frac{2\sum_{k=1}^{N} x_k a_{ki}}{a} - \frac{b_i}{b}\right]\ln\left[\frac{Z^V + 2.414B}{Z^V - 0.414B}\right] \qquad \text{2-16}$$

$$\ln(\phi_i) = \frac{b_m}{b}\left(Z^L - 1\right) - \ln\left(Z^L - B\right) - \frac{A}{2\sqrt{2}B}\left[\frac{2\sum_{k=1}^{N} x_k a_{ki}}{a} - \frac{b_i}{b}\right]\ln\left[\frac{Z^L + 2.414B}{Z^L - 0.414B}\right] \qquad \text{2-17}$$

$$\left(Z^V\right)^3 - (1-B)\left(Z^V\right)^2 + (A - 3B^2 - 2B)Z^V - (AB - B^2 - B^3) = 0 \qquad \text{2-24}$$

$$\left(Z^L\right)^3 - (1-B)\left(Z^L\right)^2 + (A - 3B^2 - 2B)Z^L - (AB - B^2 - B^3) = 0 \qquad \text{2-25}$$

New partition coefficients are calculated using Equation 4-7, a rearrangement of the iso-fugacity relationships in Equations 2-28 and 2-29,

$$K_i = \frac{y_i}{x_i} = \frac{\phi_i^L(T,P,x)}{\phi_i^V(T,P,y)} \qquad \text{4-7}$$

The differences between each of the original K_i values and the new K_i values are calculated. If any difference is larger than a specified tolerance, the "while loop" algorithm is repeated; if not, the function returns the calculated equilibrium compositions, x_i and y_i.

4.1.1.2 *Solid-Liquid Equilibrium and Solid-Vapor Equilibrium Codes*

As discussed in Section 2.2.3, an activity coefficient relationship is often used to calculate the fugacity of a solute dissolved in a liquid phase; however, it is necessary to consistently use the Peng-Robinson equation of state to calculate fugacities for the liquid

phase so that a k_{23} value regressed using the SLE code can be applied to the SVLE code. The (2) solvent – (3) solute SLE system has two unknowns: the equilibrium mole fractions of each component in the liquid phase, x_i. The constraints are Equations 2-30 and 4-1. The structure of the SLE code is represented in a flowchart in Figure 4.3.

$$P \cdot x_3 \cdot \hat{\phi}_3^L(T, P, x) = f_3^S \qquad \text{2-30}$$

The fugacity of the pure solid solute, f_3^S, is calculated using the following relationship (Prausnitz et al., 1999),

$$f_3^S = f_3^L(T, P_{tp}) \exp\left[\frac{\Delta H_{fus}}{R}\left(\frac{1}{T_{tp}} - \frac{1}{T}\right) + \frac{v_3^S(P - P_{tp})}{RT} - \frac{\Delta C_P}{R}\left(\ln\left(\frac{T_{tp}}{T}\right) - \frac{T_{tp}}{T} + 1\right)\right] \qquad \text{2-27}$$

The molar heat of fusion, ΔH_{fus}, molar volume, v_3^S, differential molar heat capacity, ΔC_p, triple point temperature, T_{tp}, and triple point pressure, P_{tp}, for the solid solute are required inputs for the SLE code, although, often the ΔC_p is neglected in phase equilibria calculations. For simple solids – for instance naphthalene and acetaminophen – these quantities can typically be found in the DIPPR database along with the critical properties. For most pharmaceuticals, nutraceuticals, and complex molecules physical property parameter values are unknown, and for modeling purposes these quantities must be measured experimentally or estimated using a group contribution method. The Ambrose method (Ambrose, 1980), the Joback and Reid method (Joback and Reid, 1987), and the Constantinou and Gani method (Constantinou and Gani, 1994) are all commonly used to estimate critical properties. The Han and Peng method (Han and Peng, 1993) is often used to calculate the acentric factor.

For the SLE code a guess for the mole fraction of the solute in the liquid phase is a required input parameter, and because the liquid phase mole fractions must sum to unity, a guess for the mole fraction of the solvent in the liquid phase is also specified automatically. The fugacity coefficient for the solute in the liquid phase is calculated using Equations 2-17 and 2-25, and then a new value of the liquid phase mole fraction of the solute is calculated,

$$x_3 = \frac{f_3^S(T,P)}{P \cdot \phi_3^L(T,P,x)} \qquad \text{4-8}$$

If the difference between the guess for x_3 and the x_3 calculated using Equation 4-8 is less than the tolerance, the liquid phase composition is returned as the output of the function; if not, the new calculated x_3 becomes the initial guess and the calculation is repeated.

The (1) antisolvent – solute SVE system has two unknowns: the equilibrium mole fractions of each component in the vapor phase, y_i. The constraints are Equations 2-31 and 4-1.

$$P \cdot y_3 \cdot \hat{\phi}_3^V(T,P,y) = f_3^S \qquad \text{2-31}$$

The structure of this code is precisely the same as the SLE code, which is represented in a flowchart in Figure 4.3. In the SVE case, an initial guess for the solubility of the solute in the vapor phase is a required input parameter. The fugacity coefficient of the solute in the vapor phase is calculated using Equations 2-17 and 2-25, and the fugacity of the solid solute is again calculated using Equation 2-27. The new mole fraction of the solute in the vapor phase is calculated using the following relationship,

$$y_3 = \frac{f_3^S(T,P)}{P \cdot \phi_3^V(T,P,y)} \qquad \text{4-9}$$

4.1.1.3 *Solid-Vapor-Liquid Equilibrium Code*

The (1) antisolvent – (2) solvent – (3) solute SVLE equilibrium system has six unknowns when the precipitated solute phase is assumed to be pure: the equilibrium mole fractions of each of the components in the fluid phases. Equations 2-28, 2-29, 2-30, 2-32, 4-1, and 4-2 are the constraints. The structure of the SVLE equilibrium code is represented in a flowchart in Figure 4.4.

$$P \cdot y_3 \cdot \hat{\phi}_3^V(T,P,y) = P \cdot x_3 \cdot \hat{\phi}_3^L(T,P,x) \qquad \text{2-32}$$

The fugacity of the solid solute in Equation 2-30 is calculated using Equation 2-27. For the SVLE code a guess for the solubility of the solute in the equilibrium liquid phase, x_3^{guess}, is a required input parameter.

The partition coefficients for each of the three components, K_i, are calculated using Equation 4-2. Initial guesses for the mole fractions of each component in the vapor and liquid phases are calculated in terms of the K_i values,

$$x_2 = \frac{1 + (K_1 - K_3) \cdot x_3 - K_1}{K_2 - K_1} \qquad \text{4-10}$$

$$x_1 = 1 - x_3 - x_2 \qquad \text{4-11}$$

$$y_i = K_i x_i \qquad \text{4-12}$$

New K_i values are calculated using the fugacity coefficients for each component in the vapor and liquid phases, as determined using Equations 2-16 and 2-17, in Equation 4-7. Then, a new value of the solubility of the solute in the liquid phase is calculated,

$$x_3 = \frac{f_3^S(T,P)}{P \cdot \phi_3^L(T,P,x)} \qquad \text{4-13}$$

If the difference between the new x_3 value and the initial guess is less than the tolerance, the equilibrium compositions of the vapor and liquid phases are returned; if not, the K_i values are used to calculate new guesses for the mole fractions and the calculations are repeated.

4.1.2 Verifying the Validity of Phase Equilibrium Codes with Published Solubility Data

To verify the validity of the Mathcad phase equilibrium codes, PREOS model fits to literature solubility data were reproduced using published binary interaction parameters. Ng and Robinson report compositions for the VLE system (1) CO_2 - (2) toluene at 311K as a function of pressure (Ng and Robinson, 1978), and binary interaction parameters for this pair, k_{12}=0.0900 and l_{12}=0.0000, were regressed by Dixon and Johnston (Dixon and Johnston, 1991). Bubble and dew point curves were generated for this system using the VLE Mathcad code (Figure 4.5). The model correctly captures the solubility behavior, indicating that the VLE code works.

Solubility data for the most widely studied supercritical fluid-solute pair, (1) CO_2 – (3) naphthalene, were used to test the SVE code. McHugh and Paulaitis report the solubility of naphthalene in CO_2 at 308K and 328K as a function of pressure (McHugh and Paulaitis, 1980), and binary interaction parameters for this pair, k_{13}=0.1001 and l_{13}=0.0000, were regressed by Garnier et al. (Garnier et al., 1999). As shown in Figure 4.6, the SVE code accurately predicts the naphthalene solubility in the supercritical phase at both temperatures, even predicting the crossover pressure, indicating that the SVE code works.

The structure of the SLE code is precisely the same as the structure of the SVE code. In both cases a fluid phase is in equilibrium with a pure solute phase, and verifying only the SVE code was considered adequate.

Dixon and Johnston measured the liquid phase composition of the three-component SVLE system (1) CO_2 – (2) toluene – (3) naphthalene at 298 K as a function of pressure (Dixon and Johnston, 1991). Kikic and coworkers fit these data with a model using the PREOS to represent the fluid phases (Kikic et al., 1997). For the (1) CO_2 – (2) toluene pair, Kikic et al. employed the binary interaction parameters k_{12}=0.0900 and l_{12}=0.0000, as regressed by Dixon and Johnston; for the (2) toluene – (3) naphthalene pair, they obtained adequate representation of the ternary data by setting both k_{23} and l_{23} to zero; for the (1) CO_2 - (3) naphthalene pair, they regressed k_{13}=0.0940 and l_{13}=-0.0240 from the liquid-phase composition data. As shown in Figure 4.7, the fits Kikic and coworkers achieved to the three-component composition data were satisfactorily reproduced, indicating that the SVLE codes works.

4.2 Sensitivity Analysis on Phase Equilibrium Codes: Methods Employed and Error Calculations

A parametric sensitivity analysis was performed on the two-component VLE, SLE, and SVE codes and on the three-component SVLE code to determine the relative importance of each binary interaction parameter to the models' solubility predictions. The hypothesis that adequate representation of binary and ternary composition data is obtained by regressing only a single binary interaction parameter, k_{ij}, for each pair of components was tested. Additionally, the effect of altering the ΔH_{fus}, T_c, and P_c of the solute compound on the shape of the SVE model's solubility prediction curves was examined.

Because the phase equilibrium codes return solubility predictions for an input temperature and pressure, the sensitivity analysis involved comparing average errors in

predicted compositions for incremental changes in binary interaction parameter values. The regressed binary interaction parameter for each pair of components, k_{ij}, corresponds to a minimum absolute root-mean-square (RMS) deviation in the solubility prediction when the second binary interaction parameter, l_{ij}, is set to zero.

$$RMS = \sum_{i=1}^{N} \frac{1}{N} \left(x_{\exp_i} - x_{calc_i} \right)^2 \tag{4-14}$$

For the binary systems, two sets of average errors were calculated – one with the experimental solubility values as the base case and another with model-predicted solubility values, when k_{ij} was set at its regressed value, as the base case. The former provides an indication of the magnitude of the error in the fit to experimental data and quantifies the effect of altering the model parameter values on the goodness-of-fit; the latter provides an indication of how sensitive, on average, the model's solubility predictions are to each binary interaction parameter.

Because solubility data are not currently available for the ternary system, only the error incurred using the model's prediction of the composition with all three regressed binary interaction parameters as the base case was calculated. Only the solubilities of CO_2 and acetaminophen in the vapor and liquid phases are considered in the analysis. Both the RMS error and the average absolute relative deviation (AARD) of the solubility predictions were calculated when each k_{ij} was individually increased and decreased by 10% of its regressed value and all other parameters were held at their regressed values.

$$RMS = \sum_{i=1}^{N} \frac{1}{N} \left(x_{base_i} - x_{change_i} \right)^2 \tag{4-15}$$

$$AARD = \sum_{i=1}^{N} \frac{1}{N} \left| \frac{x_{base_i} - x_{change_i}}{x_{base_i}} \right| \cdot 100\% \tag{4-16}$$

The error incurred when each l_{ij} was individually increased and decreased by 10% of the corresponding regressed k_{ij} parameter value was calculated to determine if the model predictions are more sensitive to changes in k_{ij} or l_{ij} values.

The ΔH_{fus}, T_c, and P_c of the solute were individually increased and decreased by 10% of the parameter value to determine the effect of altering each parameter on the shape of the SVE model's solubility curve predictions. These parameter values are typically estimated for complex pharmaceutical molecules, and thus errors in these parameter values could contribute to poor model fits to SVE solubility data.

Table 4.1 Physical property parameter values. Unless otherwise indicated, all values were taken from the DIPPR Database (Rowley et al., 2002).

	CO_2	Ethanol	Toluene	Acetaminophen	Naphthalene	Resveratrol
MW	44.01	46.07	92.14	151.16	128.17	228.20[a]
T_c (K)	304	514	592	736	748	894[b]
P_c (bar)	73.83	61.37	41.08	42.60	40.50	51.40[b]
ω	0.225	0.644	0.264	0.800	0.302	0.961[c]
T_m (K)	-----	-----	-----	441	353	539[a]
T_{tp} (K)[d]	-----	-----	-----	441	353	539
P_{tp} (bar)	-----	-----	-----	0.0484	0.00991	unknown
ΔH_{fus} (J/mol)	-----	-----	-----	27,000	18,980	unknown
v_s (l/mol)	-----	-----	-----	0.117	0.112	unknown
ΔC_p (J/mol K)	-----	-----	-----	99.8[e]	53.7[f]	unknown

[a] Taken from MSDS, http://www.caymanchem.com
[b] (Berna et al., 2001) approximated by authors using Ambrose Method (Ambrose, 1980)
[c] (Berna et al., 2001) approximated by authors using Han and Peng Method (Han and Peng, 1993)
[d] Approximated as the normal melting temperature
[e] (Neau et al., 1997)
[f] Estimated as the ΔS_{fus} of naphthalene, taken from http://webbook.nist.gov (Syunyarv et al., 1984)

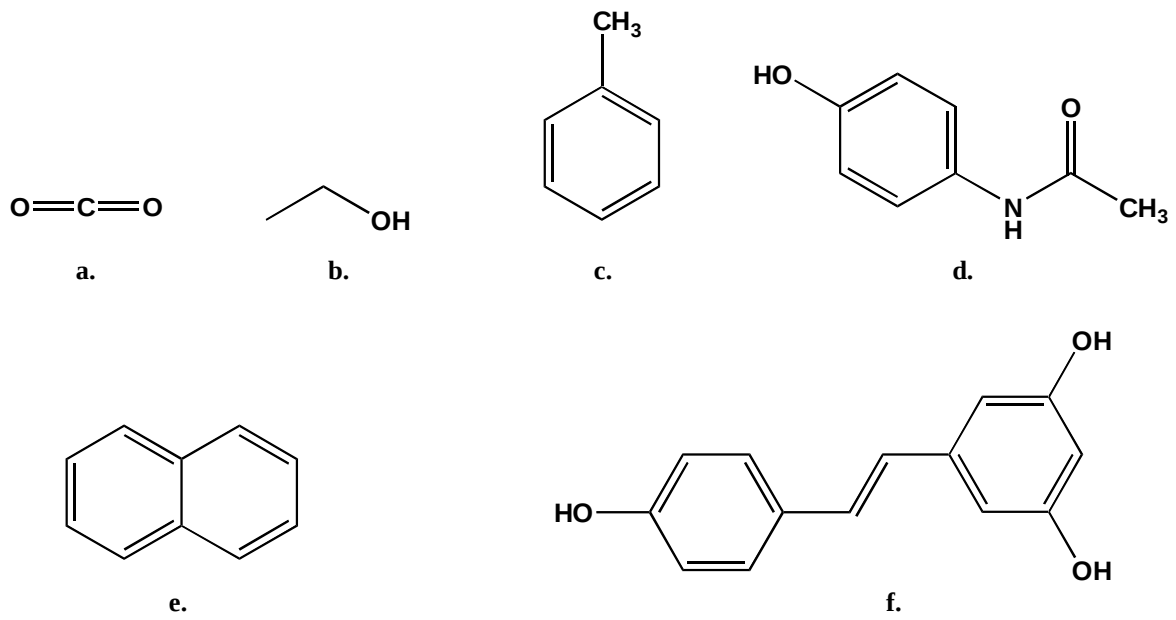

Figure 4.1 The molecular structures of (a) CO_2, (b) ethanol, (c) toluene, (d) acetaminophen, (e) naphthalene, and (f) resveratrol.

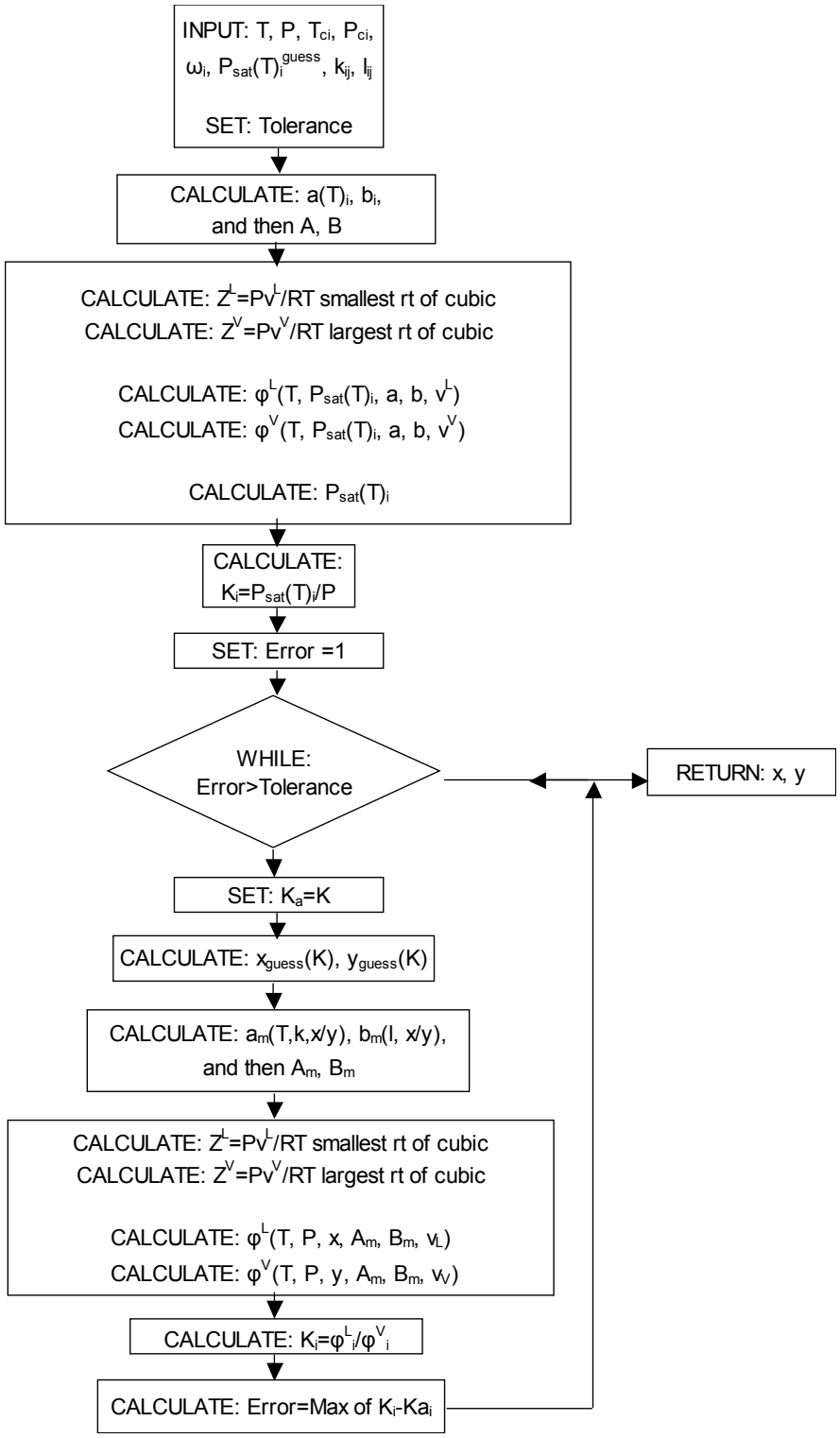

Figure 4.2 A flowchart showing required inputs, calculation steps, and outputs for the VLE Mathcad code listed in Section B.1 of Appendix B.

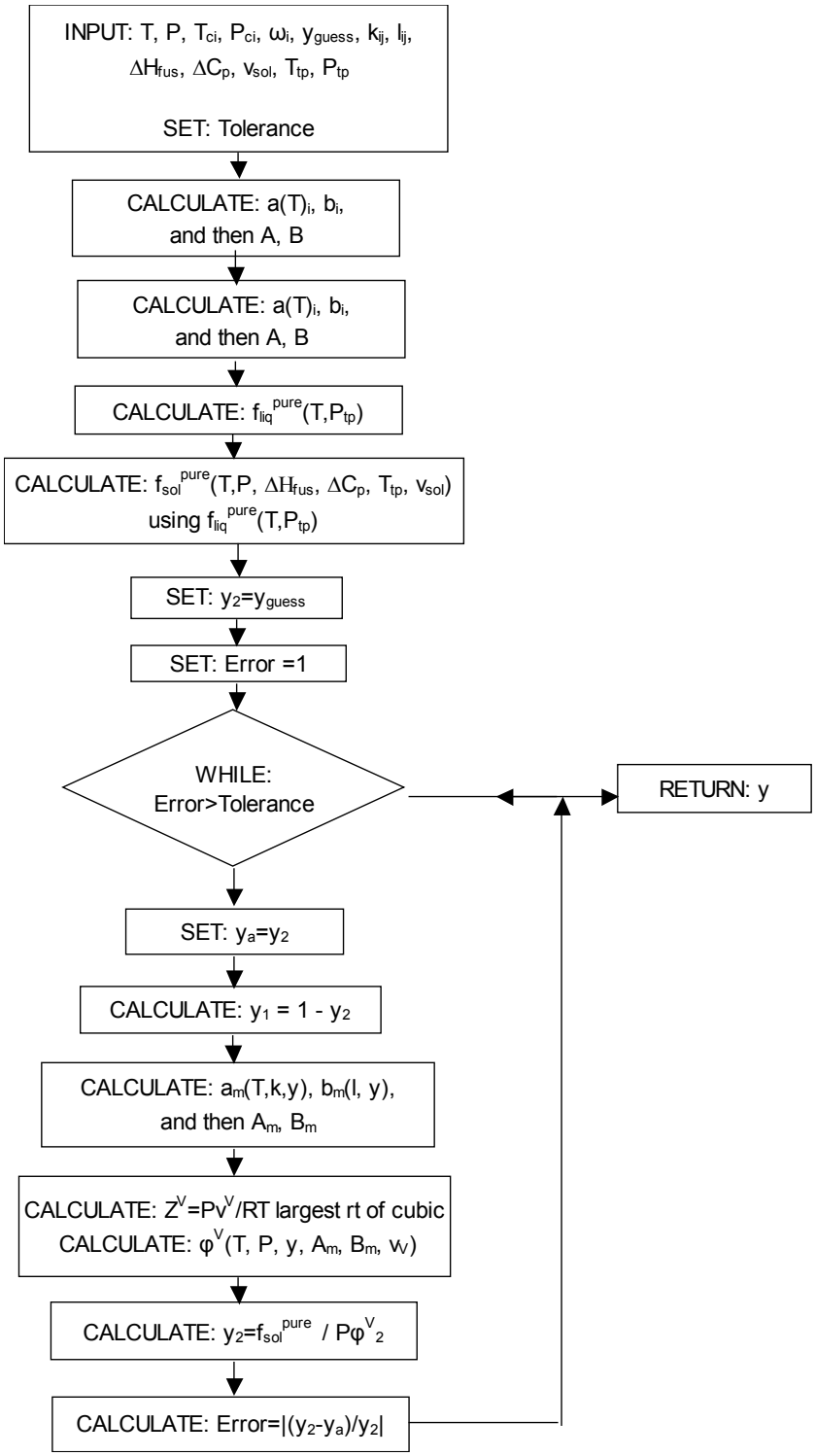

Figure 4.3 A flowchart showing required inputs, calculation steps, and outputs for the SLE and SVE Mathcad codes in Sections B.2 and B.3 of Appendix B.

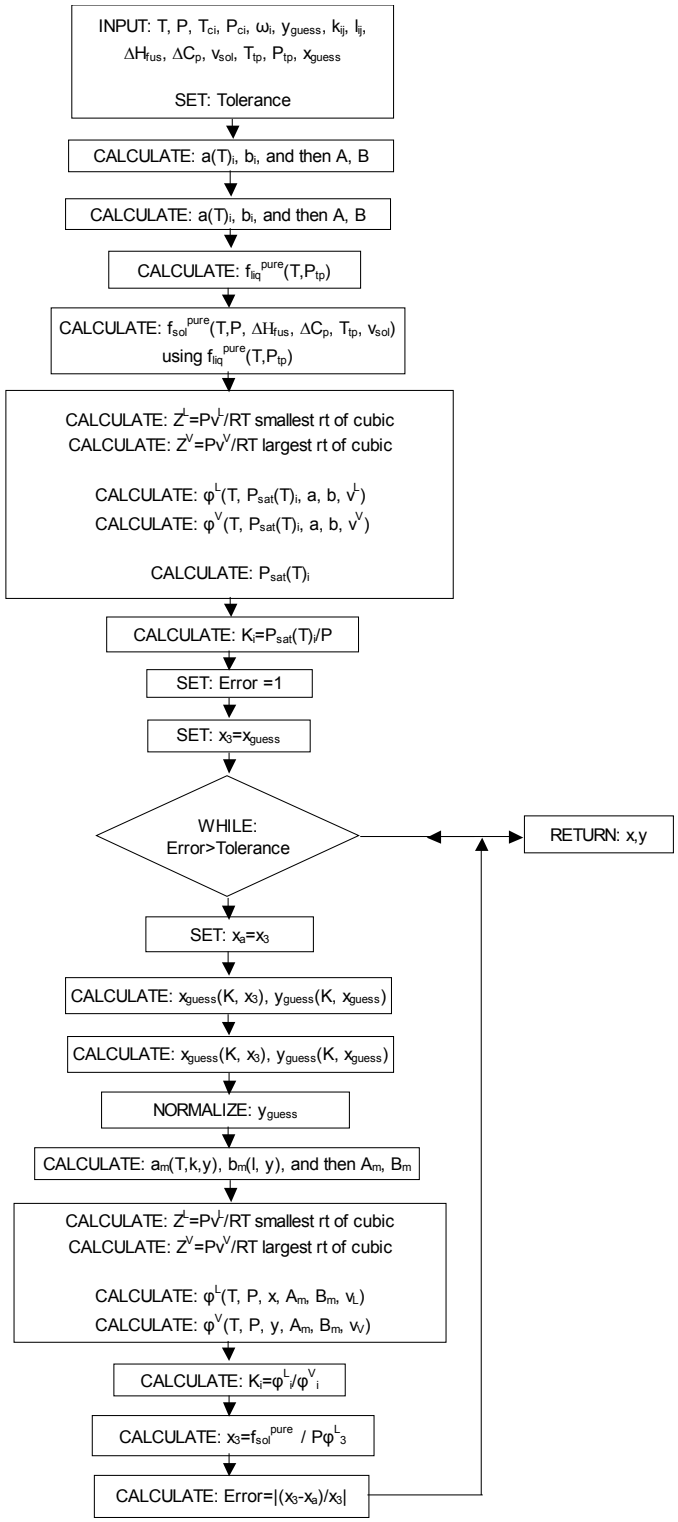

Figure 4.4 A flowchart showing required inputs, calculation steps, and outputs for the SVLE Mathcad code listed in Section B.4 of Appendix B.

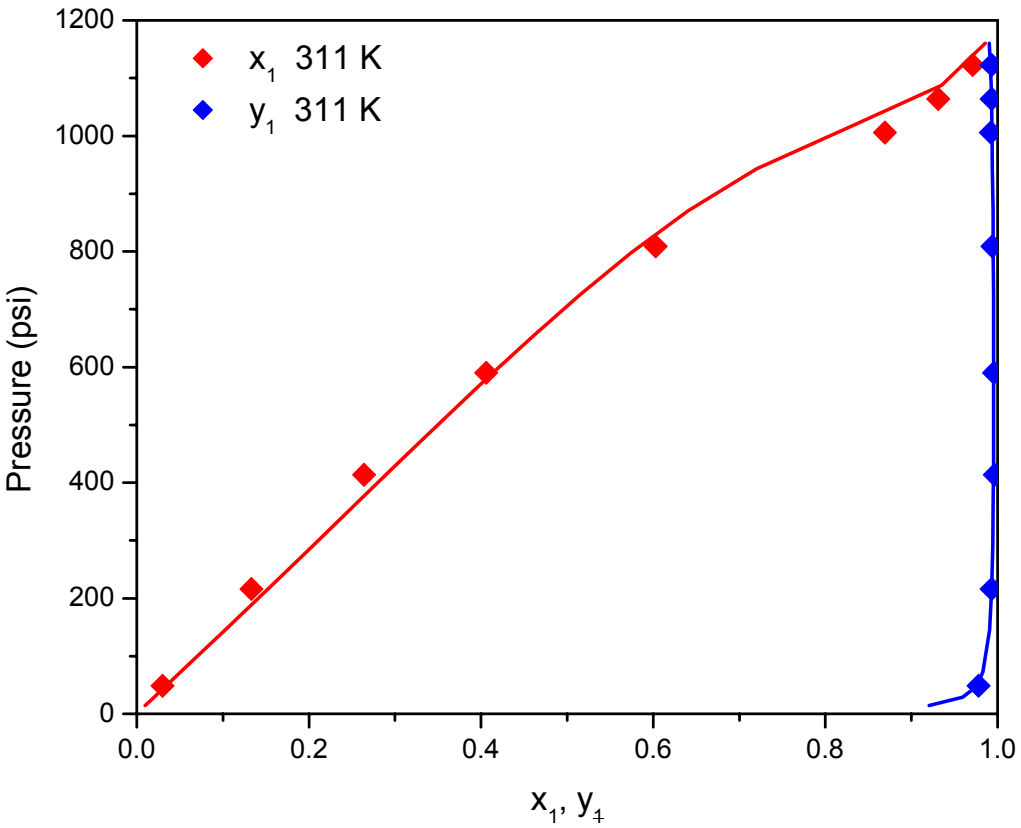

Figure 4.5 The solubility of (1) CO_2 in (2) toluene at 311 K (Ng and Robinson, 1978), shown with the VLE model fit using k_{12}=0.0900 (Dixon and Johnston, 1991).

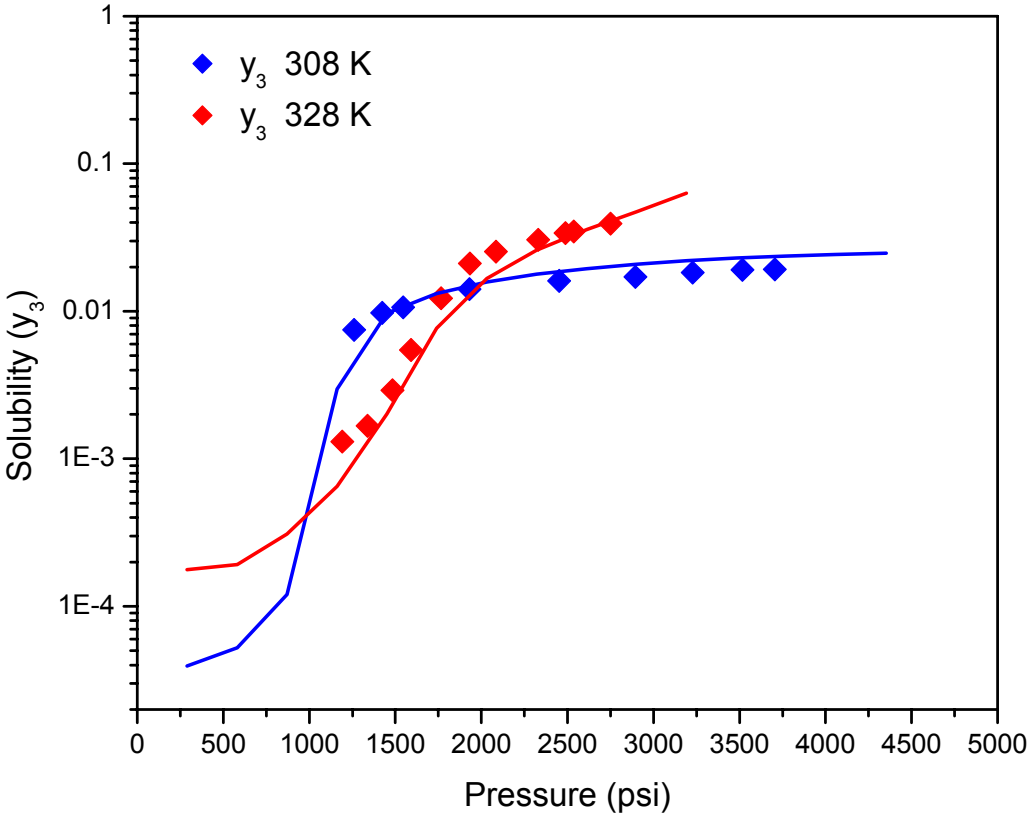

Figure 4.6 The solubility of (3) naphthalene in (1) CO_2 at 308 K and 328 K (McHugh and Paulaitis, 1980), shown with the SVE model fits using k_{13}=0.1001 (Garnier et al., 1999).

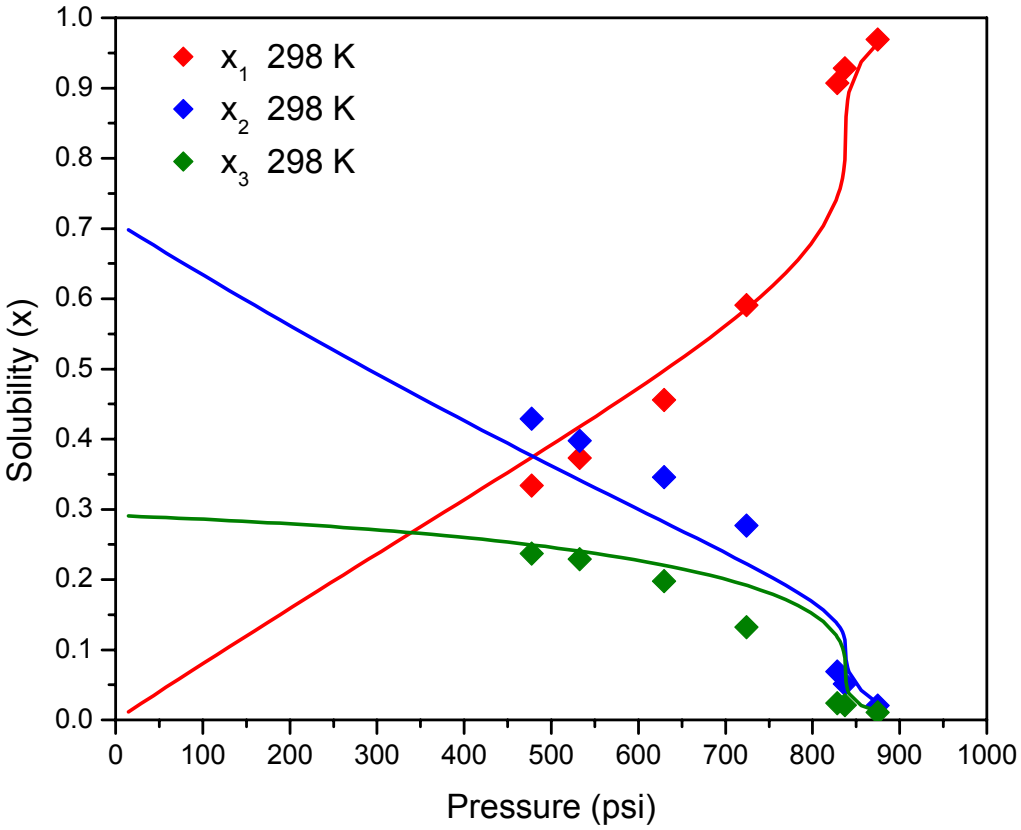

Figure 4.7 The liquid phase composition of the system (1) CO_2 – (2) toluene – (3) naphthalene at 298 K (Dixon and Johnston, 1991), shown with the SVLE model fit using the following binary interaction parameter values: k_{12}=0.0900 and l_{12}=0.0000; k_{23}=0.0000 and l_{23}=0.0000; k_{13}=0.0940 and l_{13}=-0.0240 (Kikic et al., 1997).

4.3 References

Ambrose, D. (1980). Vapor-Liquid Critical Properties, NPL Rep. Chem. 107, National Physical Laboratory, Teddington.

Berna, A., A. Chafer and J. B. Monton (2001). "High-pressure solubility data of the system resveratrol (3) plus ethanol (2) plus CO2 (1)." Journal of Supercritical Fluids **19**(2): 133-139.

Constantinou, L. and R. Gani (1994). "New Group-Contribution Method for Estimating Properties of Pure Compounds." Aiche Journal **40**(10): 1697-1710.

Dixon, D. J. and K. P. Johnston (1991). "Molecular Thermodynamics of Solubilities in Gas Antisolvent Crystallization." Aiche Journal **37**(10): 1441-1449.

Garnier, S., E. Neau, P. Alessi, A. Cortesi and I. Kikic (1999). "Modelling solubility of solids in supercritical fluids using fusion properties." Fluid Phase Equilibria **160**: 491-500.

Han, B. X. and D. Y. Peng (1993). "A Group-Contribution Correlation for Predicting the Acentric Factors of Organic-Compounds." Canadian Journal of Chemical Engineering **71**(2): 332-334.

Joback, K. G. and R. C. Reid (1987). "Estimation of Pure-Component Properties from Group-Contributions." Chemical Engineering Communications **57**(1-6): 233-243.

Kikic, I., M. Lora and A. Bertucco (1997). "A thermodynamic analysis of three-phase equilibria in binary and ternary systems for applications in rapid expansion of a supercritical solution (RESS), particles from gas-saturated solutions (PGSS), and supercritical antisolvent (SAS)." Industrial & Engineering Chemistry Research **36**(12): 5507-5515.

McHugh, M. and M. E. Paulaitis (1980). "Solid Solubilities of Naphthalene and Biphenyl in Supercritical Carbon-Dioxide." Journal of Chemical and Engineering Data **25**(4): 326-329.

Neau, S. H., S. V. Bhandarkar and E. W. Hellmuth (1997). "Differential molar heat capacities to test ideal solubility estimations." Pharmaceutical Research **14**(5): 601-605.

Ng, H. J. and D. B. Robinson (1978). "Equilibrium Phase Properties of Toluene-Carbon Dioxide System." Journal of Chemical and Engineering Data **23**(4): 325-327.

Prausnitz, J. M., R. N. Lichtenthaler and E. G. d. Azevedo (1999). Molecular Thermodynamics of Fluid Phase Equilibria. Upper Saddle River, NJ, Prentice Hall.

Rowley, R. L., W. V. Wilding, J. L. Oscarson, N. A. Zundel, T. L. Marshall, T. E. Daubert and R. P. Danner (2002). DIPPR Data Compilation of Pure Component Properties. New York, Design Institute for Physical Properties, AIChE.

Syunyarv, Z. I., B. P. Tumanyan, S. I. Kolesnikov and N. I. Zhokhova (1984). "Some anomalies in melting points of binary mixtures of solid hydrocarbons." Zhurnal prikladnoi khimii (Leningrad, R.S.F.S.R.) **57**: 666-669.

5.0 RESULTS AND DISCUSSION

5.1 Fitting Binary Interaction Parameters for CO_2-Ethanol and Ethanol-Acetaminophen Pairs

5.1.1 Modeling the Solubility of CO_2 in Ethanol at 298 K

Kordikowski and coworkers measured bubble point values for the VLE system CO_2-ethanol at 298 K as a function of pressure. They obtained a good fit to their solubility data using the PREOS with k_{12}=0.0890 and l_{12}=0.0000 (Kordikowski et al., 1995), but in the present study, k_{12}=0.1045 was regressed for the same data set using the VLE PREOS model. The apparent discrepancy is due to a difference in the objective functions that were minimized to determine the binary interaction parameters. The value k_{ij}=0.0890 corresponds to a minimum in the root-mean-squared (RMS) error between the predicted and experimentally measured liquid phase CO_2 mole fractions (Equation 4-14), while k_{ij}=0.0890 corresponds to a minimum in the absolute average deviation (AAD) error between the predicted and experimentally measured vapor pressures (Equation 5-1).

$$RMS = \sum_{i=1}^{N} \frac{1}{N} \left(x_{1\exp_i} - x_{1calc_i} \right)^2 \qquad \text{4-14}$$

$$AAD = \sum_{i=1}^{N} \frac{1}{N} \left| P^{sat}{}_{\exp_i} - P^{sat}{}_{calc_i} \right| \cdot 100\% \qquad \text{5-1}$$

In the present study, the RMS error in solubility is used as the objective function due to the structure of the Mathcad codes, which require the equilibrium temperature and pressure of the mixture as inputs and return the compositions of the vapor and liquid phases. Because k_{12}=0.0890 is widely used in the literature, this value is retained for the CO_2-ethanol pair in the remainder of this study. Figure 5.1 shows Kordikowski's bubble point data at 298K

along with the PREOS model predictions for the bubble and dew point curves when k_{12}=0.0890. The PREOS satisfactorily captures the solubility behavior of this system.

5.1.2 Modeling the Solubility of Acetaminophen in Ethanol at 1 atm

For SLE the fugacity of the pure solid solute was calculated using the following relationship,

$$f_3^S = f_3^L\left(T, P_{tp}\right)\exp\left[\frac{\Delta H_{fus}}{R}\left(\frac{1}{T_{tp}} - \frac{1}{T}\right) + \frac{v_3^S\left(P - P_{tp}\right)}{RT} - \frac{\Delta C_P}{R}\left(\ln\left(\frac{T_{tp}}{T}\right) - \frac{T_{tp}}{T} + 1\right)\right] \quad \text{2-27}$$

At the high pressures required for supercritical fluid extraction, the molar differential heat capacity term is very small compared to the first two terms in the exponential, and is typically neglected in phase equilibrium calculations, however, for low pressure solubility calculations, the contribution can be significant. Unfortunately, the value of the molar differential heat capacity is not available for most solid compounds. The solute's molar entropy of fusion, ΔS_{fus}, is often used as an approximation for ΔC_p. At the melting point ΔS_{fus} can be calculated as the molar heat of fusion, ΔH_{fus}, divided by the melting temperature, T_m. Depending on the solute, using ΔS_{fus} or setting ΔC_p to zero may provide an adequate fit to the solubility data (Neau et al., 1997). Neau and coworkers determined the ΔC_p for acetaminophen, 99.8 J/mol K, by extrapolating the measured molar heat capacities of liquid acetaminophen and solid acetaminophen to the melting temperature and then taking the difference (Figure 5.2).

Granberg and Rasmusson measured the solubility of acetaminophen in pure ethanol at 1 atm as a function of temperature (Granberg and Rasmuson, 1999). The dashed line in Figure 5.3 represents the best SLE model fit to their data using the truncated form of

Equation 2-27, and the solid line represents the best SLE model fit to their data when the ΔC_p term is included. Clearly, the latter case provides a better representation of the data. This result is consistent with several reports in the literature in which the contribution of ΔC_p to the calculated activity of acetaminophen was found to be significant (Neau et al., 1997; Gracin et al., 2002). The value of the binary interaction parameter corresponding to a minimum in the RMS error for the solubility prediction is k_{23}=0.0099.

5.2 Static Equilibrium Solubility of Acetaminophen in Supercritical CO_2

5.2.1 Experimental Solubility at 323 K

Static equilibrium experiments were performed using the apparatus shown in Figure 3.1 to determine the solubility of acetaminophen in supercritical CO_2 at 323 K as a function of pressure. Over the pressure range 1500 psi – 4000 psi the equilibrium mole fraction of acetaminophen in the vapor phase ranged over 2 orders of magnitude, from 10^{-6}-10^{-4}, with solubility generally increasing with pressure (Table 3.1). As expected, due to the polar nature of the solute molecule, acetaminophen is sparingly soluble in supercritical CO_2. In contrast, the solubilities of several non-polar low vapor pressure solutes such as naphthalene and biphenyl in supercritical CO_2 are as high as 10^{-3} – 10^{-1} mole fraction (McHugh and Paulaitis, 1980).

Bristow and coworkers measured the solubility of acetaminophen in pure and modified CO_2 at 313K and 353K over the pressure range 1100 psi to 4000 psi using a dynamic through-flow extraction system (Bristow et al., 2001). Their solubility data for acetaminophen in pure CO_2 and the results from the present study are shown in Figure 5.4.

The current results fall within the range of Bristow's data, however, the solubilities are significantly higher than one would expect to achieve by interpolating between their data sets. The lower acetaminophen concentrations measured by Bristow may indicate that they were unable to measure true equilibrium solubility values with their dynamic solubility apparatus. They acknowledge that for the extraction of acetaminophen into ethanol-modified CO_2, the solubilities they obtained using their dynamic through-flow extraction system are significantly lower than the solubilities they obtained using a static recirculation system.

5.2.2 Correlation of Experimental Solubility Data

The acetaminophen solubility data were correlated using the SVE PREOS model to fit the binary interaction parameter for the CO_2-acetaminophen pair. A minimum in the RMS error between the calculated and predicted solubilities corresponds to k_{13}=0.2614. As shown in Figure 5.5, this model fit does not provide a good representation of the solubility data. While the solubility of many non-polar, low vapor pressure organic solids in supercritical CO_2 has been adequately represented using this method (Schmitt and Reid, 1986), other researchers have similarly had trouble representing the solubility of polar drug substances (Weinstein et al., 2004). The PREOS model captures the general trend of the data – increasing solubility with increasing pressure – but the model under-predicts the solubility across most of the pressure range of interest, save the highest pressures, where it over-predicts the solubility.

The shape of the solubility data appears curious at first glance (especially when viewed against the solubility curve predicted using the PREOS model); however, a cursory

review of the available literature related to the solubility of drug compounds in supercritical CO_2 indicates that the data exhibit the expected trend with pressure for polar drug compounds (Yamini et al., 2001; Asghari-Khiavi and Yamini, 2003; Duarte et al., 2004). Weinstein et al. studied the equilibrium solubility of three anti-inflammatory drugs in liquid and supercritical CO_2 at 298 K, 308 K, and 318 K, over the pressure range 1015 psi to 4050 psi using a static equilibrium apparatus (Weinstein et al., 2004). The solubility curve for benzocaine in CO_2 at 318K is the same shape as the curve for acetaminophen in CO_2 at 323K, and the data are on the same order of magnitude. As shown in Figure 5.6, the solubility curve for lidocaine in CO_2 at 318 K has the same characteristic shape as acetaminophen and benzocaine, but the solubility is much higher. Weinstein and coworkers were unsuccessful in their attempt to fit their data using a PREOS model.

Coutsikos and coworkers examined the ability of a modified PREOS model to predict the solubility behavior of solid-supercritical fluid binary systems and also ternary systems that include modifiers (Coutsikos et al., 2003). They obtained adequate predictions for the solubilities of aromatic hydrocarbons, aliphatic acids, and some alcohols in CO_2. Their predictions were poor for complex solids, including naproxen and cholesterol. The authors note the problem of possible errors in the predicted values of critical properties of compounds, which are input variables for all cubic equations of state. For complex solids these quantities often have not or cannot be measured, and values calculated using common estimation methods can yield large errors (Macnaughton et al., 1996). Coutsikos and coworkers acknowledge that this may have an effect on predicted solubilities.

The effect of individually increasing and decreasing ΔH_{fus}, P_c, and T_c for acetaminophen by 10% of the parameter value on the SVE model's solubility prediction was examined. As shown in Figure 5.7, across the entire pressure range the predicted solubility is increased when ΔH_{fus} is decreased by 10% of its value, and the predicted solubility is decreased when ΔH_{fus} is increased by 10% of its value; however, the shape of the prediction curve remains unchanged in both cases, and the data are no better represented. As shown in Figure 5.8, altering P_c by 10% has a negligible effect on the SVE model's solubility prediction, but the predictions are much more sensitive to changes in T_c. Increasing T_c by 10% decreases the predicted solubilities significantly across the entire pressure range, while decreasing T_c by 10% increases the predicted solubilities. Altering the critical property parameter values does not change the general shape of the curve. The curve is not shifted to the right, and the altered parameters do not provide a better fit to the solubility data for the (1) CO_2 – (3) acetaminophen system. Using an empirical equation to fit the experimental solubility data in many cases eliminates the need for physical property parameter data for the solid solute. This is a common approach in the literature to effectively capture the solubility behavior of drug compounds and other complex molecules in supercritical CO_2 (Chrastil, 1982; Garmroodi et al., 2004), but it cannot be predictive.

The empirical density-based relationship suggested by Weinstein and coworkers (Weinstein et al., 2004) was employed to model the CO_2-acetaminophen solubility data. First, the natural log of the enhancement factor was plotted versus the density of the supercritical fluid phase (approximated as the density of pure supercritical CO_2 at 323 K and

the pressure of the data point), as shown in Figure 5.9. The enhancement factor, *E*, is the ratio of the experimental solubility to the solubility in an ideal gas,

$$E = \frac{y_3 \cdot P}{P_{subl_3}} \qquad 5\text{-}2$$

The sublimation pressure of the solid solute, P_{subl3}, was approximated using a modified Clausius-Clapeyron equation,

$$\ln\left(P_{subl_3}\right) = \frac{T_b}{T_c} \cdot \ln\left(P_c\right) \cdot \frac{\left(1 - \frac{T_c}{T}\right)}{\left(1 - \frac{T_b}{T_c}\right)} \qquad 5\text{-}3$$

The dashed blue line in Figure 5.9 is the best-fit linear regression of the data set, and the solid blue line is the regression of the data set when the two lowest density data points are omitted. The regressed parameters in Equation 5-4 were used to fit the solubility as a function of density (Equation 5-5) for each of the two cases.

$$\ln\left(E\right) = A + c\rho_1 \qquad 5\text{-}4$$

$$y_3 = \frac{P_{subl_3}}{P} \cdot \exp\left(A + c\rho_1\right) \qquad 5\text{-}5$$

The dashed line in Figure 5.10 represents the exponential solubility predictions based on the parameters fit for the entire data set, and the solid line represents the exponential solubility predictions based on the parameters fit when the two lowest density data points were omitted. The latter case provides a better fit to the data. The corresponding *AARD* for this fit, calculated using Equation 5-6, is 46.64%, compared to the *AARD* of 341.94% for the fit obtained using the PREOS model.

$$AARD = \sum_{i=1}^{N} \frac{1}{N} \left| \frac{y_{\exp_i} - y_{calc_i}}{y_{\exp_i}} \right| \cdot 100\% \qquad 5\text{-}6$$

Based on the shape of the solubility data as a function of density, an empirical polynomial fit was applied to the data set,

$$\ln(E) = A + B\rho_1 + C\rho_1^{\ 2} \qquad 5\text{-}7$$

$$y_3 = \frac{P_{subl_3}}{P} \cdot \exp\left(A + B\rho_1 + C\rho_1^{\ 2}\right) \qquad 5\text{-}8$$

The solid line in Figure 5.11 is a quadratic regression to the data (Equation 5-7), and the exponential prediction for the solubility based on using parameters from the regressed polynomial fit is the solid line shown in Figure 5.12 (Equation 5-8). The *AARD* for this fit is 31.05%, slightly better than the empirical linear fit to the data.

While it is clear that the solubility of acetaminophen in CO_2 cannot be represented using the PREOS, the SVLE model employs this relationship to represent the fugacity of the two fluid phases. Accordingly, the regressed k_{13}=0.2614 was still used to make predictions about the CO_2-ethanol-acetaminophen system.

5.3 Prediction of Three-Component Ternary Phase Behavior of the System CO_2-Ethanol-Acetaminophen

In the GAS process an antisolvent is dissolved into a solute solution by increasing the system pressure, which leads to a volumetric expansion of the liquid phase. The result is a reduction in solvent power, which causes the pure solute to precipitate. At the point of precipitation, SVLE occurs. The solute is the focus when GAS precipitation is used to form pharmaceutical particles, and it is important to know how a given solute partitions between

the equilibrium phases as a function of temperature and pressure in order to design an efficient separation scheme. The solubility of acetaminophen in CO_2-expanded ethanol, x_3, and in the CO_2-rich vapor phase, y_3, was predicted using the SVLE PREOS model.

5.3.1 Solubility of Acetaminophen in Gas-Expanded Liquid Phase as a Function of Pressure at Different Temperatures

The solubility predictions for acetaminophen in CO_2-exanded ethanol as a function of pressure at temperatures 293 K to 303 K are shown in Figure 5.13. As expected, at a given temperature x_3 decreases with increasing pressure. In practice, this decrease in equilibrium solubility as a function of pressure leads to supersaturation of a solute solution when the solution is pressurized from 1 atm, the driving force for GAS precipitation. At a given pressure, x_3 increases with temperature. This was true of the solubility of acetaminophen in ethanol at 1 atm (Figure 5.3), and the predictions indicate that the trend continues across the entire pressure range of interest. Dense gases are more soluble in liquids at lower temperatures, and so a higher pressure is required at elevated temperatures to achieve a given liquid phase mole fraction of CO_2, x_1. The pressure and temperature trends exhibited by these predicted solubility curves are consistent with those seen for the liquid phase solute mole fractions measured by Liu and coworkers for the system CO_2-ethyl acetate-o-hydroxybenzoic acid (Liu et al., 2000), as shown in Figure 5.14.

The shape of the x_3 curve for the system CO_2-ethanol-acetaminophen (Figure 5.13) is the same as the shape of the solubility data for the system CO_2-ethyl acetate-o-hydroxybenzoic acid (Figure 5.14) – an almost linear decrease in solubility at a given temperature with increasing pressure; however, this is quite different than the shape of the liquid phase solubility curve for the system CO_2-toluene-naphthalene (Figure 4.7). The

SVLE model predictions for x_3 for the acetaminophen and naphthalene systems as a function of pressure and temperature are contrasted in Figure 5.15. The trend with temperature for the two systems is the same: at a given pressure, the solubility increases with increasing temperature. Acetaminophen is only sparingly soluble in CO_2 (Figure 3.3), and so the CO_2 acts as an antisolvent across the entire pressure range. In contrast, naphthalene is much more soluble in CO_2 (Figure 4.6), and so the CO_2 acts as a cosolvent at low and moderate pressures; at higher pressures a sudden drop-off in solubility is observed. The latter case is advantageous in processing, as a large change in solubility can be effected through a small change in pressure. This can result in recompression cost savings.

Several authors have found that in a simple three-component GAS precipitation system a solute will usually precipitate at similar x_1 values, regardless of the temperature (Kikic et al., 1997; Thiering et al., 2000). This is not surprising because the volume expansion curves for an antisolvent-solvent pair at different temperatures will often coincide when plotted against x_1 (Kordikowski et al., 1995). Figure 5.16 shows the predicted acetaminophen solubility in the liquid phase plotted against the CO_2 solubility in the liquid phase. The solubility curves shown in this way now partly collapse on each other. At low pressures, the effect is less pronounced, and acetaminophen is still more soluble at higher temperatures for a given x_1, presumably due to the higher sublimation pressure of the solute. Similar results were calculated by Kikic and coworkers for the system CO_2-toluene-naphthalene (Kikic et al., 1997).

At all temperatures examined, a significant change in the equilibrium solute solubility is effected over the pressure range of interest, indicating that GAS precipitation

should be considered a viable means to precipitate acetaminophen from CO_2-expanded ethanol for purification or for forming particles with specific characteristics.

5.3.2 Solubility of Acetaminophen in the Vapor Phase

In GAS precipitation, it is desirable for the solute of interest to be very soluble in the solvent-rich phase, but insoluble in the antisolvent-rich phase, to facilitate an efficient separation. Predictions for the solubility of acetaminophen in the CO_2-rich vapor phase as a function of temperature and pressure are shown in Figure 5.17. At a given pressure y_3 increases with temperature, due in part to the rise in sublimation pressure with increasing temperature. At higher temperatures the vapor pressure of ethanol is also higher, causing more ethanol to partition into the vapor phase. This has the effect of *modifying* the CO_2-rich vapor phase, making the polar acetaminophen more soluble.

At a given temperature y_3 decreases slightly at low pressures, levels out over much of the pressure range of interest, and finally increases sharply approaching the critical pressure of CO_2. At the pressure where y_3 begins to increase, the majority of the acetaminophen has already precipitated out of solution; therefore, it is not necessary to go to pressures any higher than this before filtering the solids. Although some product may be lost, the vapor phase mole fraction of acetaminophen, ranging from 5.0^{-8} - 4.5^{-7}, is orders of magnitude lower than the liquid phase mole fraction of acetaminophen, indicating that even at high pressure the solute prefers the condensed phases. Essentially, any lost product is not really *lost* at all. The filtered vapor and liquid solutions can be separated by lowering the pressure, and the *used* liquid can then be recycled to dissolve more acetaminophen for GAS precipitation. As long as contaminants are not introduced to the system, there is no reason

that any small amount of solute partitioning into the vapor phase cannot be recovered in the recycled stream in the next run.

5.4 Sensitivity Analysis on Phase Equilibrium Codes

A sensitivity analysis was performed on the VLE, SLE, SVE, and SVLE models to determine the relative importance of each binary interaction parameter to the solubility predictions. The methods and calculations are described in Section 4.2, and the tabulated results are listed in Table 5.1 for the binary systems with experimental data as the base case, in Table 5.2 for the binary systems with the model predictions using regressed parameters as the base case, and in Table 5.3 for the ternary system with the model predictions using the regressed parameters as the base case.

For the system CO_2-ethanol at 298 K, increasing k_{12} by 10% resulted in a decrease in the error in the model's bubble point curve prediction. This is expected because the k_{12} value regressed in the present study is higher than the value reported by Kordikowski and coworkers (Kordikowski et al., 1995), as discussed in Section 5.1.1. When k_{12}=0.0890 is retained, the error in the solubility prediction can be reduced slightly by fitting a second parameter, l_{12}, although, the VLE model's bubble point and dew point predictions are much more sensitive to changes in k_{12} than to changes in l_{12}. The dew point predictions are less sensitive than the bubble point predictions to changes in either parameter.

For the system ethanol-acetaminophen at 1 atm, increasing k_{23} increases the predicted x_3 values, and decreasing k_{23} decreases the predicted x_3 values across the whole

temperature range. The model prediction is sensitive to the k_{23} parameter, although not dramatically so, and insensitive to changes in l_{23} of the same magnitude.

The experimental solubility data for the CO_2-acetaminophen system at 323 K is shown in Figure 5.18 with the SVE model's solubility predictions as a function of pressure. The curves predicted when the k_{13} and l_{13} parameters are altered by 10% in either direction are also shown. While it is clear from the plot that the model's solubility prediction is sensitive to k_{13} over the pressure range, the shape of the prediction is unchanged, and the parameter changes do not improve the model fit to the data. The prediction is not sensitive to changes in l_{13}. It should be noted that for SVE data that spans several orders of magnitude, minimizing the absolute RMS error in the solubility, as was done here, favors a better fit to the higher solubility points. Minimizing the AARD for the solubility predictions favors a better fit to the lower solubility data points, but the representation of the overall data set is not improved in doing so.

For the SVLE system, predictions for the solubility of acetaminophen in CO_2-expanded ethanol and for the solubility of acetaminophen in the equilibrium vapor phase at 298 K are of primary interest in the present study. The prediction for x_3 is affected by k_{12}, k_{23}, k_{23}, and l_{12}, although the effect is not large for any parameter. As shown in Figure 5.19, altering the k_{12} parameter affects the solubility prediction over the range of pressures, but most significantly at high pressures when the solubility drops to near zero. The effect on the solubility predictions from changing the l_{12} parameter mimics the effect of changing k_{12}, but the magnitude of the effect is much smaller. As shown in Figure 5.20, changing the k_{23} parameter only affects the low-pressure prediction for x_3, and of the three k_{ij} parameters, this

parameter has the least effect on the x_3 solubility prediction. As shown in Figure 5.21, changing the k_{13} parameter affects the solubility predictions at moderate pressures, but the predictions remain unchanged at the low pressure and high pressure extremes.

While the model fit to the binary SVE CO_2-acetaminophen solubility data was quite poor, it is encouraging that changing the k_{13} parameter does little to change the shape of the predicted x_3 curve, and only changes the magnitude of the prediction by a maximum of approximately 10%. This indicates that obtaining a bad fit to the antisolvent-solute solubility data does not automatically prevent making a decent prediction for x_3 in the ternary system. The sensitivity analysis for SVLE indicates that in the liquid phase the interactions between the antisolvent and the solvent are the most significant, but that the solvent-solute and antisolvent-solute liquid phase interactions are non-negligible.

Altering k_{13} is found to have the most significant effect on the predictions for the vapor phase mole fraction of acetaminophen. As shown in Figure 5.22, the predictions were most affected at moderate to high pressures. The y_3 predictions were negligibly affected by changes in each of the other binary interaction parameters, indicating that the antisolvent-solute interactions have the greatest effect on the prediction of the solubility of acetaminophen in the CO_2-rich phase. Even so, for this particular system y_3 is so small that the possibility of some error in the prediction due to a poor fit for k_{13} does not prevent making adequate predictions of y_3 for our purposes.

5.5 Conclusions and Suggestions for Future Work

5.5.1 Conclusions

The solubility of acetaminophen in supercritical CO_2 at 323 K was measured using a static equilibrium apparatus. The PREOS model was unable to provide an adequate fit to the SVE solubility data, which is consistent with the literature reports for other polar drug compounds dissolved in supercritical CO_2. A much better representation of the solubility data is obtained using empirical density-based correlations. While useful for obtaining fits to experimental data, the density correlations are not predictive. Binary interaction parameters were successfully fit from solubility data for the pairs CO_2-ethanol and ethanol-acetaminophen.

The three regressed binary interaction parameters were used in the SVLE model to predict the fluid phase compositions. While solubility data are not available for the CO_2-ethanol-acetaminophen system with which to compare the model predictions, the trends in the predicted curves for x_3 as a function of temperature and pressure are consistent with solubility data trends found for other systems in the literature. The change in x_3 caused by dissolving pressurized CO_2 in the liquid phase indicates that GAS precipitation of acetaminophen from CO_2-expanded ethanol could be a potentially viable method for purifying this pharmaceutical compound or forming particles with desired characteristics.

The concentration of acetaminophen in the CO_2-rich phase is predicted to drop slightly at low pressure, level off, and finally increase near the critical pressure of CO_2. Comparison of the predictions for x_3 and y_3 indicates that most of the acetaminophen has precipitated from the liquid phase when the vapor phase concentration starts to increase.

Thus, the precipitated particles can be filtered at a pressure below this point to minimize vapor phase losses for each individual run.

The binary phase equilibrium models' solubility predictions are found to be much more sensitive to changes in the k_{ij} parameter than to changes in the l_{ij} parameter. In fact, while the l_{12} parameter was found to have a slight effect on the behavior of the CO_2-ethanol system, the other two binary systems were negligibly affected by l_{ij} parameter alterations. The solubility behavior for the VLE and SLE systems is adequately represented using a single binary interaction parameter, k_{ij}. While the SVE solubility predictions are sensitive to changes in the k_{13} parameter, the shape of the curve prediction is not altered, and the PREOS model is still unable to capture the solubility behavior of the CO_2-acetaminophen system.

The SVLE model's prediction for x_3 is sensitive to all three k_{ij} parameters, although not dramatically so. A poor fit to SVE data resulting in a questionable k_{13} value should not eliminate the ability to obtain a decent prediction for x_3. The SVLE model's prediction for y_3 is only sensitive to the k_{13} binary interaction parameter. These solubility predictions can be used as a starting point for designing an efficient GAS precipitation process for acetaminophen dissolved in ethanol.

5.5.2 Future Work

Equipment limitations prevented taking solubility measurements for acetaminophen in CO_2 at higher pressures. If possible, the static equilibrium system should be modified by replacing the parts with lower pressure ratings to allow measurements at higher pressures to be taken safely and to determine the pressure at which the solubility levels off at a given

temperature. More data should also be taken for this binary system at temperatures other than 323 K and with and without polar modifiers that could enhance the solubility.

Errors in the predictions for the physical property parameter values for complex molecules, including pharmaceuticals and nutraceuticals, can affect the ability of a cubic equation of state to capture the solubility behavior. For the system CO_2-acetaminophen, it would be telling to simultaneously fit k_{13}, T_{c3}, and P_{c3} to try and obtain a better fit to the data.

With tested Mathcad codes in place to represent VLE, SLE, SVE, and SVLE, predictions can be made for the GAS precipitation of nutraceuticals from ester solvents. It will be necessary to measure the solubilities of select nutraceutical compounds in ester solvents as a function of temperature and in CO_2 as a function of temperature and pressure to regress the appropriate binary interaction parameters for the ternary model. The SVLE model can be improved upon by incorporating group contribution excess Gibbs free energy functions or substituting alternative cubic equations of state for Peng-Robinson. Above all, measurements of the liquid phase solubility of nutraceuticals of interest in CO_2-expanded solvents are needed. SVLE solubility data is scarce in the literature, and experimental data can help to validate and improve model predictions.

Table 5.1 The sensitivity analysis results for the binary systems using the experimental data as the base case.

Vapor-Liquid Equilibrium (1) CO_2 + (2) Ethanol T=298 K; P=15-60 bar; n=18			
		x_1 AARD (%)	x_1 RMS
Regressed Parameters			
k_{12}=0.0890	l_{12}=0.0000	13.55%	1.37E-2
Parameter Variation			
k_{12} + 10%	0.0979	7.32%	7.76E-3
k_{12} - 10%	0.0801	22.71%	2.07E-2
l_{12} + 10%	0.0089	9.14%	8.35E-3
l_{12} - 10%	-0.0089	17.34%	1.82E-2

Solid-Liquid Equilibrium (2) Ethanol + (3) Acetaminophen P=1 atm; T=270-310K; n=8			
		x_3 AARD (%)	x_3 RMS
Regressed Parameters			
k_{23}=0.0099	l_{23}=0.0000	1.94%	4.55E-6
Parameter Variation			
k_{23} + 10%	0.0109	2.65%	6.91E-6
k_{23} - 10%	0.0089	2.00%	7.36E-6
l_{23} + 10%	0.0010	1.94%	4.56E-6
l_{23} - 10%	-0.0010	1.94%	4.54E-6

Solid-Vapor Equilibrium (1) CO_2 + (3) Acetaminophen T=323 K; P=100-300 bar; n=11			
		y_3 AARD (%)	y_3 RMS
Regressed Parameters			
k_{13}=0.2614	l_{13}=0.0000	341.94%	4.58E-10
Parameter Variation			
k_{13} + 10%	0.2875	214.55%	5.43E-10
k_{13} - 10%	0.2353	547.40%	6.83E-10
l_{13} + 10%	0.0261	341.95%	4.58E-10
l_{13} - 10%	-0.0261	341.95%	4.58E-10

Table 5.2 The sensitivity analysis results for the binary systems using the model prediction with the regressed parameters as the base case.

Vapor-Liquid Equilibrium
(1) CO_2 + (2) Ethanol
T=298 K; P=15-60 bar; n=25

Regressed Parameters		x_1	y_1	x_1	y_1
k_{12}=0.0890	l_{12}=0.0000	AARD (%)	AARD (%)	RMS	RMS
Parameter Variation					
k_{12} + 10%	0.0979	8.54%	0.01%	4.01E-3	1.03E-8
k_{12} - 10%	0.0801	7.40%	0.01%	9.97E-4	1.16E-8
l_{12} + 10%	0.0089	1.82%	0.00%	1.19E-4	1.20E-11
l_{12} - 10%	-0.0089	1.85%	0.00%	1.43E-4	8.00E-12

Solid-Liquid Equilibrium
(2) Ethanol + (3) Acetaminophen
P=1 atm; T=270-310K; n=20

Regressed Parameters		x_3	x_3
k_{23}=0.0099	l_{23}=0.0000	AARD (%)	RMS
Parameter Variation			
k_{23} + 10%	0.0109	3.73%	2.49E-6
k_{23} - 10%	0.0089	3.83%	2.62E-6
l_{23} + 10%	0.0010	0.01%	5.50E-11
l_{23} - 10%	-0.0010	0.01%	5.00E-11

Solid-Vapor Equilibrium
(1) CO_2 + (3) Acetaminophen
T=323 K; P=100-300 bar; n=30

Regressed Parameters		y_3	y_3
k_{13}=0.2614	l_{13}=0.0000	AARD (%)	RMS
Parameter Variation			
k_{13} + 10%	0.2875	27.13%	5.91E-11
k_{13} - 10%	0.2353	41.28%	1.53E-10
l_{13} + 10%	0.0261	0.00%	1.13E-19
l_{13} - 10%	-0.0261	0.00%	1.13E-19

Table 5.3 The sensitivity analysis results for the ternary system using the model prediction with the regressed parameters as the base case.

Solid-Vapor-Liquid Equilibrium
(1) CO_2 + (2) Ethanol + (3) Acetaminophen
T=298 K; P=1-64 bar; n=64

Regressed Parameters

k_{12}=0.0890	l_{12}=0.0000	k_{23}=0.0099	l_{23}=0.0000	k_{13}=0.2614	l_{13}=0.0000

Parameter Variation		AARD (%) x_1	x_3	y_1	y_3
k_{12} + 10%	0.0979	7.80%	109.90%	0.01%	0.05%
k_{12} - 10%	0.0801	8.09%	13.29%	0.01%	0.06%
l_{12} + 10%	0.0089	1.82%	46.39%	0.00%	0.01%
l_{12} - 10%	-0.0089	1.82%	5.38%	0.00%	0.01%
k_{23} + 10%	0.0109	0.39%	3.04%	0.00%	0.00%
k_{23} - 10%	0.0089	0.40%	3.15%	0.00%	0.00%
l_{23} + 10%	0.0010	0.03%	0.04%	0.00%	0.00%
l_{23} - 10%	-0.0010	0.03%	0.04%	0.00%	0.00%
k_{13} + 10%	0.2875	0.85%	14.37%	0.00%	6.96%
k_{13} - 10%	0.2353	0.91%	19.61%	0.00%	7.78%
l_{13} + 10%	0.0261	0.15%	0.32%	0.00%	0.00%
l_{13} - 10%	-0.0261	0.15%	0.32%	0.00%	0.00%

Parameter Variation		RMS x_1	x_3	y_1	y_3
k_{12} + 10%	0.0979	2.61E-3	5.69E-6	7.27E-9	1.60E-20
k_{12} - 10%	0.0801	1.44E-3	4.64E-6	8.38E-9	1.54E-20
l_{12} + 10%	0.0089	1.10E-3	3.43E-7	1.06E-10	3.87E-22
l_{12} - 10%	-0.0089	5.99E-4	3.18E-7	2.81E-11	1.30E-22
k_{23} + 10%	0.0109	7.27E-7	1.09E-6	6.00E-10	3.99E-24
k_{23} - 10%	0.0089	7.84E-7	1.16E-6	6.19E-10	4.19E-24
l_{23} + 10%	0.0010	3.24E-9	1.09E-10	0.00E0	0.00E-0
l_{23} - 10%	-0.0010	3.22E-9	1.19E-10	0.00E0	0.00E-0
k_{13} + 10%	0.2875	6.44E-6	3.17E-6	1.47E-10	6.02E-17
k_{13} - 10%	0.2353	7.82E-6	4.01E-6	2.00E-10	8.44E-17
l_{13} + 10%	0.0261	4.02E-7	3.23E-9	0.00E0	1.56E-28
l_{13} - 10%	-0.0261	3.97E-7	3.30E-9	0.00E0	1.56E-28

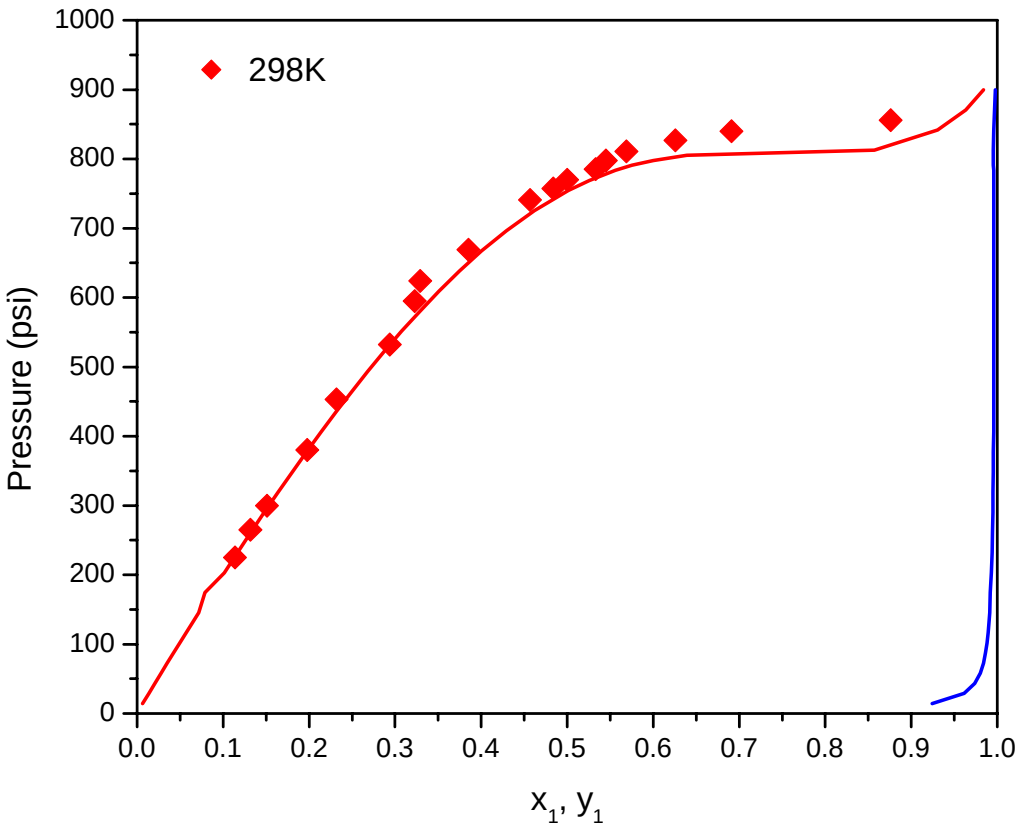

Figure 5.1 The solubility of (1) CO_2 in (2) ethanol at 298 K (Kordikowski et al., 1995), shown with the VLE model fit using the value of k_{12}=0.0890 that Kordikowski et al. regressed.

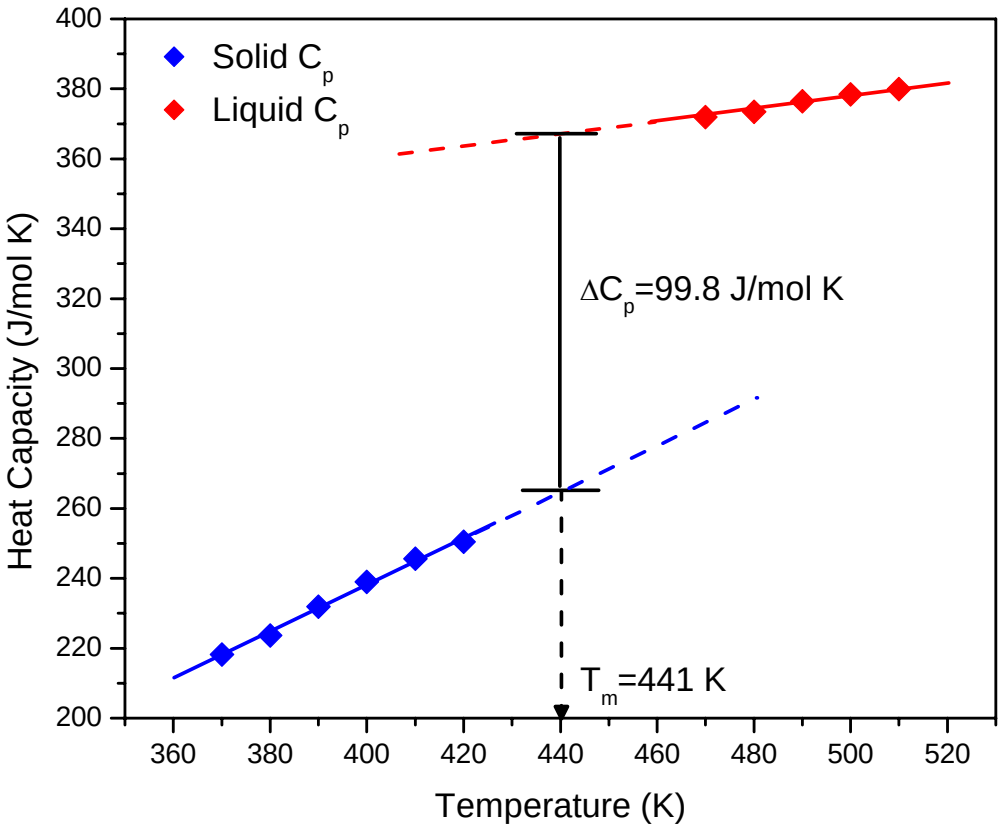

Figure 5.2 Neau and coworkers determined the differential heat capacity of acetaminophen, ΔC_p, by extrapolating the linear trend in heat capacity for solid and liquid acetaminophen to the melting point temperature, T_m, and taking the difference (Neau et al., 1997).

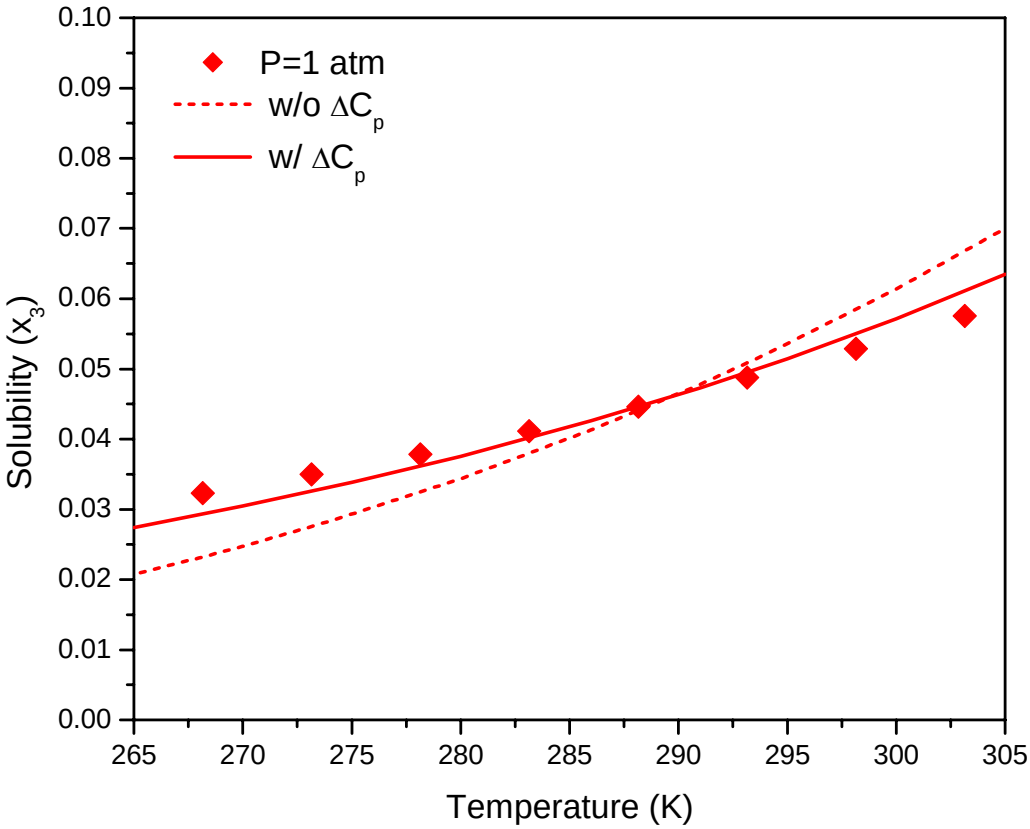

Figure 5.3 The solubility of (3) acetaminophen in (2) ethanol at 1 atm as a function of temperature (Granberg and Rasmuson, 1999). The dashed line represents the SLE model fit to the data when the differential heat capacity term is neglected from the expression for the fugacity of the solid phase; the solid line represents the fit when the differential heat capacity term is included, k_{23}=0.0099.

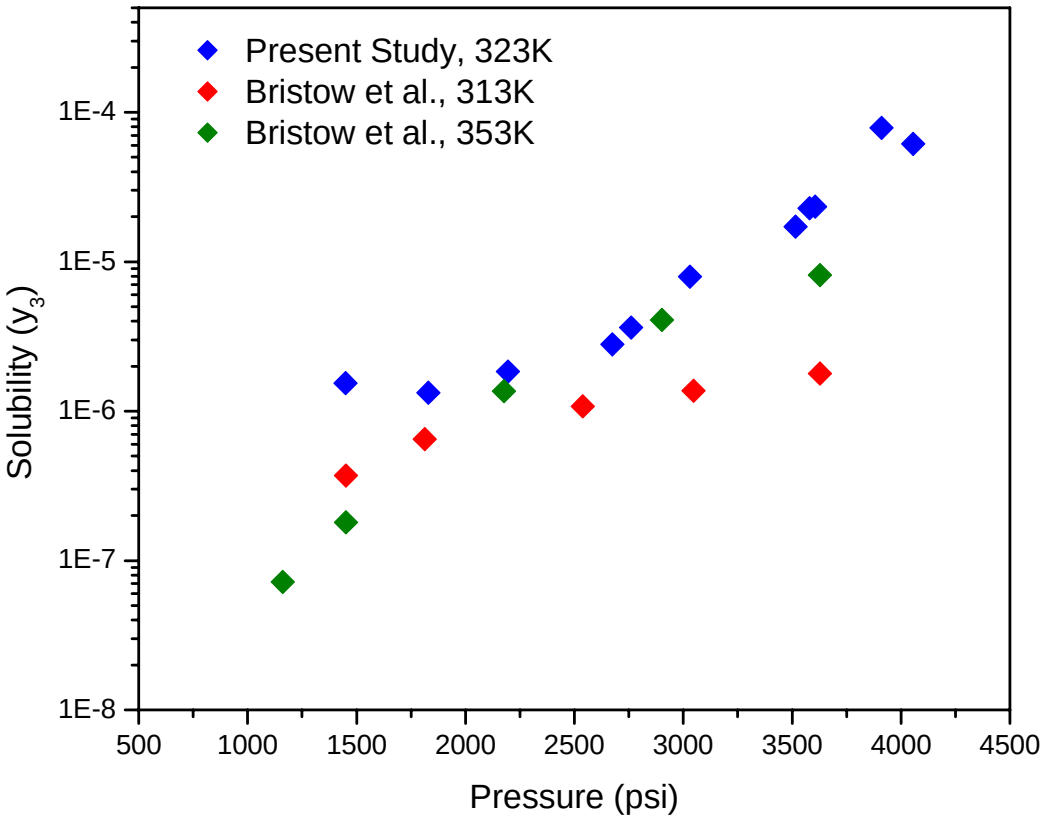

Figure 5.4 The solubility of (3) acetaminophen in (1) supercritical CO_2 at 323 K obtained using a static recirculation apparatus, compared to data taken by Bristow et al, 2001 at 313 K and 353 K using a dynamic through-flow apparatus coupled with off-line analysis.

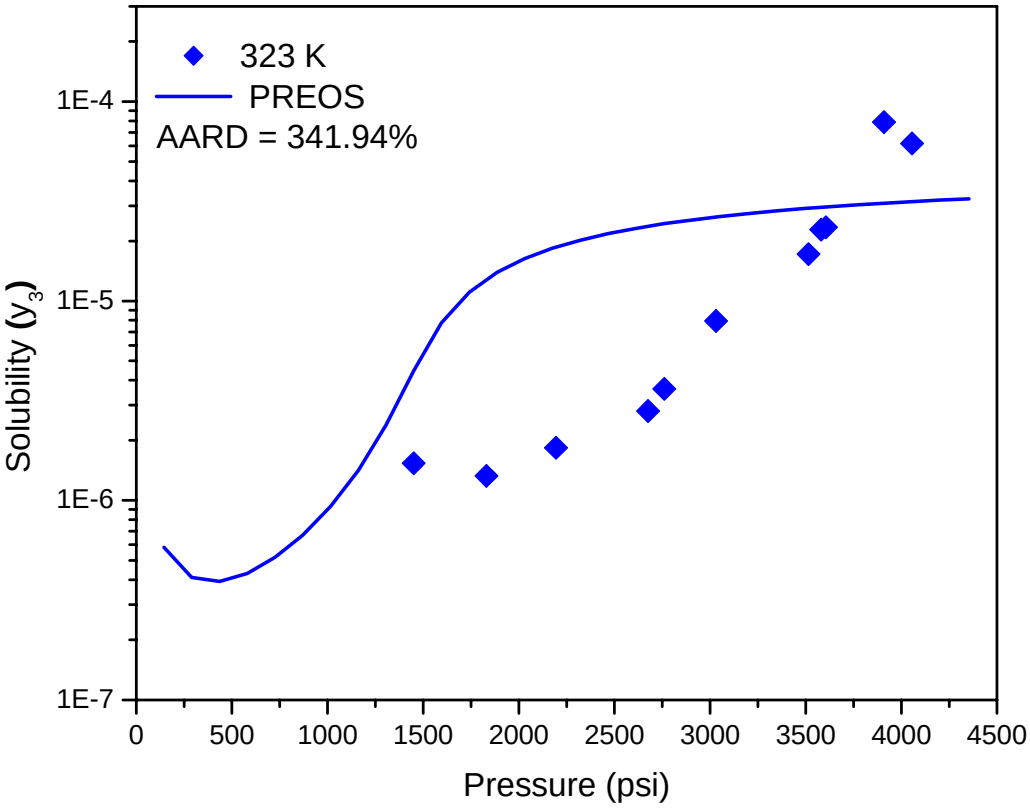

Figure 5.5 The best fit obtained for the solubility of (3) acetaminophen in (1) supercritical CO_2 at 323.15 K as a function of pressure using the Peng-Robinson equation of state, k_{13}=0.2614.

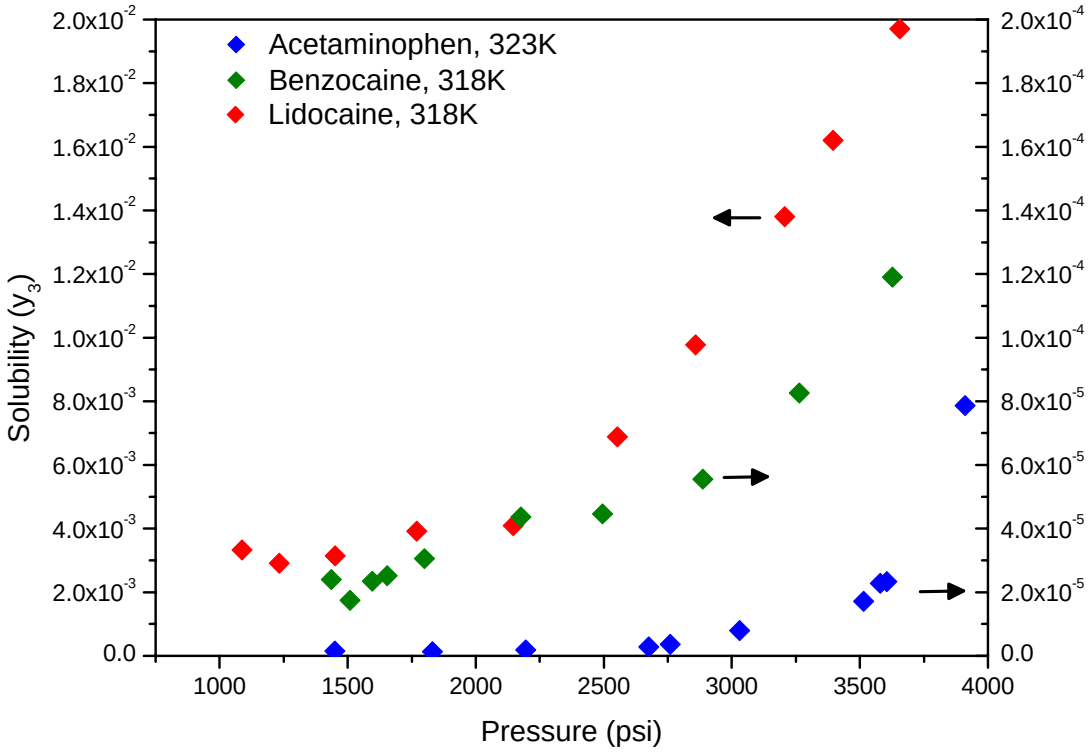

Figure 5.6 The solubility of (3) acetaminophen in (1) supercritical CO_2 at 323 K compared to the solubility of (3) benzocaine and (3) lidocaine at 318 K (Weinstein et al., 2004).

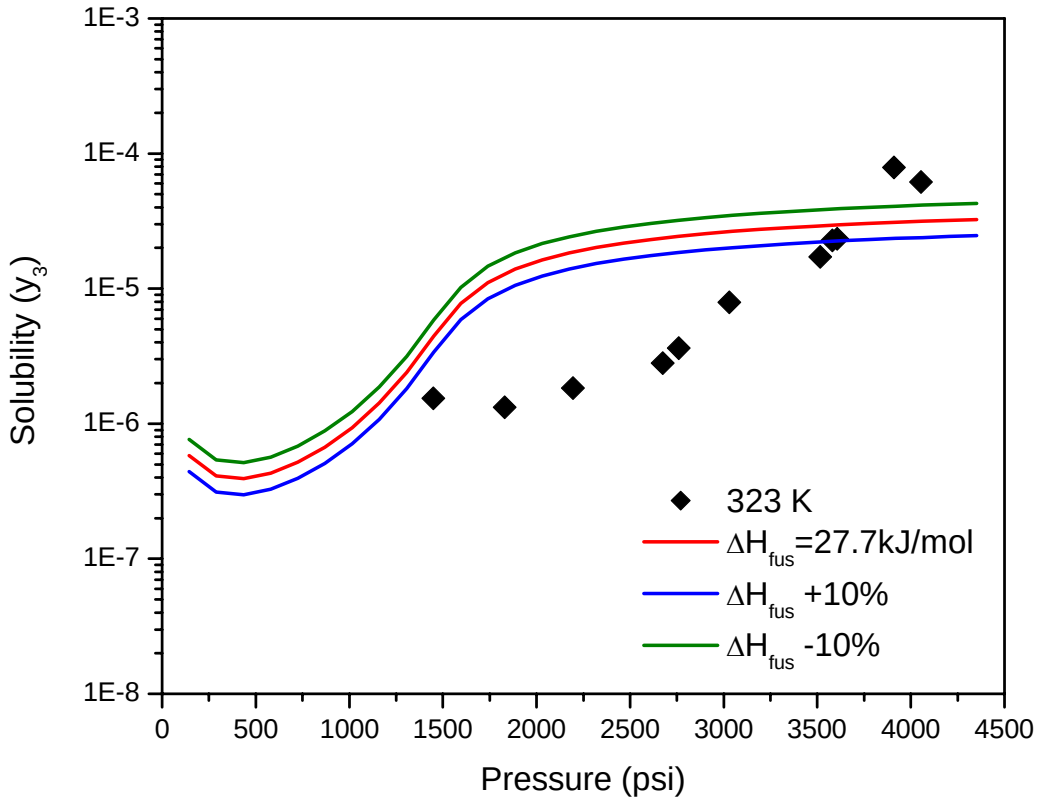

Figure 5.7 The sensitivity of the prediction for the SVE vapor phase solubility of (3) acetaminophen in (1) CO_2 to the ΔH_{fus} of acetaminophen at 323 K.

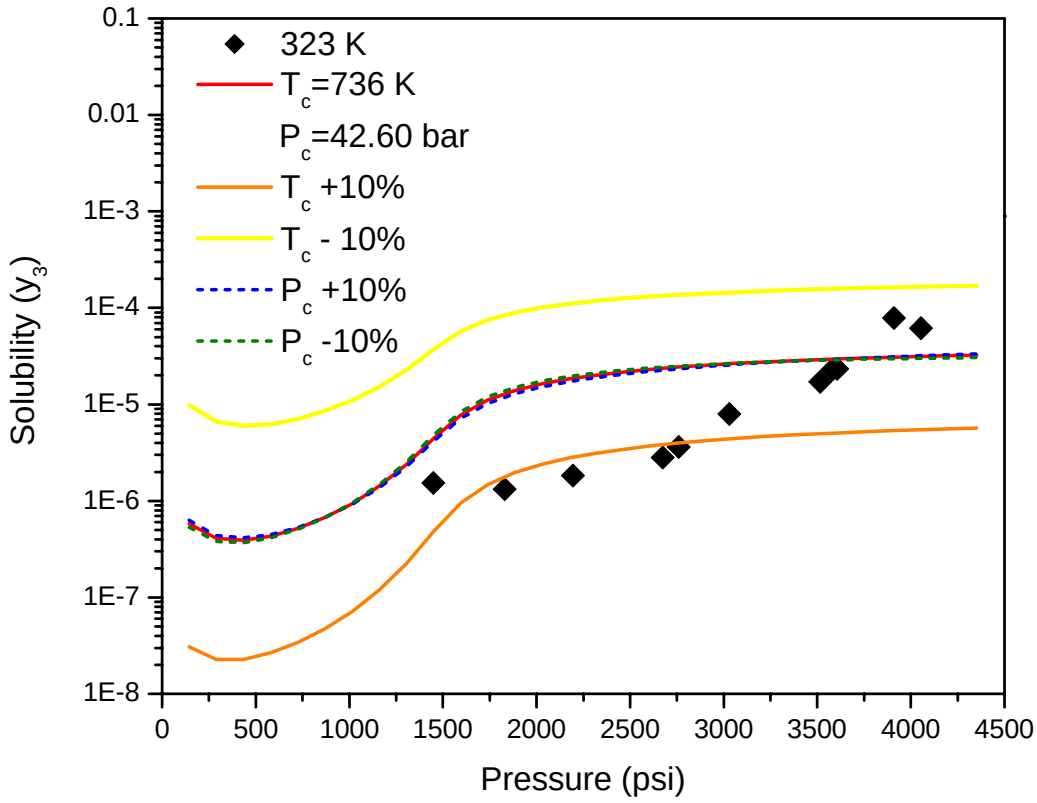

Figure 5.8 The sensitivity of the SVE prediction for the vapor phase solubility of (3) acetaminophen in (1) CO_2 to the T_c and P_c of acetaminophen at 323 K.

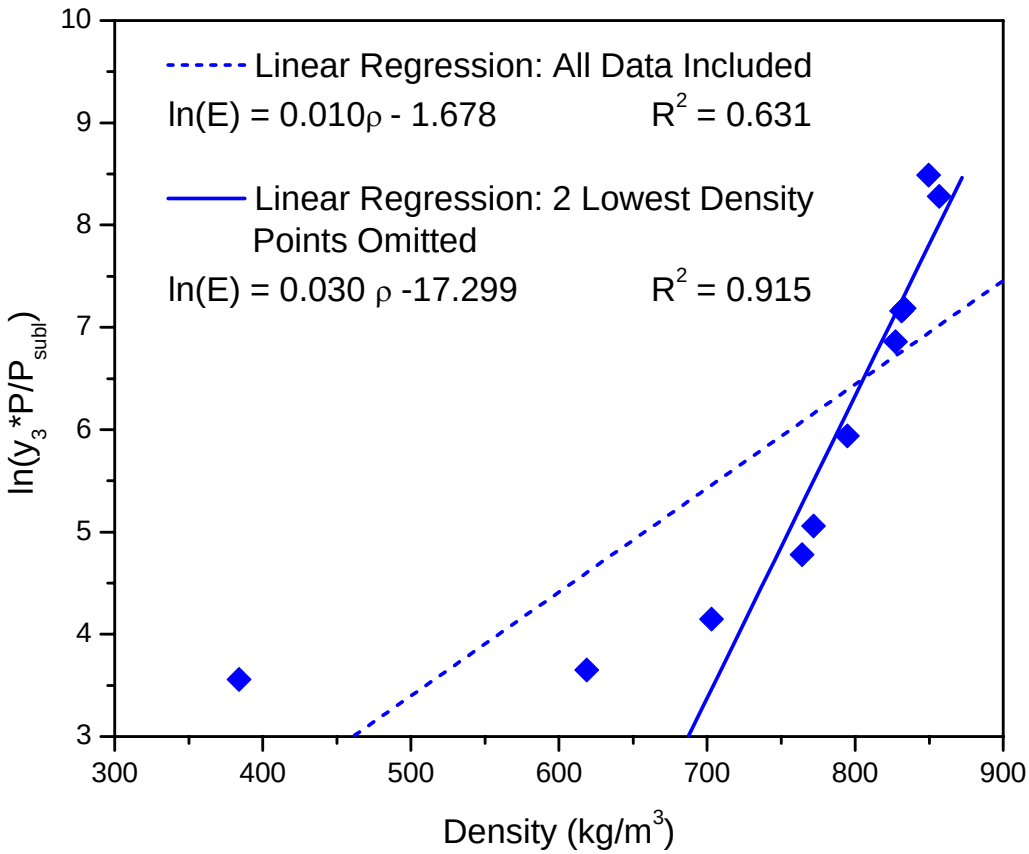

Figure 5.9 A linear regression to fit the parameters for an empirical density-based model. The dashed line represents the linear regression to the data when all data points are considered. The solid line represents the linear regression to the data when the two lowest density data points are omitted.

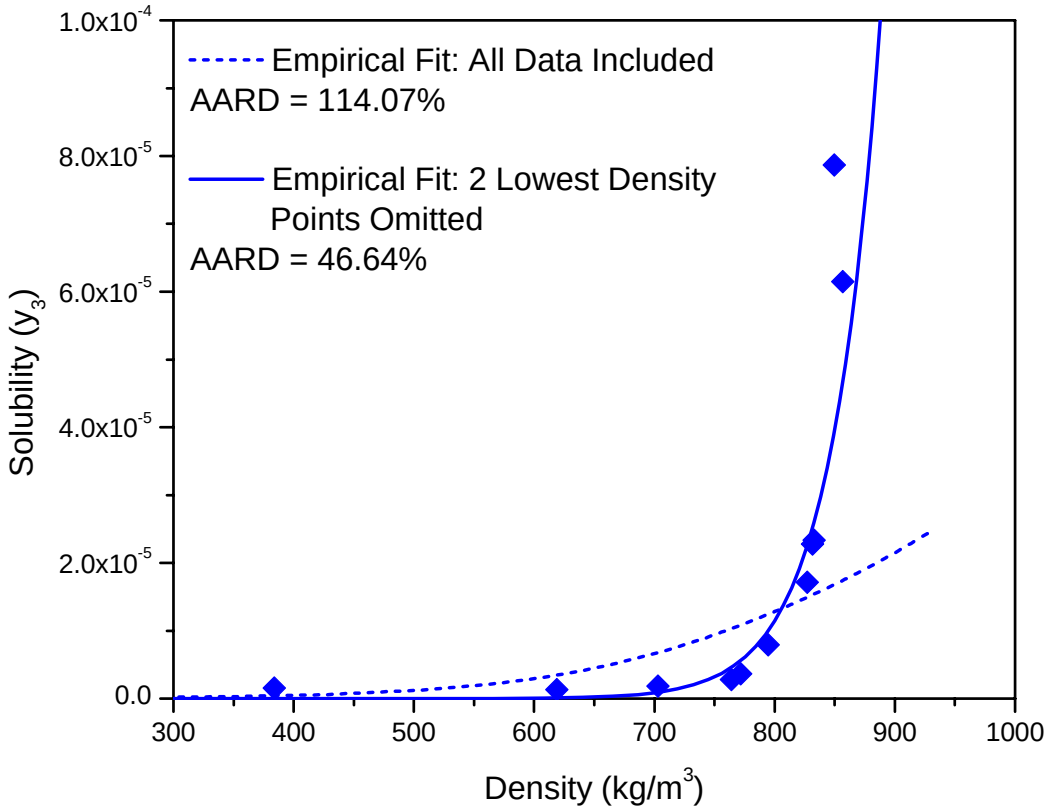

Figure 5.10 The empirical exponential fit to the (1) CO_2 – (3) acetaminophen solubility data using the parameters regressed from the linear approximation. The dashed line is the fit to the solubility data when all data points are considered. The solid line is the fit to the solubility data when the two lowest density data points are omitted.

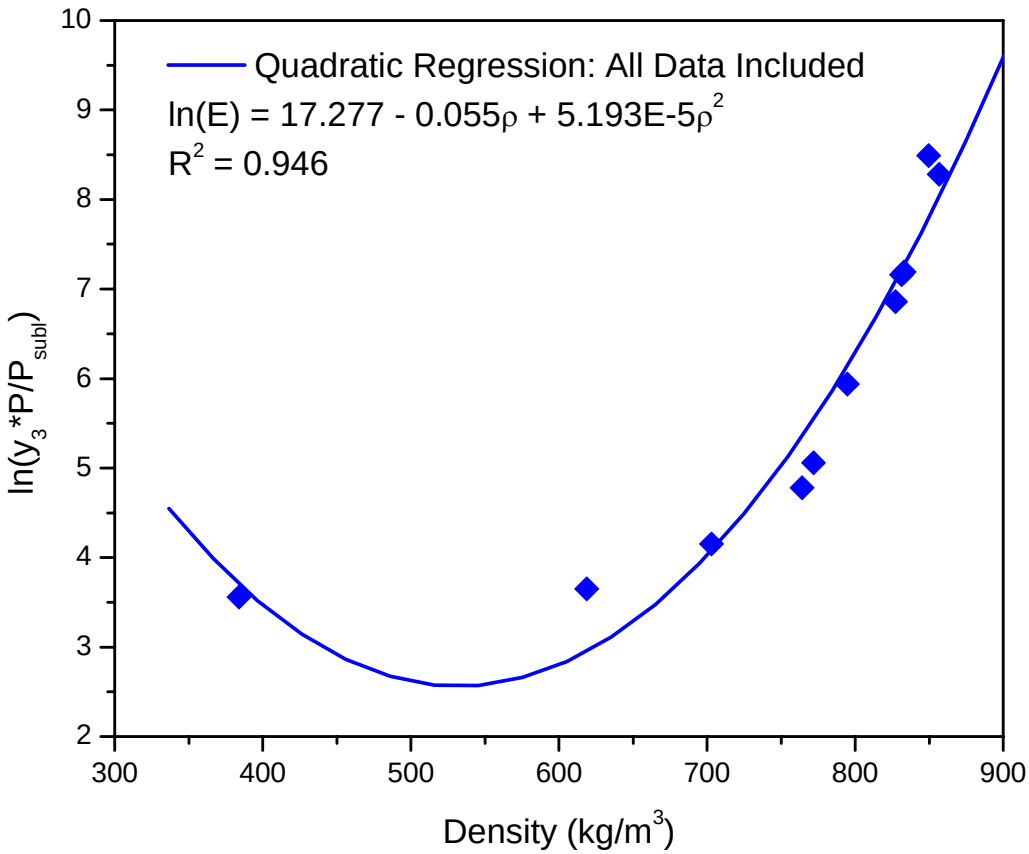

Figure 5.11 A quadratic regression to fit the parameters for an empirical density-based model. The solid line represents the quadratic regression to the data when all data points are considered.

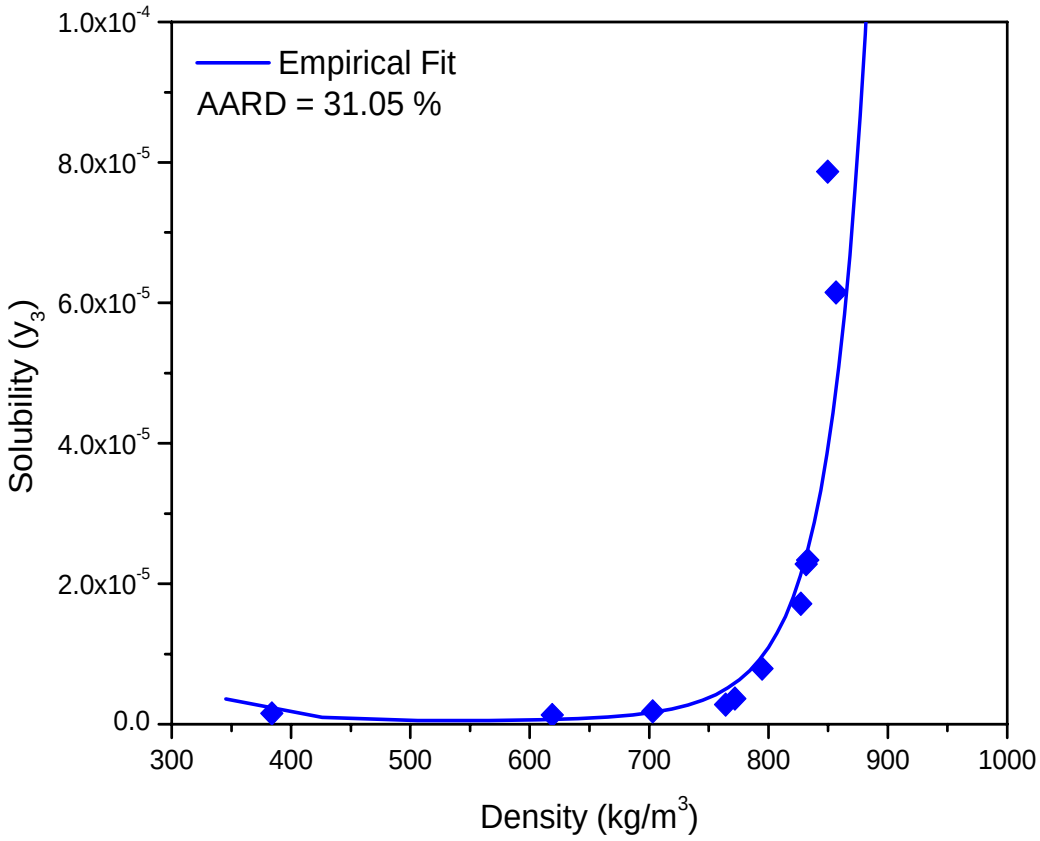

Figure 5.12 The empirical exponential fit to the (1) CO_2 – (3) acetaminophen solubility data using the parameters regressed from the quadratic approximation with all data points considered.

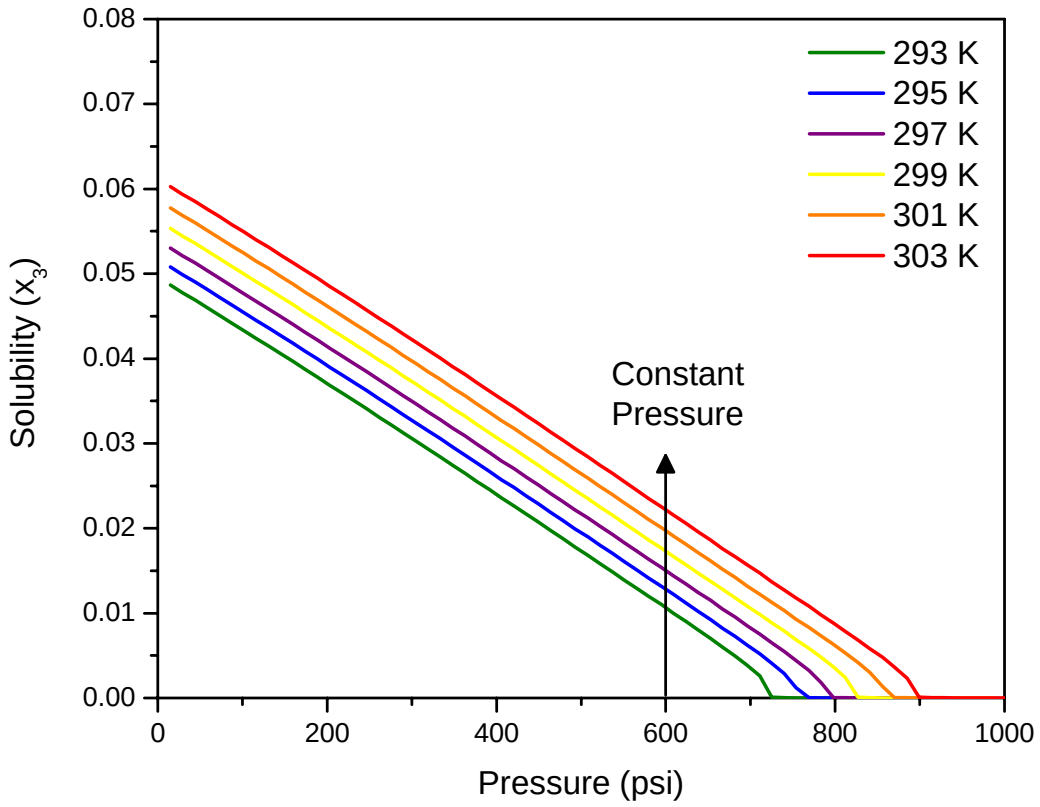

Figure 5.13 Predictions for the solubility of (3) acetaminophen in (1) CO_2-expanded (2) ethanol as a function of temperature and pressure; k_{12}=0.0890, k_{23}=0.0099, and k_{13}=0.2614.

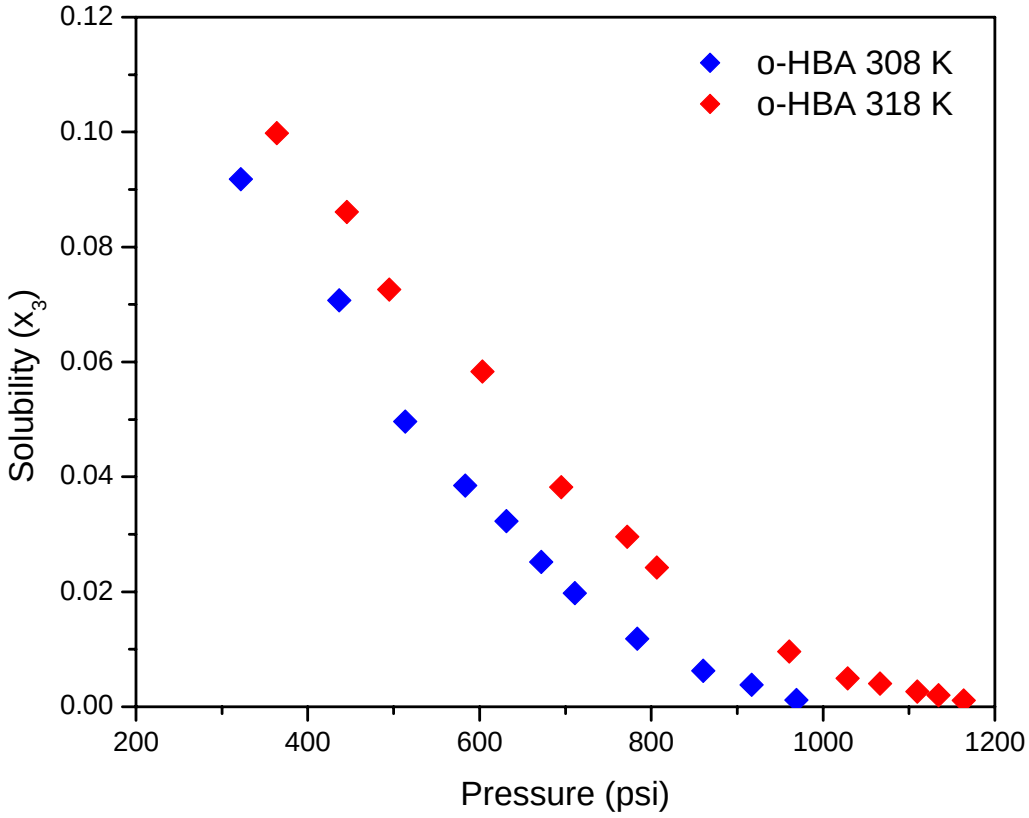

Figure 5.14 The solubility of (3) ortho-hydroxybenzoic acid in (1) CO_2-expanded (2) ethyl acetate at 308 K and 328 K (Liu et al., 2000).

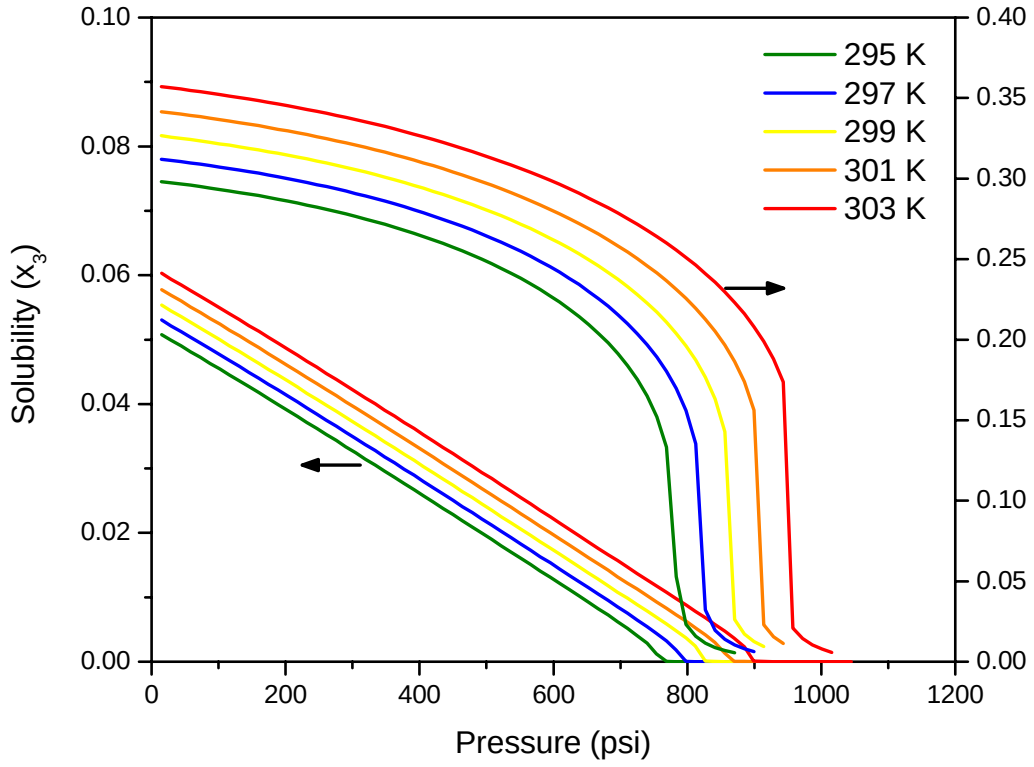

Figure 5.15 A comparison of the trends in the solubility predictions for the naphthalene and acetaminophen GAS systems with temperature and pressure. For the system (1) CO_2 - (2) toluene – (3) naphthalene CO_2 acts as a cosolvent at low to moderate pressures and an antisolvent at high pressures; k_{12}=0.0900, l_{12}=0.0000, k_{13}=0.0940, l_{13}=-0.0240, k_{23}=0.0000, l_{23}=0.0000 (Kikic et al., 1997). For the system (1) CO_2 – (2) ethanol - (3) acetaminophen CO_2 acts as an antisolvent across the entire pressure range; k_{12}=0.0890, k_{13}=0.2614, k_{23}=0.0099.

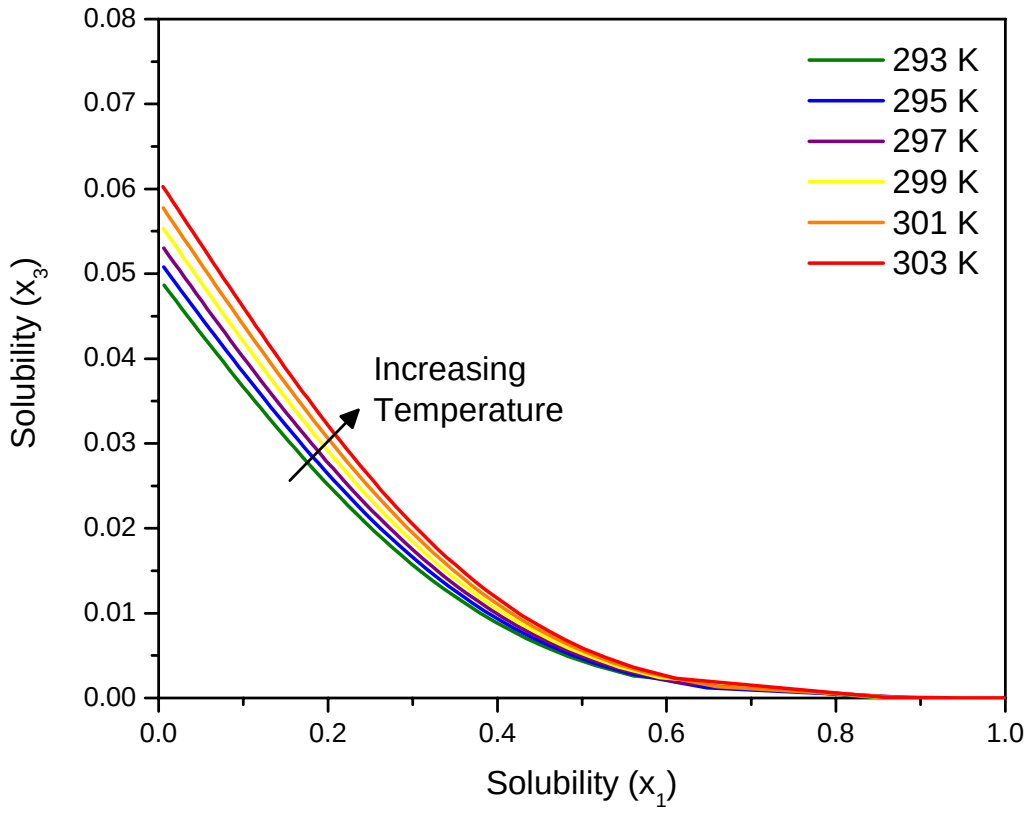

Figure 5.16 Predictions for the solubility of (3) acetaminophen in (1) CO_2-expanded (2) ethanol as a function of temperature and mole fraction of CO_2 in the liquid phase; k_{12}=0.0890, k_{23}=0.0099, and k_{13}=0.2614.

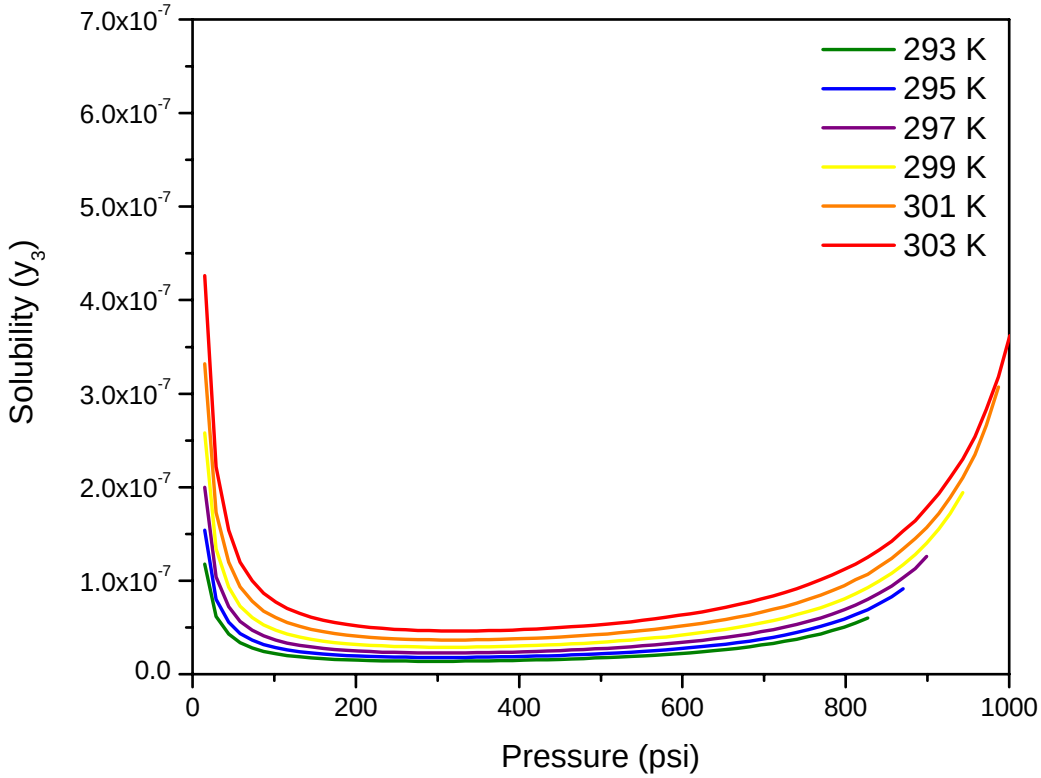

Figure 5.17 Predictions for the solubility of acetaminophen in the (1) CO_2 – (2) ethanol – (3) acetaminophen GAS system vapor phase as a function of temperature and pressure; k_{12}=0.0890, k_{23}=0.0099, and k_{13}=0.2614.

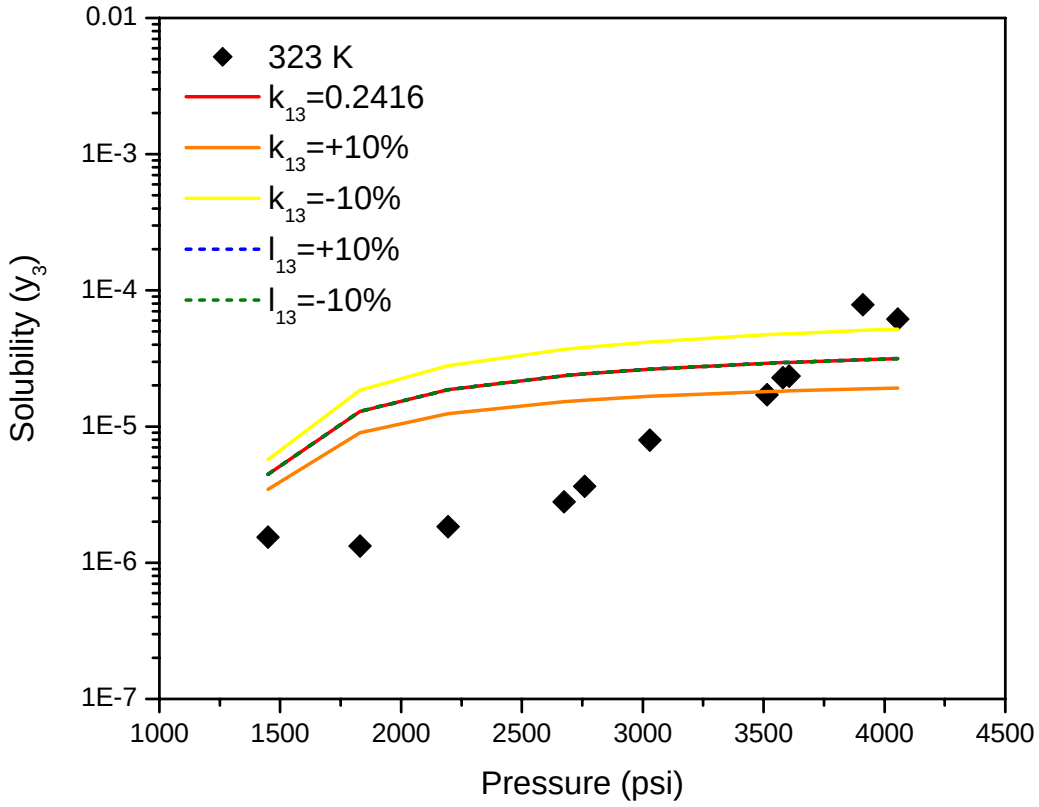

Figure 5.18 The sensitivity of the prediction for the SVE vapor phase solubility of (3) acetaminophen in (1) supercritical CO_2 to the k_{13} and l_{13} parameters at 323 K.

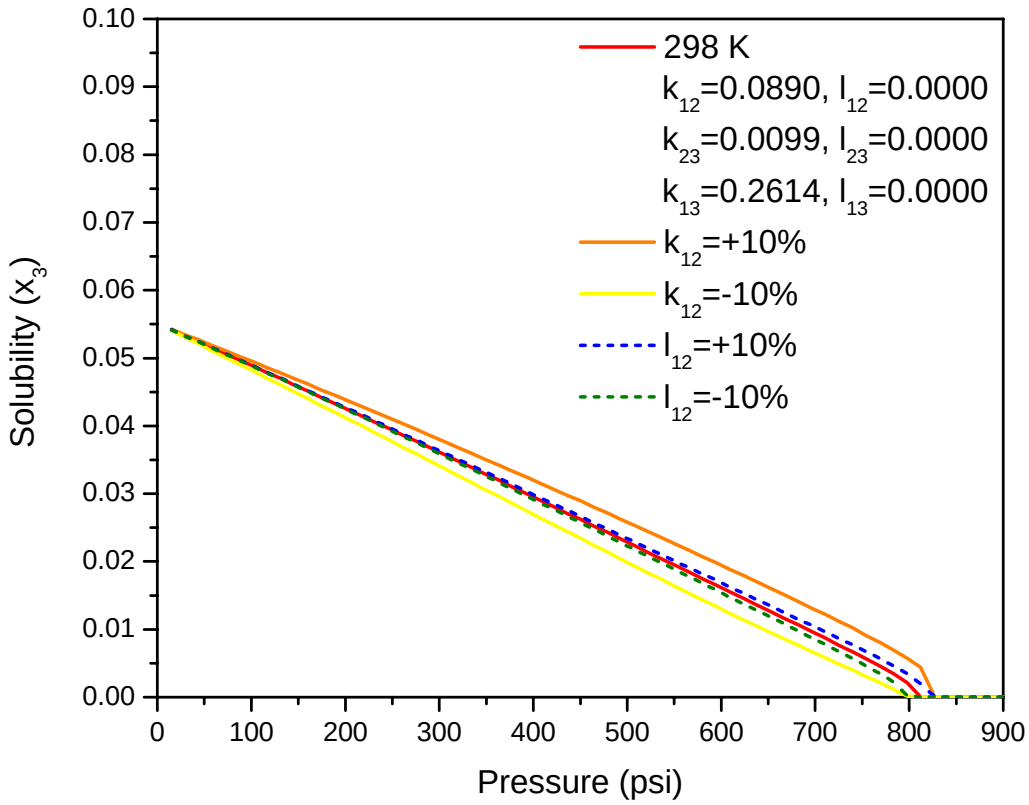

Figure 5.19 The sensitivity of the SVLE prediction for the liquid phase solubility of (3) acetaminophen in (1) CO_2-expanded (2) ethanol to the k_{12} and l_{12} parameters at 298 K.

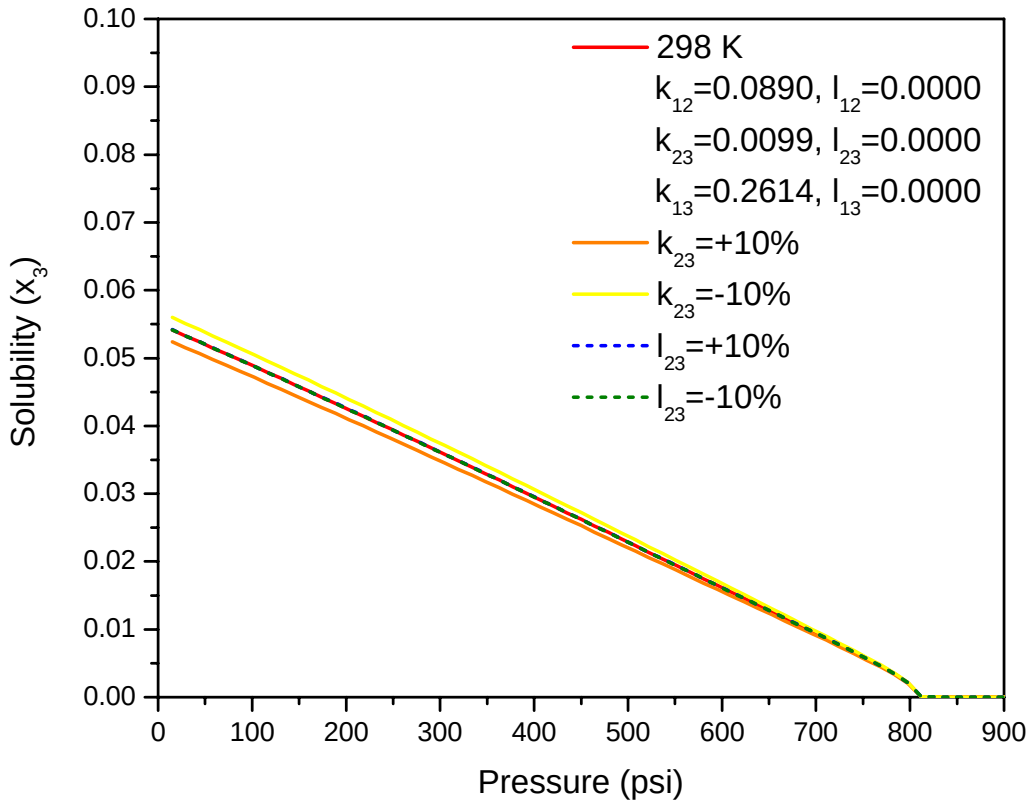

Figure 5.20 The sensitivity of the SVLE prediction for the liquid phase solubility of (3) acetaminophen in (1) CO_2-expanded (2) ethanol to the k_{23} and l_{23} parameters at 298 K.

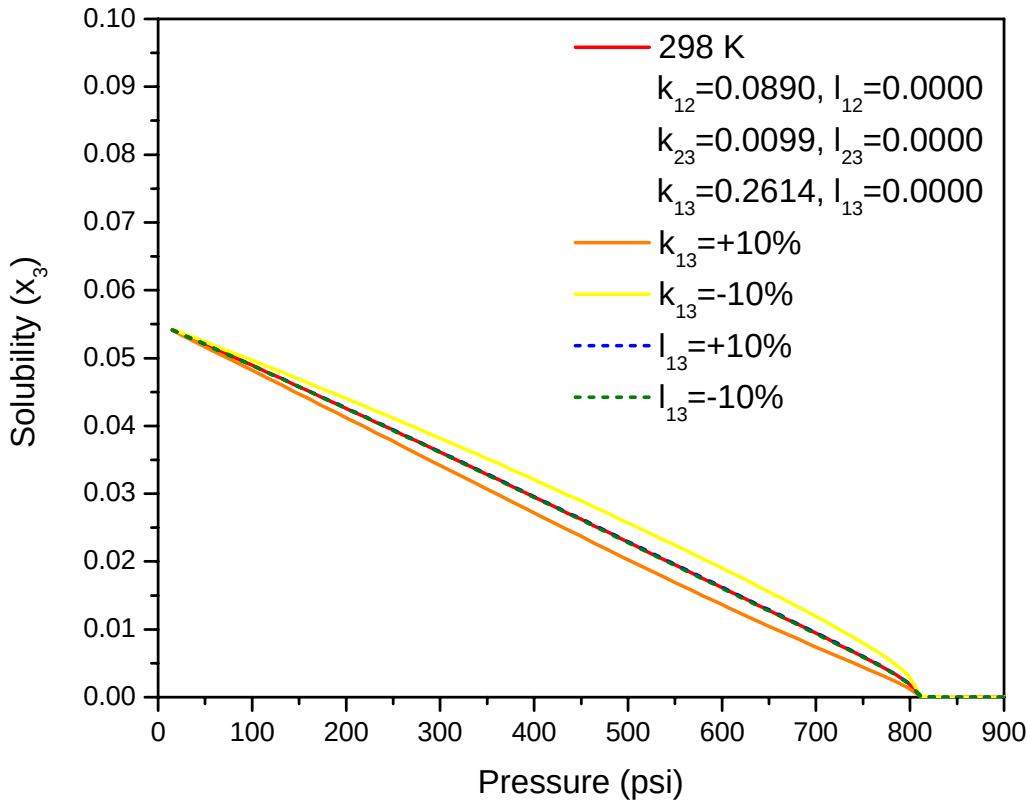

Figure 5.21 The sensitivity of the SVLE prediction for the liquid phase solubility of (3) acetaminophen in (1) CO_2-expanded (2) ethanol to the k_{13} and l_{13} parameters at 298 K.

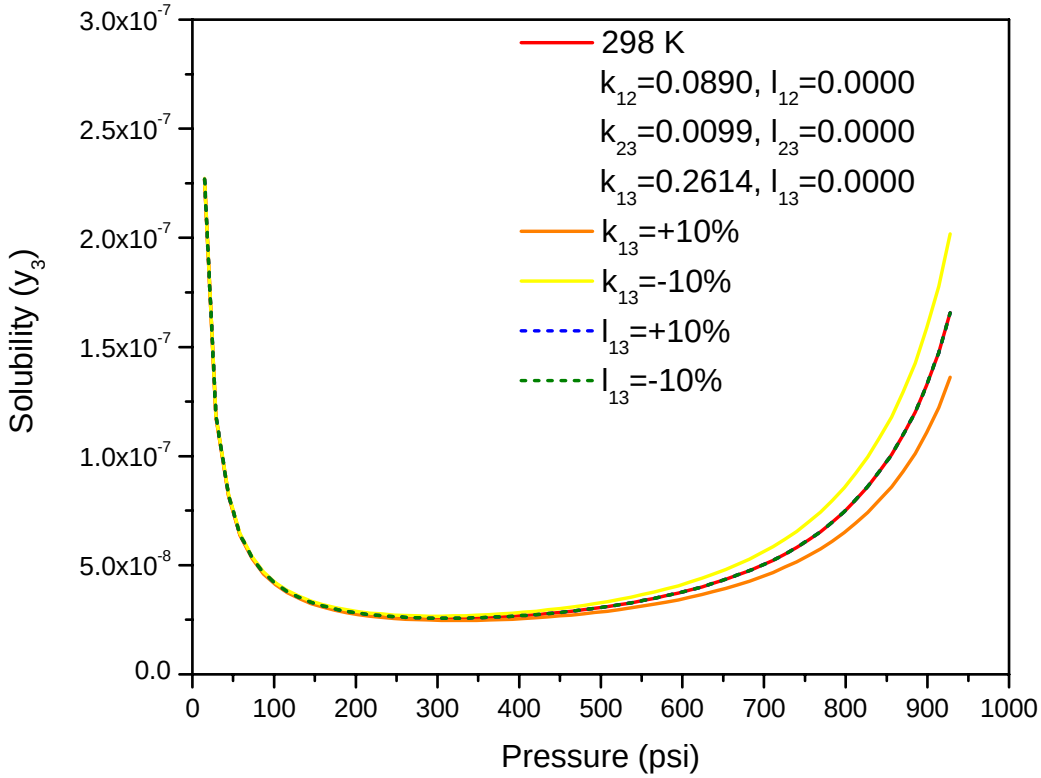

Figure 5.22 The sensitivity of the SVLE prediction for the vapor phase solubility of acetaminophen to k_{13} and l_{13} for the system CO_2-ethanol-acetaminophen at 298 K.

5.6 References

Asghari-Khiavi, M. and Y. Yamini (2003). "Solubility of the drugs bisacodyl, methimazole, methylparaben, and Iodoquinol in supercritical carbon dioxide." Journal of Chemical and Engineering Data **48**(1): 61-65.

Bristow, S., B. Y. Shekunov and P. York (2001). "Solubility analysis of drug compounds in supercritical carbon dioxide using static and dynamic extraction systems." Industrial & Engineering Chemistry Research **40**(7): 1732-1739.

Chrastil, J. (1982). "Solubility of Solids and Liquids in Supercritical Gases." Journal of Physical Chemistry **86**(15): 3016-3021.

Coutsikos, P., K. Magoulas and G. M. Kontogeorgis (2003). "Prediction of solid-gas equilibria with the Peng-Robinson equation of state." Journal of Supercritical Fluids **25**(3): 197-212.

Duarte, A. R. C., P. Coimbra, H. C. de Sousa and C. M. M. Duarte (2004). "Solubility of flurbiprofen in supercritical carbon dioxide." Journal of Chemical and Engineering Data **49**(3): 449-452.

Garmroodi, A., J. Hassan and Y. Yamini (2004). "Solubilities of the drugs benzocaine, metronidazole benzoate, and naproxen in supercritical carbon dioxide." Journal of Chemical and Engineering Data **49**(3): 709-712.

Gracin, S., T. Brinck and A. C. Rasmuson (2002). "Prediction of solubility of solid organic compounds in solvents by UNIFAC." Industrial & Engineering Chemistry Research **41**(20): 5114-5124.

Granberg, R. A. and A. C. Rasmuson (1999). "Solubility of paracetamol in pure solvents." Journal of Chemical and Engineering Data **44**(6): 1391-1395.

Kikic, I., M. Lora and A. Bertucco (1997). "A thermodynamic analysis of three-phase equilibria in binary and ternary systems for applications in rapid expansion of a supercritical solution (RESS), particles from gas-saturated solutions (PGSS), and supercritical antisolvent (SAS)." Industrial & Engineering Chemistry Research **36**(12): 5507-5515.

Kordikowski, A., A. P. Schenk, R. M. VanNielen and C. J. Peters (1995). "Volume expansions and vapor-liquid equilibria of binary mixtures of a variety of polar solvents and certain near- critical solvents." Journal of Supercritical Fluids **8**(3): 205-216.

Liu, Z., D. Li, G. Yang and B. Han (2000). "Solubility of hydroxybenzoic acid isomers in ethyl acetate expanded with CO2." Journal of Supercritical Fluids **18**: 111-119.

Macnaughton, S. J., I. Kikic, N. R. Foster, P. Alessi, A. Cortesi and I. Colombo (1996). "Solubility of anti-inflammatory drugs in supercritical carbon dioxide." Journal of Chemical and Engineering Data **41**(5): 1083-1086.

McHugh, M. and M. E. Paulaitis (1980). "Solid Solubilities of Naphthalene and Biphenyl in Supercritical Carbon-Dioxide." Journal of Chemical and Engineering Data **25**(4): 326-329.

Neau, S. H., S. V. Bhandarkar and E. W. Hellmuth (1997). "Differential molar heat capacities to test ideal solubility estimations." Pharmaceutical Research **14**(5): 601-605.

Schmitt, W. J. and R. C. Reid (1986). "Solubility of Monofunctional Organic-Solids in Chemically Diverse Supercritical Fluids." Journal of Chemical and Engineering Data **31**(2): 204-212.

Thiering, R., F. Dehghani, A. Dillow and N. R. Foster (2000). "The influence of operating conditions on the dense gas precipitation of model proteins." Journal of Chemical Technology and Biotechnology **75**(1): 29-41.

Weinstein, R. D., K. R. Muske, J. Moriarty and E. K. Schmidt (2004). "The solubility of benzocaine, lidocaine, and procaine in liquid and supercritical carbon dioxide." Journal of Chemical and Engineering Data **49**(3): 547-552.

Yamini, Y., J. Hassan and S. Haghgo (2001). "Solubilities of some nitrogen-containing drugs in supercritical carbon dioxide." Journal of Chemical and Engineering Data **46**(2): 451-455.

APPENDIX A RESVERATROL: MODEL NUTRACEUTICAL FOR EXTRACTION WITH ESTER SOLVENTS AND GAS PRECIPITATION

A.1 Resveratrol Background

A.1.1 Health Benefits of Resveratrol

Resveratrol is an antioxidant found in the skins of red grapes. Concentrations of resveratrol have been detected in several varieties of wine (Goldberg et al., 1995; Jeandet et al., 1995; Lamikanra et al., 1996). Some evidence suggests that resveratrol may help to explain the "French paradox" – that the French have a statistically lower occurrence of heart disease, stroke, and certain cancers. Resveratrol has been shown to have chemopreventive properties (Bhat and Pezzuto, 2002), to inhibit platelet aggregation, and to function as an anti-inflammatory agent (Fremont, 2000).

A.1.2 Stability of Resveratrol

The structure of resveratrol is shown in Figure 4.1. Due to the presence of the double bond, resveratrol can exist in either the *trans* or *cis* conformation. The trans-conformation is the naturally occurring isomer found in grapes, but both isomers have been detected in wines. Trans-resveratrol is very sensitive to UV light. Trela and Waterhouse report that while solutions of trans-resveratrol are fairly stable in normal lab lighting conditions for short periods of time, the equilibrium in these conditions favors the cis conformation. In lab samples unprotected from light, 80% of the resveratrol isomerized to the cis conformation over 30 days (Trela and Waterhouse, 1996). Figure A.1 shows the curves for absorbance versus wavelength that Trela and Waterhouse reported for trans and cis-resveratrol in ethanol. Trans-resveratrol in ethanol yields a characteristic double peak

with the λ_{max}=308nm, the same concentration of cis-resveratrol in ethanol yields a smaller single peak with the λ_{max} =288 nm (Trela and Waterhouse, 1996).

A.1.3 Supercritical Fluid Extraction of Resveratrol

Several authors have performed studies to extract polyphenols into pure and modified CO_2 under dynamic conditions to study the effect of operating variables on percent recoveries: Palma and Taylor extracted polyphenols, including resveratrol, from spiked sand into ethanol-modified CO_2 and ethyl acetate modified CO_2 (Palma and Taylor, 1999), Tena and coworkers extracted polyphenols, including resveratrol, from an inert support into pure and methanol-modified CO_2 (Tena et al., 1998), Pascual-Marti and coworkers extracted resveratrol from dried grape skins into ethanol-modified CO_2 (Pascual-Marti et al., 2001). Very little work has been done to quantify the solubility of resveratrol in pure or modified CO_2 or to model the solubility behavior. Berna and coworkers measured the solubility of resveratrol in ethanol-modified CO_2 at 313 K as a function of modifier percentage at pressures from 80 bar to 140 bar. They fit their data using the Peng-Robinson and Soave-Redlich-Kwong equations of state (Berna et al., 2001).

A.2 Ester Solvents

Alkyl aryl esters, including benzoates, salicylates, and cinnamates, are promising solvents for extracting nutraceuticals from plants. As mentioned in Section 1.1, these esters are GRAS (Generally Recognized As Safe), and their substituent groups can be chosen to achieve a desired polarity, allowing specific nutraceuticals to be targeted. Typically, these esters are not water soluble, allowing for an efficient separation of the ester extract solution

from water and plant tissue; however, ethyl lactate, a water miscible ester solvent (UusiPenttila et al., 1996), was found to dissolve more resveratrol than its hydrophobic counterparts. This high resveratrol solubility in the polar solvent is expected due to resveratrol's three hydroxyl groups. The basic structures of benzoates, salicylates, cinnamates, and lactates are shown in Figure A.2.

These ester solvents are particularly well suited for use in GAS precipitation due to their CO_2-miscibility. The liquid phase volume expansion of CO_2 dissolved in n-butyl salicylate is shown in Figure A.3. With increasing pressure, CO_2 dissolves into the ester solvent, expanding it. Eventually, the vapor and liquid phases become miscible. In order to design and implement an efficient separation scheme using these esters, knowledge of the solubility of CO_2 in esters as function of temperature and pressure is required. VLE data has been published for binary mixtures of CO_2 with the following esters of interest: ethyl benzoate (Feng et al., 2001), methyl benzoate (Bamberger and Maurer, 1994), and methyl salicylate (Cheng et al., 2000). VLE data for CO_2-ethyl lactate is currently unavailable in the literature.

A.3 Solubility of Resveratrol in Various Solvents

Simple tests were performed to determine the room temperature solubility of resveratrol in various ester solvents as an initial solvent screening step. Resveratrol was found to be insoluble in isopropyl salicylate, n-butyl salicylate, benzyl salicylate, benzyl lactate, benzyl propionate, n-butyl cinnamate, isopropyl cinnamate, and benzyl isobutyrate.

The solubilities of resveratrol in isopropyl benzoate, ethyl lactate, ethanol, n-butyl benzoate, ethyl benzoate, and benzyl benzoate at 297 K are reported in Table A.1.

A.4 Testing the Light Sensitivity of Resveratrol in Solution

A 0.022 mg/mL solution of resveratrol in isopropyl benzoate was exposed to a 100 watt long wave mercury spot lamp with peak emission at 365nm for 3 hours. The absorbance spectrum of the solution was taken before and after the exposure using a UV-Visible Spectrophotometer (Jasco V-550). The absorbance curves are shown in Figure A.4. Before the exposure, the shape of the absorbance curve resembled the curve obtained by Trela and Waterhouse for trans-resveratrol in ethanol, a double peak (Figure A.1); after the exposure, the shape of the absorbance curve resembled the curve obtained by Trela and Waterhouse for cis-resveratrol in ethanol, a single peak with a maximum shifted to a slightly lower wavelength. This result was expected for such long exposure to high intensity light; however, the effect of sample exposure to short term lab lighting conditions was not known.

A simple experiment was performed to gain insight into the stability of resveratrol in solution when exposed to lab light. The absorbance was measured every thirty minutes for a 0.004 mg/mL solution of resveratrol in isopropyl benzoate that was continuously exposed to lab light. The absorbance spectra changed very little over three hours (Figure A.5), indicating that resveratrol in ester solvent solutions is probably stable for at least three hours when exposed to normal lab light. A small peak does appear at 300nm, but the change with time is not consistent: first, a peak appears after 30 minutes, the peak height is higher after 60 minutes, the height drops after 90minutes, and it continues to drop with time. Another

experiment of this type should be conducted to explore this further. The new peak is not the expected shape for a cis-resveratrol peak, but may instead indicate sample contamination.

A.5 Attempt to Measure and Model the Solubility of Resveratrol in CO_2

The absorbance spectrum of a sample of resveratrol extracted into CO_2 at 323 K using the static equilibrium apparatus (Figure 3.1) and collected in ethanol is shown in Figure A.6. The shape of the curve resembles the characteristic shape of cis-resveratrol in solution, with the λ_{max}=288nm. This indicates that resveratrol is isomerizing during the supercritical fluid extraction process. As a result, the amount of resveratrol extracted into CO_2 at a given pressure could not be quantified. Cis-resveratrol is not commercially available, nor is it stable, and so Beer's Law calibration curves can only be constructed for trans-resveratrol in solution.

In order to fit the solubility of resveratrol in supercritical CO_2 using the method outlined for SVE in Section 4.1.1.2, the heat of fusion is required to calculate the fugacity of the solid resveratrol. The ΔH_{fus} was measured for four resveratrol samples using a differential scanning calorimeter (TA Instruments, Q100). The experiments were performed using a ramp rate of 10°C/min under a nitrogen atmosphere. The results for the four samples were inconsistent, as shown in Figure A.7: heat of fusion values from 124.42 J/g to 218.80 J/g were obtained. This may be due to isomerization of resveratrol in the vicinity of the melting temperature.

Table A.1 The room temperature (297 K) solubility of resveratrol in various solvents.

Solvent	Solubility (mg/mL)
Isopropyl benzoate	2.33
Ethyl lactate	51.00
Ethanol	50.00*
n-Butyl benzoate	1.87
Ethyl benzoate	5.31
Benzyl benzoate	1.31

*Taken from the Sigma Product Information Sheet for Resveratrol (Sigma-Aldrich, 1997)

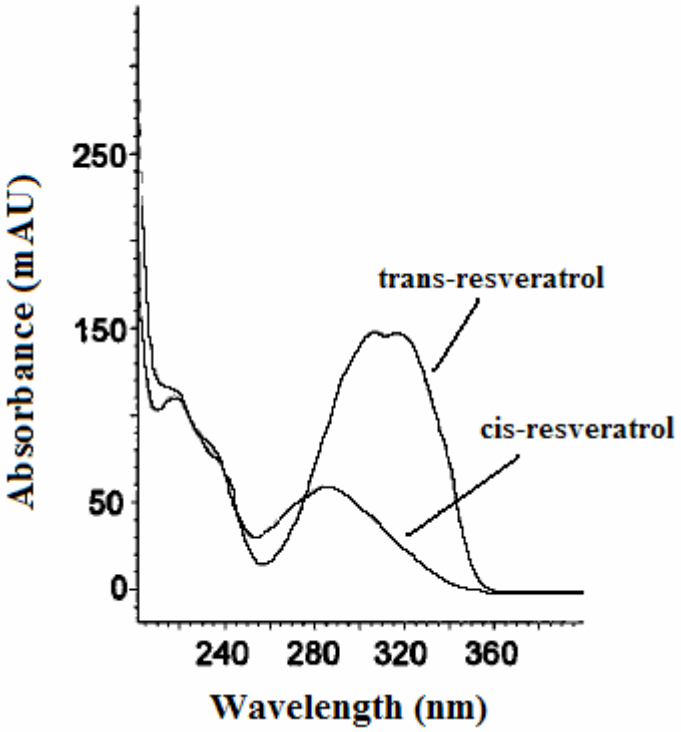

Figure A.1 The absorbance spectra of trans-resveratrol and cis-resveratrol in ethanol. Taken from (Trela and Waterhouse, 1996).

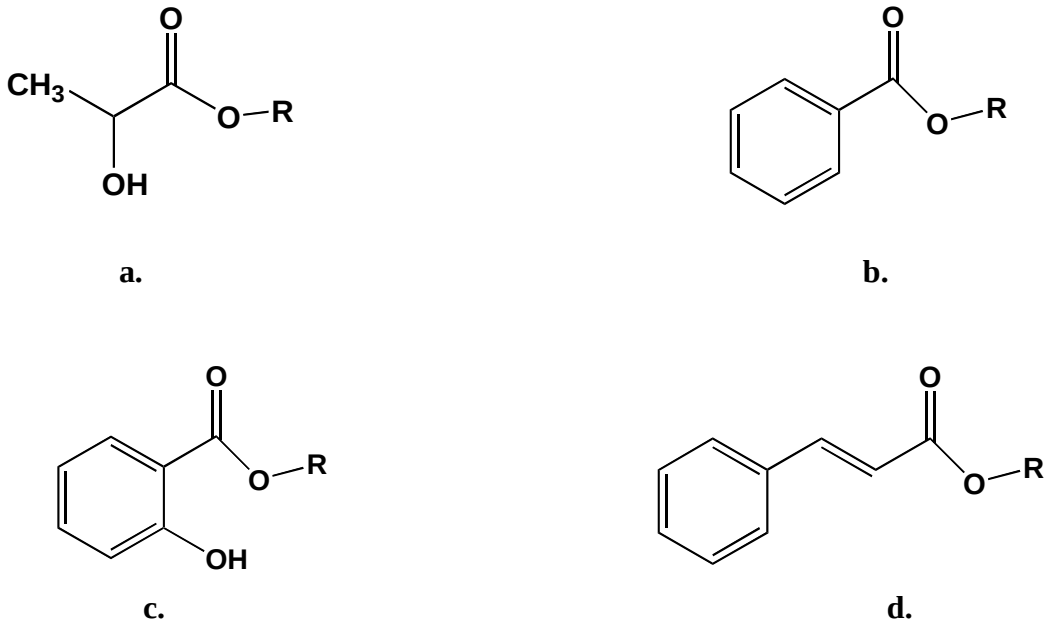

Figure A.2 The molecular structure of ester solvents: (a) lactates, (b) benzoates, (c) salicylates, and (d) cinnamates.

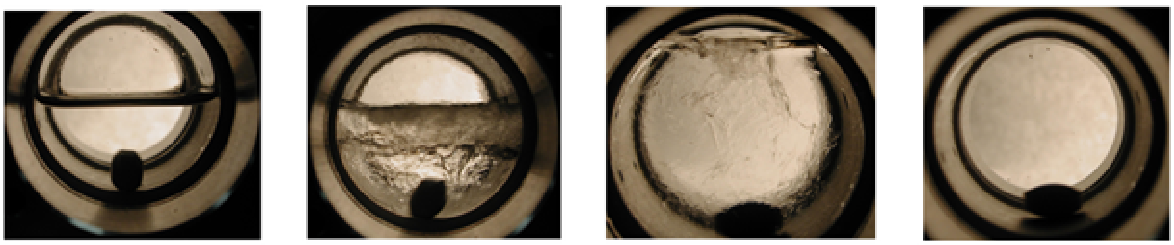

Figure A.3 The liquid phase volume of expansion of CO_2 dissolved in n-butyl salicylate. Photos taken by Nael Zaki.

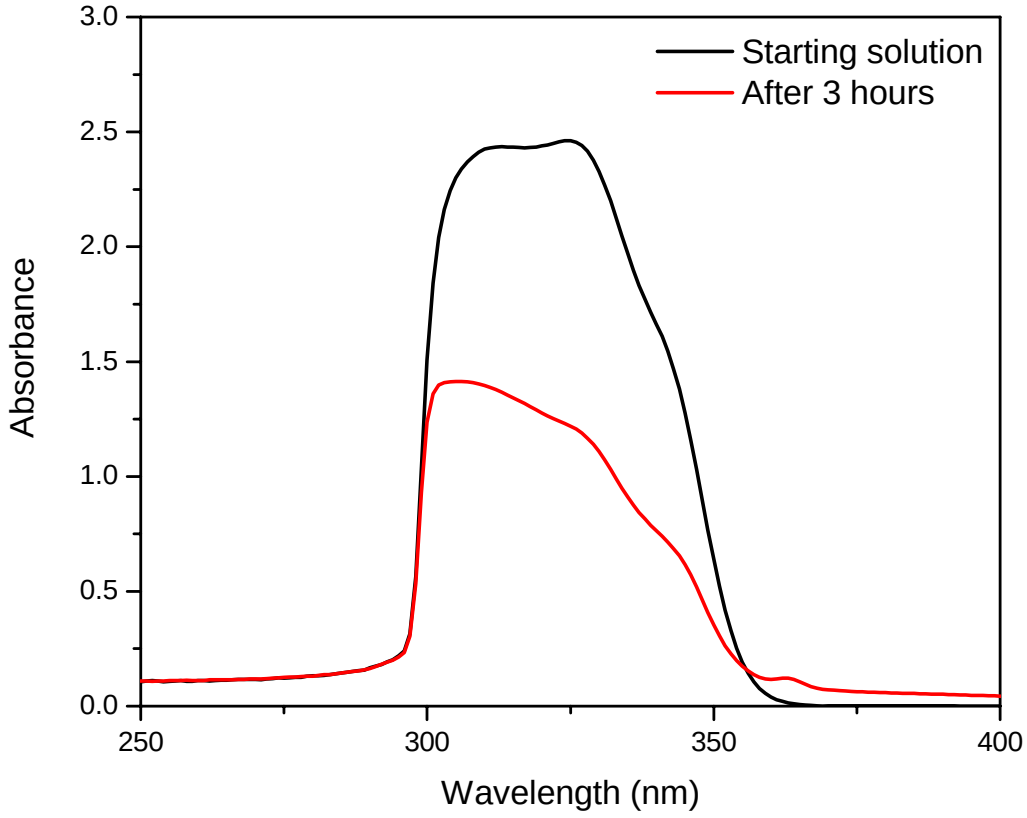

Figure A.4 The absorbance spectra for a solution of resveratrol in isopropyl benzoate before and after exposure to a 100 watt longwave mercury spotlamp with peak emission at 365nm for 3 hours.

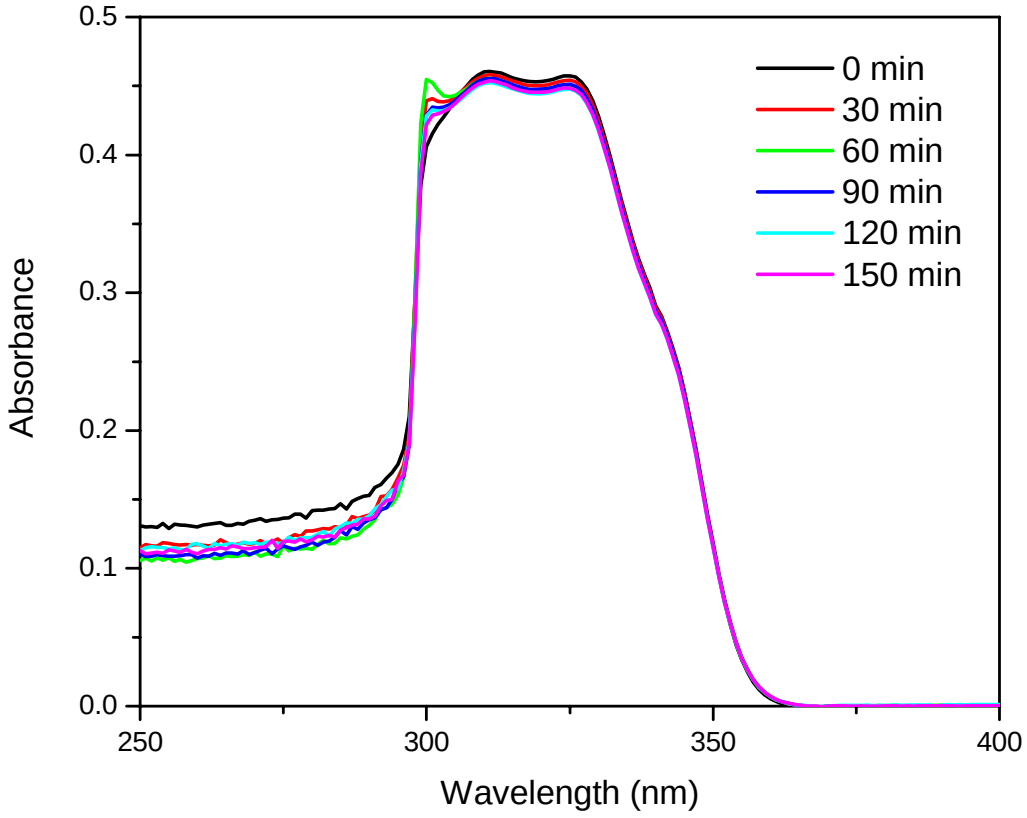

Figure A.5 The absorbance spectra for resveratrol in isopropyl benzoate as a function of time when exposed to lab light.

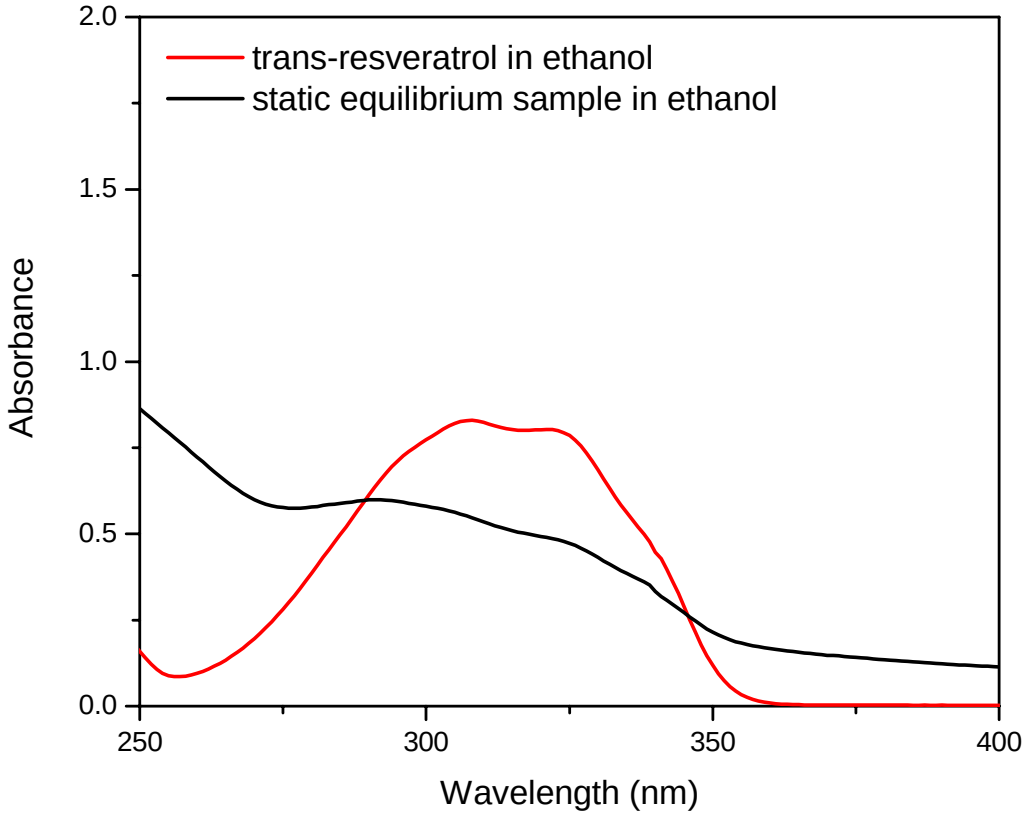

Figure A.6 The measured absorbance spectra for resveratrol in ethanol. The red curve corresponds to a one of the samples used to form the calibration curve for trans-resveratrol in ethanol. Note the characteristic trans-resveratrol double peak. The black curve corresponds to a sample from a static equilibrium extraction experiment at 323 K. This curve is the characteristic shape displayed by cis-resveratrol. The two curves do not correspond to the same sample, the tran-resveratrol peak is shown only for visual reference.

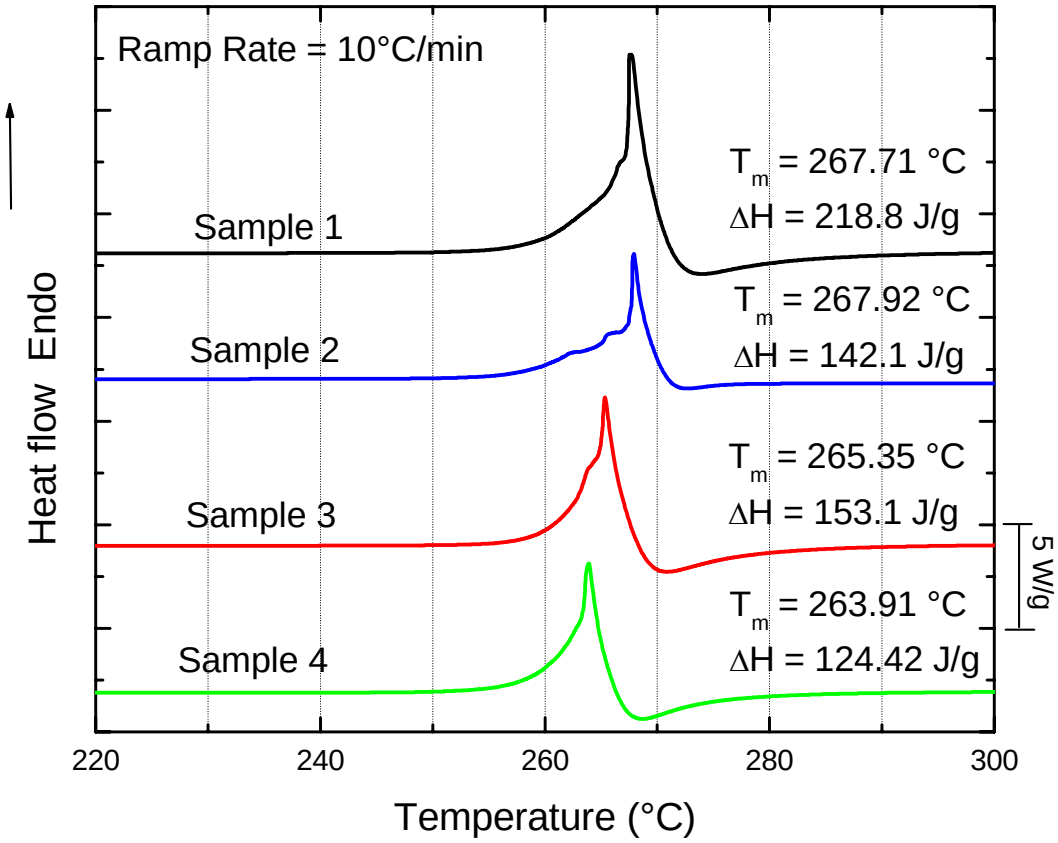

Figure A.7 The heat flow versus temperature for four samples of resveratrol measured using a differential scanning calorimeter. The area under the curve was integrated to determine the ΔH_{fus} at the melting point.

A.6 References

Bamberger, A. and G. Maurer (1994). "High-Pressure Vapor-Liquid-Equilibria in Binary-Mixtures of Carbon-Dioxide and Aromatic-Hydrocarbons - Experimental-Data and Correlation for Co2 Plus Acetophenone, Co2 Plus 1-Chloronaphthalene, Co2 Plus Methyl Benzoate and Co2 Plus N-Propylbenzene." Journal of Supercritical Fluids **7**(2): 115-127.

Berna, A., A. Chafer and J. B. Monton (2001). "High-pressure solubility data of the system resveratrol (3) plus ethanol (2) plus CO2 (1)." Journal of Supercritical Fluids **19**(2): 133-139.

Bhat, K. P. L. and J. M. Pezzuto (2002). Cancer chemopreventive activity of resveratrol. Alcohol and Wine in Health and Disease. **957:** 210-229.

Cheng, K. W., S. J. Kuo, M. Tang and Y. P. Chen (2000). "Vapor-liquid equilibria at elevated pressures of binary mixtures of carbon dioxide with methyl salicylate, eugenol, and diethyl phthalate." Journal of Supercritical Fluids **18**(2): 87-99.

Feng, L. C., K. W. Cheng, M. Tang and Y. P. Chen (2001). "Vapor-liquid equilibria of carbon dioxide with ethyl benzoate, diethyl succinate and isoamyl acetate binary mixtures at elevated pressures." Journal of Supercritical Fluids **21**(2): 111-121.

Fremont, L. (2000). "Minireview - Biological effects of resveratrol." Life Sciences **66**(8): 663-673.

Goldberg, D. M., J. Yan, E. Ng, E. P. Diamandis, A. Karumanchiri, G. Soleas and A. L. Waterhouse (1995). "A Global Survey of Trans-Resveratrol Concentrations in Commercial Wines." American Journal of Enology and Viticulture **46**(2): 159-165.

Jeandet, P., R. Bessis, M. Sbaghi, P. Meunier and P. Trollat (1995). "Resveratrol Content of Wines of Different Ages - Relationship with Fungal Disease Pressure in the Vineyard." American Journal of Enology and Viticulture **46**(1): 1-4.

Lamikanra, O., C. C. Grimm, J. B. Rodin and I. D. Inyang (1996). "Hydroxylated stilbenes in selected American wines." Journal of Agricultural and Food Chemistry **44**(4): 1111-1115.

Palma, M. and L. T. Taylor (1999). "Statistical design for optimization of extraction of polyphenols from an inert matrix using carbon dioxide-based fluids." Analytica Chimica Acta **391**(3): 321-329.

Pascual-Marti, M. C., A. Salvador, A. Chafer and A. Berna (2001). "Supercritical fluid extraction of resveratrol from grape skin of Vitis vinifera and determination by HPLC." Talanta **54**(4): 735-740.

Sigma-Aldrich (1997). Product Information: Resveratrol. **Sigma Product No. R5010**.

Tena, M. T., A. Rios and M. Valcarcel (1998). "Supercritical fluid extraction of t-resveratrol and other phenolics from a spiked solid." Fresenius Journal of Analytical Chemistry **361**(2): 143-148.

Trela, B. C. and A. L. Waterhouse (1996). "Resveratrol: Isomeric molar absorptivities and stability." Journal of Agricultural and Food Chemistry **44**(5): 1253-1257.

UusiPenttila, M., R. J. Richards, P. Blowers, B. A. Torgerson and K. A. Berglund (1996). "Liquid-liquid equilibria of selected dibasic ester plus water plus solvent ternary systems." Journal of Chemical and Engineering Data **41**(2): 235-238.

Bamberger, A. and G. Maurer (1994). "High-Pressure Vapor-Liquid-Equilibria in Binary-Mixtures of Carbon-Dioxide and Aromatic-Hydrocarbons - Experimental-Data and Correlation for Co2 Plus Acetophenone, Co2 Plus 1-Chloronaphthalene, Co2 Plus Methyl Benzoate and Co2 Plus N-Propylbenzene." Journal of Supercritical Fluids **7**(2): 115-127.

Berna, A., A. Chafer and J. B. Monton (2001). "High-pressure solubility data of the system resveratrol (3) plus ethanol (2) plus CO2 (1)." Journal of Supercritical Fluids **19**(2): 133-139.

Bhat, K. P. L. and J. M. Pezzuto (2002). Cancer chemopreventive activity of resveratrol. Alcohol and Wine in Health and Disease. **957:** 210-229.

Cheng, K. W., S. J. Kuo, M. Tang and Y. P. Chen (2000). "Vapor-liquid equilibria at elevated pressures of binary mixtures of carbon dioxide with methyl salicylate, eugenol, and diethyl phthalate." Journal of Supercritical Fluids **18**(2): 87-99.

Feng, L. C., K. W. Cheng, M. Tang and Y. P. Chen (2001). "Vapor-liquid equilibria of carbon dioxide with ethyl benzoate, diethyl succinate and isoamyl acetate binary mixtures at elevated pressures." Journal of Supercritical Fluids **21**(2): 111-121.

Fremont, L. (2000). "Minireview - Biological effects of resveratrol." Life Sciences **66**(8): 663-673.

Goldberg, D. M., J. Yan, E. Ng, E. P. Diamandis, A. Karumanchiri, G. Soleas and A. L. Waterhouse (1995). "A Global Survey of Trans-Resveratrol Concentrations in Commercial Wines." American Journal of Enology and Viticulture **46**(2): 159-165.

Jeandet, P., R. Bessis, M. Sbaghi, P. Meunier and P. Trollat (1995). "Resveratrol Content of Wines of Different Ages - Relationship with Fungal Disease Pressure in the Vineyard." American Journal of Enology and Viticulture **46**(1): 1-4.

Lamikanra, O., C. C. Grimm, J. B. Rodin and I. D. Inyang (1996). "Hydroxylated stilbenes in selected American wines." Journal of Agricultural and Food Chemistry **44**(4): 1111-1115.

Palma, M. and L. T. Taylor (1999). "Statistical design for optimization of extraction of polyphenols from an inert matrix using carbon dioxide-based fluids." Analytica Chimica Acta **391**(3): 321-329.

Pascual-Marti, M. C., A. Salvador, A. Chafer and A. Berna (2001). "Supercritical fluid extraction of resveratrol from grape skin of Vitis vinifera and determination by HPLC." Talanta **54**(4): 735-740.

Sigma-Aldrich (1997). Product Information: Resveratrol. **Sigma Product No. R5010**.

Tena, M. T., A. Rios and M. Valcarcel (1998). "Supercritical fluid extraction of t-resveratrol and other phenolics from a spiked solid." Fresenius Journal of Analytical Chemistry **361**(2): 143-148.

Trela, B. C. and A. L. Waterhouse (1996). "Resveratrol: Isomeric molar absorptivities and stability." Journal of Agricultural and Food Chemistry **44**(5): 1253-1257.

UusiPenttila, M., R. J. Richards, P. Blowers, B. A. Torgerson and K. A. Berglund (1996). "Liquid-liquid equilibria of selected dibasic ester plus water plus solvent ternary systems." Journal of Chemical and Engineering Data **41**(2): 235-238.

APPENDIX B CODE LISTING

In this appendix, the Mathcad codes used to generate the model data for this thesis are provided. Appendix B.1 contains the code used to calculate the compositions of the vapor and liquid phases in the case of vapor-liquid equilibria. Appendix B.2 contains the code used to calculate the composition of the liquid phase in the case of solid-liquid equilibria, when the solid phase is assumed to be pure. Appendix B.3 contains the code used to calculate the composition of the vapor phase in the case of solid-vapor equilibria, when the solid phase is assumed to be pure. Appendix B.4 contains the code used to calculate the compositions of the vapor and liquid phases in the case of solid-vapor liquid equilibrium, when the solid phase is assumed to be pure. In all four codes the Peng-Robinson equation of state was used to represent the fluid phases. These codes were run on a PC with a Windows XP operating system, using Mathcad Professional, Version 7.

B.1 Vapor-Liquid Equilibrium Code with Binary Interaction Parameter Regression Function

Define system:

Component #1: Carbon Dioxide (Anti-solvent)

Component #2: Ethanol (Organic Solvent)

Tolerance for code: $Tol := 0.00000000000001$

Number of components: $N := 2$

Counter: $i := 1..N$

Define Ideal Gas Constant (L kPa/mol K):

$R := 8.31451$

Required Inputs:

Calculations:

Temperature (K): $T := 298.15$

Pressure (bar): $P_{input} := 1$

$P := P_{input} \cdot 100$

Pressure (kPa) --> $P = 100$

Input Component Parameters:

Critical Temperatures (K): $T_c := \begin{bmatrix} 304.2 \\ 514 \end{bmatrix}$

Critical Pressures (bar): $P_{cbar} := \begin{bmatrix} 73.8 \\ 61.37 \end{bmatrix}$

$P_c := 100 \cdot P_{cbar}$

Critical Pressure (kPa) --> $P_c = \begin{bmatrix} 7.38 \cdot 10^3 \\ 6.137 \cdot 10^3 \end{bmatrix}$

Acentric factor: $\omega := \begin{bmatrix} 0.225 \\ 0.643558 \end{bmatrix}$

Initial Guesses to Specify:

Guess for Pure Component Vapor Pressures at T (bar):

$P_{guessbar} := \begin{bmatrix} 10 \\ .001 \end{bmatrix}$

$P_{guess} := 100 \cdot P_{guessbar}$

Guess for Pure Component Vapor Pressures at T (kPa) --> $P_{guess} = \begin{bmatrix} 1 \cdot 10^3 \\ 0.1 \end{bmatrix}$

System Parameters to Specify:

Define Binary Interaction Parameters for Peng-Robinson EOS:

$$k := \begin{bmatrix} 0 & 0.0466 \\ 0.0466 & 0 \end{bmatrix} \qquad l := \begin{bmatrix} 0.000 & 0.000 \\ 0.000 & 0.000 \end{bmatrix}$$

Peng-Robinson Equation of State:

Calculate Pure Component Values:

$$\kappa_i := 0.37464 + 1.54226 \cdot \omega_i - 0.26992 \cdot \left(\omega_i\right)^2 \qquad \alpha_T(T,i) := \left[1 + \kappa_i \cdot \left(1 - \sqrt{\frac{T}{T_{c_i}}}\right)\right]^2$$

$$a_i := 0.457235528921382 \cdot \frac{R^2 \cdot \left(T_{c_i}\right)^2}{P_{c_i}} \qquad b_i := 0.0777960739038884 \cdot \frac{R \cdot T_{c_i}}{P_{c_i}}$$

Quadratic Mixing Rules:

$$a\alpha_{rm}(a\alpha, x, k) := \sum_{i=1}^{N} \sum_{j=1}^{N} x_i \cdot x_j \cdot \left(1 - k_{i,j}\right) \cdot \sqrt{a\alpha_i \cdot a\alpha_j}$$

$$b_{rm}(b, x) := \sum_{i=1}^{N} \sum_{j=1}^{N} \frac{\left[x_i \cdot x_j \cdot \left(1 - l_{i,j}\right) \cdot \left(b_i + b_j\right)\right]}{2}$$

Vapor Pressure Calculations -- Pure Component Form:

Function to Calculate the Compressibility Factor of the Vapor Phase:

$$VP\_Calc\_Z_V(T, P, A, B) := \left| \begin{array}{l} c_1 \leftarrow B^3 + B^2 - A \cdot B \\ c_2 \leftarrow A - 3 \cdot B^2 - 2 \cdot B \\ c_3 \leftarrow B - 1 \\ c_4 \leftarrow 1 \\ Z \leftarrow \text{polyroots}(c) \\ Z_V \leftarrow Z_3 \\ Z_V \end{array} \right.$$

Function to Calculate the Compressibility Factor of the Liquid Phase:

$$\mathrm{VP\_Calc\_Z}_L(T,P,A,B) := \left| \begin{array}{l} c_1 \leftarrow B^3 + B^2 - A\cdot B \\ c_2 \leftarrow A - 3\cdot B^2 - 2\cdot B \\ c_3 \leftarrow B - 1 \\ c_4 \leftarrow 1 \\ Z \leftarrow \mathrm{polyroots}(c) \\ Z_L \leftarrow Z_1 \\ Z_L \end{array} \right.$$

Function to Calculate the Fugacity Coefficient of the Vapor Phase:

$$\mathrm{VP\_Calc\_}\phi_V(T,P,a,b) := \left| \begin{array}{l} A \leftarrow \dfrac{a\cdot P}{R^2\cdot T^2} \\ B \leftarrow \dfrac{b\cdot P}{R\cdot T} \\ Z_V \leftarrow \mathrm{VP\_Calc\_Z}_V(T,P,A,B) \\ \phi_V \leftarrow \exp\left[\left(Z_V - 1\right) - \ln\left(Z_V - B\right) - \dfrac{A}{2\cdot\sqrt{2}\cdot B}\cdot\ln\left[\dfrac{Z_V + \left(1+\sqrt{2}\right)\cdot B}{Z_V + \left(1-\sqrt{2}\right)\cdot B}\right]\right] \\ \phi_V \end{array} \right.$$

Function to Calculate the Fugacity Coefficient of the Liquid Phase:

$$
\begin{aligned}
VP\_Calc\_\phi_L(T,P,a,b) := \;& A \leftarrow \frac{a \cdot P}{R^2 \cdot T^2} \\
& B \leftarrow \frac{b \cdot P}{R \cdot T} \\
& Z_L \leftarrow VP\_Calc\_Z_L(T,P,A,B) \\
& \phi_L \leftarrow \exp\left[\left(Z_L - 1\right) - \ln\left(Z_L - B\right) - \frac{A}{2 \cdot \sqrt{2} \cdot B} \cdot \ln\left[\frac{Z_L + \left(1 + \sqrt{2}\right) \cdot B}{Z_L + \left(1 - \sqrt{2}\right) \cdot B}\right]\right] \\
& \phi_L
\end{aligned}
$$

Function to Calculate the Vapor Pressure (bar) of Pure Components:

$$
\begin{aligned}
Calc\_P_{sat}(T) := \;& \text{for } i \in 1..N \\
& \quad P_{vap_i} \leftarrow P_{guess_i} \\
& \quad a \leftarrow a_i \cdot \alpha_T(T,i) \\
& \quad b \leftarrow b_i \\
& \quad e \leftarrow 1 \\
& \quad \text{while } e > Tol \\
& \quad\quad \phi_V \leftarrow VP\_Calc\_\phi_V\left(T, P_{vap_i}, a, b\right) \\
& \quad\quad \phi_L \leftarrow VP\_Calc\_\phi_L\left(T, P_{vap_i}, a, b\right) \\
& \quad\quad P_{vap_i} \leftarrow P_{vap_i} \cdot \frac{\phi_L}{\phi_V} \\
& \quad\quad e \leftarrow \left|\left(\frac{\phi_L}{\phi_V}\right) - 1\right| \\
& \quad P_{sat_i} \leftarrow P_{vap_i} \\
& P_{sat}
\end{aligned}
$$

Phase Equilibria Calculations -- Mixture Form

Function to Calculate the Molar Volume of the Vapor Phase:

$$
\begin{aligned}
\mathrm{Calc\_v}_V(T,P,y,k) := \;& \text{for } i \in 1..N \\
& \quad a\alpha_i \leftarrow a_i \cdot \alpha_T(T,i) \\
& a\alpha_m \leftarrow a\alpha_{rm}(a\alpha, y, k) \\
& b_m \leftarrow b_{rm}(b, y) \\
& c_1 \leftarrow b_m^3 + \frac{b_m^2 \cdot R \cdot T - a\alpha_m \cdot b_m}{P} \\
& c_2 \leftarrow \frac{a\alpha_m - 2 \cdot b_m \cdot R \cdot T}{P} - 3 \cdot b_m^2 \\
& c_3 \leftarrow b_m - \frac{R \cdot T}{P} \\
& c_4 \leftarrow 1 \\
& v \leftarrow \mathrm{polyroots}(c) \\
& v_V \leftarrow v_3 \\
& v_V
\end{aligned}
$$

Function to Calculate the Molar Volume of the Liquid Phase:

$$
\begin{aligned}
\mathrm{Calc\_v}_L(T,P,x,k) := \;& \text{for } i \in 1..N \\
& \quad a\alpha_i \leftarrow a_i \cdot \alpha_T(T,i) \\
& a\alpha_m \leftarrow a\alpha_{rm}(a\alpha, x, k) \\
& b_m \leftarrow b_{rm}(b, x) \\
& c_1 \leftarrow b_m^3 + \frac{b_m^2 \cdot R \cdot T - a\alpha_m \cdot b_m}{P} \\
& c_2 \leftarrow \frac{a\alpha_m - 2 \cdot b_m \cdot R \cdot T}{P} - 3 \cdot b_m^2 \\
& c_3 \leftarrow b_m - \frac{R \cdot T}{P} \\
& c_4 \leftarrow 1 \\
& v \leftarrow \mathrm{polyroots}(c) \\
& v_L \leftarrow \mathrm{if}\left(\left|\mathrm{Im}(v_1)\right| < 10^{-15}, v_1, v_3\right) \quad \text{if } x_N = 1 \\
& v_L \leftarrow v_1 \quad \text{otherwise} \\
& v_L
\end{aligned}
$$

Function to Calculate the Fugacity Coefficient of the Vapor Phase:

$$
\begin{aligned}
\mathrm{Calc\_}\phi_V(T,P,y,k) := \;& \text{for } i \in 1..N \\
& \quad a\alpha_i \leftarrow a_i \cdot \alpha_T(T,i) \\
& a\alpha_m \leftarrow a\alpha_{rm}(a\alpha, y, k) \\
& b_m \leftarrow b_{rm}(b, y) \\
& v \leftarrow \mathrm{Calc\_v}_V(T,P,y,k) \\
& Z \leftarrow \frac{P \cdot v}{R \cdot T} \\
& \text{for } i \in 1..N \\
& \quad \phi term \leftarrow \ln\left[\frac{v + \left(1+\sqrt{2}\right)\cdot b_m}{v + \left(1-\sqrt{2}\right)\cdot b_m}\right] \\
& \quad \phi_i \leftarrow \exp\left[\frac{b_i}{b_m}\cdot(Z-1) - \ln\left[Z\cdot\left(1-\frac{b_m}{v}\right)\right] \ldots \right. \\
& \qquad \left. + \frac{1}{2\cdot\sqrt{2}\cdot b_m \cdot R \cdot T}\cdot\left[\frac{a\alpha_m \cdot b_i}{b_m} - 2\cdot\sum_{j=1}^{N} y_j\cdot\left(1-k_{i,j}\right)\cdot\sqrt{a\alpha_i \cdot a\alpha_j}\right]\cdot\phi term\right] \\
& \phi
\end{aligned}
$$

Function to Calculate the Fugacity Coefficient of the Liquid Phase:

$$
\begin{aligned}
\mathrm{Calc\_}\phi_L(T,P,x,k) := \;& \text{for } i \in 1..N \\
& \quad a\alpha_i \leftarrow a_i \cdot \alpha_T(T,i) \\
& a\alpha_m \leftarrow a\alpha_{rm}(a\alpha,x,k) \\
& b_m \leftarrow b_{rm}(b,x) \\
& v \leftarrow \mathrm{Calc\_}v_L(T,P,x,k) \\
& Z \leftarrow \frac{P \cdot v}{R \cdot T} \\
& \text{for } i \in 1..N \\
& \quad \phi term \leftarrow \ln\left[\frac{v + \left(1+\sqrt{2}\right)\cdot b_m}{v + \left(1-\sqrt{2}\right)\cdot b_m}\right] \\
& \quad \phi_i \leftarrow \exp\left[\frac{b_i}{b_m}\cdot(Z-1) - \ln\left[Z\cdot\left(1-\frac{b_m}{v}\right)\right] \ldots \right. \\
& \qquad \left. + \frac{1}{2\cdot\sqrt{2}\cdot b_m \cdot R\cdot T}\cdot\left[\frac{a\alpha_m \cdot b_i}{b_m} - 2\cdot\sum_{j=1}^{N} x_j\cdot\left(1-k_{i,j}\right)\cdot\sqrt{a\alpha_i \cdot a\alpha_j}\right]\cdot\phi term\right] \\
& \phi
\end{aligned}
$$

Function to Calculate the Compositions of the Vapor and Liquid Phases:

$$
\begin{aligned}
\mathrm{Calc\_xy}(T,P,k) := \;& K_1 \leftarrow \frac{\mathrm{Calc\_P}_{sat}(T)_1}{P} \\
& K_2 \leftarrow \frac{\mathrm{Calc\_P}_{sat}(T)_2}{P} \\
& e \leftarrow 1 \\
& \text{while } e > \mathrm{Tol} \\
& \quad K_a \leftarrow K \\
& \quad x_1 \leftarrow \frac{K_2 - 1}{K_2 - K_1} \\
& \quad x_2 \leftarrow 1 - x_1 \\
& \quad y_1 \leftarrow K_1 \cdot x_1 \\
& \quad y_2 \leftarrow 1 - y_1 \\
& \quad \phi_V \leftarrow \mathrm{Calc\_}\phi_V(T,P,y,k) \\
& \quad \phi_L \leftarrow \mathrm{Calc\_}\phi_L(T,P,x,k) \\
& \quad K_1 \leftarrow \frac{\phi_{L_1}}{\phi_{V_1}} \\
& \quad K_2 \leftarrow \frac{\phi_{L_2}}{\phi_{V_2}} \\
& \quad e \leftarrow \max\left(\overrightarrow{\left|K - K_a\right|}\right) \\
& \mathrm{Sol}^{\langle 1 \rangle} \leftarrow x \\
& \mathrm{Sol}^{\langle 2 \rangle} \leftarrow y \\
& \mathrm{Sol}
\end{aligned}
$$

Enter Literature or Experimental Data to Regress Binary Interaction Parameters:

Example of Pressure, Temperature, Liquid-Phase, and Vapor Phase Composition Data:

$$P_0 := \begin{bmatrix} 1160 \\ 1620 \\ 2280 \\ 2960 \\ 3650 \\ 4340 \\ 5820 \end{bmatrix} \quad T_0 := \begin{bmatrix} 298.15 \\ 298.15 \\ 298.15 \\ 298.15 \\ 298.15 \\ 298.15 \\ 298.15 \end{bmatrix} \quad x_0 := \begin{bmatrix} 0.1305 \\ 0.1865 \\ 0.2624 \\ 0.3273 \\ 0.4103 \\ 0.5172 \\ 0.8139 \end{bmatrix} \quad y_0 := \begin{bmatrix} 0.9855 \\ 0.9873 \\ 0.9895 \\ 0.9906 \\ 0.9918 \\ 0.9905 \\ 0.9860 \end{bmatrix}$$

Function to Calculate the Error Between the Model's Predictions with a Given k_{12} and Experimental Data:

$$Err(k_{12}) := \left| \begin{array}{l} k \leftarrow \begin{bmatrix} 0 & k_{12} \\ k_{12} & 0 \end{bmatrix} \\ Err \leftarrow 0 \\ \text{for } i \in 1..rows(T_0) \\ \quad \left| \begin{array}{l} x\_y \leftarrow Calc\_xy(T_{0_i}, P_{0_i}, k) \\ Err \leftarrow Err + (x\_y_{1,1} - x_{0_i})^2 + (x\_y_{1,2} - y_{0_i})^2 \end{array} \right. \\ \dfrac{Err}{rows(T_0)} \end{array} \right.$$

Plot of Error vs k_{12} Value to Determine the k_{12} Corresponding to the Minimum Error:

$$k12 := 0.043, 0.044 .. 0.050$$

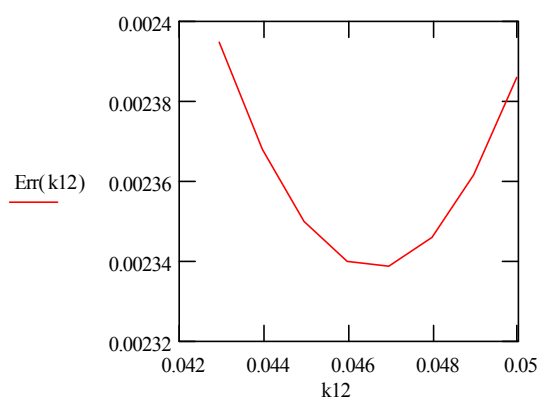

Provide an Array of Pressure Values (kPa) Over Which to Calculate Compositions at T:

$$P := \begin{bmatrix} 1000 \\ 1500 \\ 2000 \\ 2500 \\ 3000 \\ 3500 \\ 4000 \\ 4500 \\ 5000 \\ 5500 \\ 6000 \end{bmatrix}$$

Input the temperature of interest for each array:

$M := \text{rows}(P) \qquad M = 11$

$i := 1 .. M$

$X_i := \text{Calc\_xy}(T, P_i, k)_{1,1}$

$Y_i := \text{Calc\_xy}(T, P_i, k)_{1,2}$

$$X = \begin{bmatrix} 0.1019038 \\ 0.1552356 \\ 0.2104935 \\ 0.2683788 \\ 0.3299502 \\ 0.3969319 \\ 0.4724425 \\ 0.5630676 \\ 0.6859415 \\ 0.8590019 \\ 0.9626073 \end{bmatrix} \qquad Y = \begin{bmatrix} 0.9907 \\ 0.99332 \\ 0.99459 \\ 0.9953 \\ 0.99574 \\ 0.99601 \\ 0.99617 \\ 0.99624 \\ 0.99628 \\ 0.99645 \\ 0.99745 \end{bmatrix}$$

Analyze Fit to Experimental Data

With k_{12} as Defined Under "System Parameters" Above:

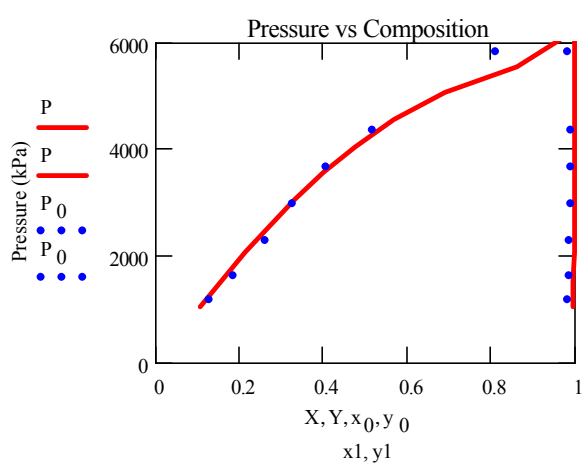

B.2 Solid-Liquid Equilibrium Code with Binary Interaction Parameter Regression Function

Define system:

Component #1: Ethanol

Component #2: Acetaminophen (Solid Solute)

Tolerance for code:

$Tol := 0.00000000000001$

Number of components: $N := 2$

Counter: $i := 1 .. N$

Define Ideal Gas Constant (L kPa/mol K):

$R := 8.31451$

Required Inputs:

Calculations:

Temperature (K): $T := 298.15$

Pressure (bar): $P_{input} := 1.01325$

$P := P_{input} \cdot 100$

Pressure (kPa) --> $P = 101.325$

Input Component Parameters:

Critical Temperatures (K): $T_c := \begin{bmatrix} 514 \\ 736 \end{bmatrix}$

Critical Pressures (bar): $P_{cbar} := \begin{bmatrix} 61.37 \\ 42.6 \end{bmatrix}$

$P_c := 100 \cdot P_{cbar}$

Critical Pressure (kPa) --> $P_c = \begin{bmatrix} 6.137 \cdot 10^3 \\ 4.26 \cdot 10^3 \end{bmatrix}$

Acentric factor: $\omega := \begin{bmatrix} 0.643558 \\ 0.799722 \end{bmatrix}$

Melting Temperature of Solid Solute (K): $T_m := 440.65$ $T_{tp} := T_m$

Triple Pt Temperature of Solute (K)--> $T_{tp} = 440.65$

Sublimation Pressure at Triple Pt (bar): $P_{tpbar} := 0.0482010$ $P_{tp} := 100 \cdot P_{tpbar}$

Triple Pt Pressure of Solute (kPa) --> $P_{tp} = 4.8201$

Molar Volume of Solid Solute (L/mol): $v2\_s := .117$

Heat of Fusion of the Solid Solute at Tm (J/mol): $\Delta H_{fus} := 27700$

Differential Heat Capacity of Solid Solute (J/mol K): $\Delta C_p := 99.8$

Initial Guess to Specify:

Initial Guess for x_2: $x_{guess} := .0001$

System Parameters to Specify:

Define Binary Interaction Parameters for Peng-Robinson EOS:

$$k := \begin{bmatrix} 0 & 0.0099 \\ 0.0099 & 0 \end{bmatrix} \qquad l := \begin{bmatrix} 0.000 & 0.000 \\ 0.000 & 0.000 \end{bmatrix}$$

Peng-Robinson Equation of State:

Calculate Pure Component Values:

$$\kappa_i := 0.37464 + 1.54226 \cdot \omega_i - 0.26992 \cdot \left(\omega_i\right)^2 \qquad \alpha_T(T, i) := \left[1 + \kappa_i \cdot \left(1 - \sqrt{\frac{T}{T_{c_i}}}\right)\right]^2$$

$$a_i := 0.457235528921382 \cdot \frac{R^2 \cdot \left(T_{c_i}\right)^2}{P_{c_i}} \qquad b_i := 0.0777960739038884 \cdot \frac{R \cdot T_{c_i}}{P_{c_i}}$$

Quadratic Mixing Rules:

$$a\alpha_{rm}(a\alpha, x, k) := \sum_{i=1}^{N} \sum_{j=1}^{N} x_i \cdot x_j \cdot \left(1 - k_{i,j}\right) \cdot \sqrt{a\alpha_i \cdot a\alpha_j} \qquad b_{rm}(b, x) := \sum_{i=1}^{N} \sum_{j=1}^{N} \frac{\left[x_i \cdot x_j \cdot \left(1 - l_{i,j}\right) \cdot \left(b_i + b_j\right)\right]}{2}$$

Phase Equilibria Calculations -- Mixture Form:

Function to Calculate the Molar Volume of the Liquid Phase:

$$
\begin{aligned}
\mathrm{Calc\_v}_L(T,P,x,k) := \;& \text{for } i \in 1..N \\
& \quad a\alpha_i \leftarrow a_i \cdot \alpha_T(T,i) \\
& a\alpha_m \leftarrow a\alpha_{rm}(a\alpha,x,k) \\
& b_m \leftarrow b_{rm}(b,x) \\
& c_1 \leftarrow b_m^3 + \frac{b_m^2 \cdot R \cdot T - a\alpha_m \cdot b_m}{P} \\
& c_2 \leftarrow \frac{a\alpha_m - 2 \cdot b_m \cdot R \cdot T}{P} - 3 \cdot b_m^2 \\
& c_3 \leftarrow b_m - \frac{R \cdot T}{P} \\
& c_4 \leftarrow 1 \\
& v \leftarrow \mathrm{polyroots}(c) \\
& v_L \leftarrow \mathrm{if}\left(\left|\mathrm{Im}(v_1)\right| < 10^{-15}, v_1, v_3\right) \quad \text{if } x_N = 1 \\
& v_L \leftarrow v_1 \quad \text{otherwise} \\
& v_L
\end{aligned}
$$

Function to Calculate the Fugacity Coefficient of the Liquid Phase:

$$
\begin{aligned}
\mathrm{Calc\_}\phi_L(T,P,x,k) := \;& \text{for } i \in 1..N \\
& \quad a\alpha_i \leftarrow a_i \cdot \alpha_T(T,i) \\
& a\alpha_m \leftarrow a\alpha_{rm}(a\alpha,x,k) \\
& b_m \leftarrow b_{rm}(b,x) \\
& v \leftarrow \mathrm{Calc\_}v_L(T,P,x,k) \\
& Z \leftarrow \frac{P \cdot v}{R \cdot T} \\
& \text{for } i \in 1..N \\
& \quad \phi term \leftarrow \ln\left[\frac{v + \left(1+\sqrt{2}\right)\cdot b_m}{v + \left(1-\sqrt{2}\right)\cdot b_m}\right] \\
& \quad \phi_i \leftarrow \exp\left[\frac{b_i}{b_m}\cdot(Z-1) - \ln\left[Z\cdot\left(1-\frac{b_m}{v}\right)\right] \ldots \right. \\
& \qquad \left. + \frac{1}{2\cdot\sqrt{2}\cdot b_m \cdot R \cdot T}\cdot\left[\frac{a\alpha_m \cdot b_i}{b_m} - 2\cdot\sum_{j=1}^{N} x_j\cdot\left(1-k_{i,j}\right)\cdot\sqrt{a\alpha_i \cdot a\alpha_j}\right]\cdot\phi term\right] \\
& \phi
\end{aligned}
$$

Function to Calculate Fugacity of the Pure, Subcooled Liquid Solute:

$$x_{pure} := \begin{bmatrix} 0 \\ 1 \end{bmatrix} \qquad \mathrm{fug2\_L}(T,P,k) := P \cdot \mathrm{Calc\_}\phi_L\left(T,P,x_{pure},k\right)_2$$

Fugacity of the Subcooled Liquid Phase (kPa) --> $\mathrm{fug2\_L}(T,P,k) = 2.83 \cdot 10^{-4}$

Function to Calculate the Fugacity of the Pure Solute in the Solid Phase:

$$\mathrm{fug2\_S}(T,P,k) := \mathrm{fug2\_L}\left(T,P_{tp},k\right)\cdot\exp\left[\frac{\Delta H_{fus}}{R}\cdot\left(\frac{1}{T_{tp}} - \frac{1}{T}\right) + \frac{v2\_s\cdot\left(P - P_{tp}\right)}{R\cdot T} - \frac{\Delta C_p}{R}\cdot\left(\ln\left(\frac{T_{tp}}{T}\right) - \frac{T_{tp}}{T} + 1\right)\right]$$

Fugacity of the Solid Phase --> $\mathrm{fug2\_S}(T,P,k) = 2.175 \cdot 10^{-5}$

Function to Calculate the Composition of the Liquid Phase:

$$\mathrm{Calc\_x}\left(x_{guess}, T, P, k\right) := \left| \begin{array}{l} x_2 \leftarrow x_{guess} \\ e \leftarrow 1 \\ \text{while } e > Tol \\ \quad \left| \begin{array}{l} x_a \leftarrow x_2 \\ x_1 \leftarrow 1 - x_2 \\ \phi_L \leftarrow \mathrm{Calc\_}\phi_L(T, P, x, k) \\ x_2 \leftarrow \dfrac{\mathrm{fug2\_S}(T, P, k)}{P \cdot \phi_{L_2}} \\ e \leftarrow \left| \dfrac{x_2 - x_a}{x_2} \right| \end{array} \right. \\ x \end{array} \right.$$

Enter Literature or Experimental Data to Regress Binary Interaction Parameters:

Example of Pressure, Temperature & Liquid-Phase Composition Data:

$$P_0 := \begin{bmatrix} 101.325 \\ 101.325 \\ 101.325 \\ 101.325 \\ 101.325 \\ 101.325 \\ 101.325 \\ 101.325 \end{bmatrix} \qquad T_0 := \begin{bmatrix} 268.15 \\ 273.15 \\ 278.15 \\ 283.15 \\ 288.15 \\ 293.15 \\ 298.15 \\ 303.15 \end{bmatrix} \qquad x_0 := \begin{bmatrix} 0.032302652 \\ 0.034977429 \\ 0.037852895 \\ 0.04115883 \\ 0.044592813 \\ 0.048790517 \\ 0.052873655 \\ 0.057540542 \end{bmatrix}$$

Function to Calculate the Error Between the Model's Predictions with a Given k_{12} and Experimental Data:

$$Err(k_{12}) := \left| \begin{array}{l} k \leftarrow \begin{bmatrix} 0 & k_{12} \\ k_{12} & 0 \end{bmatrix} \\ Err \leftarrow 0 \\ \text{for } i \in 1..rows(T_0) \\ \quad \left| \begin{array}{l} x \leftarrow Calc\_x(x_{guess}, T_{0_i}, P_{0_i}, k) \\ Err \leftarrow Err + (x_{2,1} - x_{0_i})^2 \end{array} \right. \\ \dfrac{Err}{rows(T_0)} \end{array} \right.$$

Plot of Error vs k_{12} Value to Determine the k_{12} Corresponding to the Minimum Error:

$k12 := 0.00986, 0.00988 .. 0.0100$

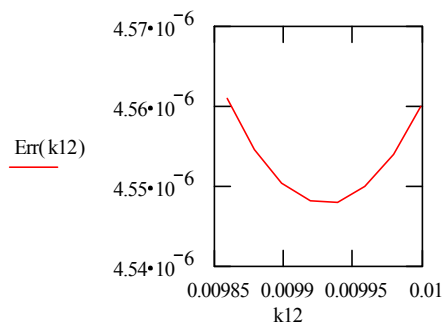

Provide an Array of Temperature Values (K) Over Which to Calculate Compositions at P:

$$T := \begin{bmatrix} 265 \\ 270 \\ 275 \\ 280 \\ 286 \\ 291 \\ 295 \\ 300 \\ 305 \end{bmatrix}$$

Input the temperature of interest for each array:

$M := rows(T) \qquad i := 1..M$

$X_i := Calc\_x(x_{guess}, T_i, P, k)_2 \qquad M = 9$

$$X = \begin{bmatrix} 0.0274454 \\ 0.0304643 \\ 0.0338227 \\ 0.0375576 \\ 0.0425951 \\ 0.0473105 \\ 0.0514586 \\ 0.0571621 \\ 0.0635009 \end{bmatrix}$$

Analyze Fit to Experimental Data

With k_{12} as Defined Under "System Parameters" Above:

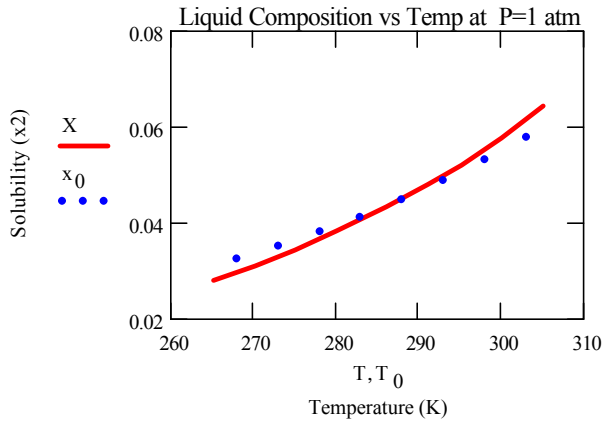

B.3 Solid-Vapor Equilibrium Code with Binary Interaction Parameter Regression Function

Define system:

Component #1: Carbon Dioxide (Anti-solvent)

Component #2: Naphthalene (Solid Solute)

Tolerance for code:

$Tol := 0.00000000000001$

Number of components: $N := 2$

Counter: $i := 1..N$

Define Ideal Gas Constant (L kPa/mol K):

$R := 8.31451$

Required Inputs:

Calculations:

Temperature (K): $T := 328.15$

Pressure (bar): $P_{input} := 1.01325$

$P := P_{input} \cdot 100$

Pressure (kPa) --> $P = 101.325$

Input Component Parameters:

Critical Temperatures (K): $T_c := \begin{bmatrix} 304.2 \\ 748.4 \end{bmatrix}$

Critical Pressures (bar): $P_{cbar} := \begin{bmatrix} 73.8 \\ 40.5 \end{bmatrix}$

$P_c := 100 \cdot P_{cbar}$

Critical Pressure (kPa) --> $P_c = \begin{bmatrix} 7.38 \cdot 10^3 \\ 4.05 \cdot 10^3 \end{bmatrix}$

Acentric factor: $\omega := \begin{bmatrix} 0.225 \\ 0.302034 \end{bmatrix}$

Melting Temperature of Solid Solute (K): $T_m := 353.434$ $T_{tp} := T_m$

Triple Pt Temperature of Solute (K)--> $T_{tp} = 353.434$

Sublimation Pressure at Triple Pt (bar): $P_{tpbar} := 0.009752$ $P_{tp} := 100 \cdot P_{tpbar}$

Triple Pt Pressure of Solute (kPa) --> $P_{tp} = 0.9752$

Molar Volume of Solid Solute (L/mol): $v2\_s := 0.1119$

Heat of Fusion of the Solid Solute at Tm (J/mol): $\Delta H_{fus} := 19060$

Differential Heat Capacity of Solid Solute (J/mol K): $\Delta C_p := 53.7$

Initial Guess to Specify:

Initial Guess for y_2: $y_{guess} := .000001$

System Parameters to Specify:

Define Binary Interaction Parameters for Peng-Robinson EOS:

$$k := \begin{bmatrix} 0 & 0.1000 \\ 0.1000 & 0 \end{bmatrix} \qquad l := \begin{bmatrix} 0.000 & 0.000 \\ 0.000 & 0.000 \end{bmatrix}$$

Peng-Robinson Equation of State:

Calculate Pure Component Values:

$$\kappa_i := 0.37464 + 1.54226 \cdot \omega_i - 0.26992 \cdot (\omega_i)^2 \qquad \alpha_T(T,i) := \left[1 + \kappa_i \cdot \left(1 - \sqrt{\frac{T}{T_{c_i}}}\right)\right]^2$$

$$a_i := 0.457235528921382 \cdot \frac{R^2 \cdot (T_{c_i})^2}{P_{c_i}} \qquad b_i := 0.0777960739038884 \cdot \frac{R \cdot T_{c_i}}{P_{c_i}}$$

Quadratic Mixing Rules:

$$a\alpha_{rm}(a\alpha, x, k) := \sum_{i=1}^{N} \sum_{j=1}^{N} x_i \cdot x_j \cdot (1 - k_{i,j}) \cdot \sqrt{a\alpha_i \cdot a\alpha_j} \qquad b_{rm}(b, x) := \sum_{i=1}^{N} \sum_{j=1}^{N} \frac{\left[x_i \cdot x_j \cdot (1 - l_{i,j}) \cdot (b_i + b_j)\right]}{2}$$

Phase Equilibria Calculations -- Mixture Form

Function to Calculate the Molar Volume of the Vapor Phase:

$$
\begin{aligned}
\mathrm{Calc\_v}_V(T,P,y,k) := \;& \text{for } i \in 1..N \\
& \quad a\alpha_i \leftarrow a_i \cdot \alpha_T(T,i) \\
& a\alpha_m \leftarrow a\alpha_{rm}(a\alpha, y, k) \\
& b_m \leftarrow b_{rm}(b, y) \\
& c_1 \leftarrow b_m^3 + \frac{b_m^2 \cdot R \cdot T - a\alpha_m \cdot b_m}{P} \\
& c_2 \leftarrow \frac{a\alpha_m - 2 \cdot b_m \cdot R \cdot T}{P} - 3 \cdot b_m^2 \\
& c_3 \leftarrow b_m - \frac{R \cdot T}{P} \\
& c_4 \leftarrow 1 \\
& v \leftarrow \mathrm{polyroots}(c) \\
& v_V \leftarrow \mathrm{if}\left(\left|\mathrm{Im}(v_3)\right| < 10^{-15}, v_3, v_1\right) \\
& v_V
\end{aligned}
$$

Function to Calculate the Molar Volume of the Liquid Phase:

$$
\begin{aligned}
\mathrm{Calc\_v}_L(T,P,x,k) := \;& \text{for } i \in 1..N \\
& \quad a\alpha_i \leftarrow a_i \cdot \alpha_T(T,i) \\
& a\alpha_m \leftarrow a\alpha_{rm}(a\alpha, x, k) \\
& b_m \leftarrow b_{rm}(b, x) \\
& c_1 \leftarrow b_m^3 + \frac{b_m^2 \cdot R \cdot T - a\alpha_m \cdot b_m}{P} \\
& c_2 \leftarrow \frac{a\alpha_m - 2 \cdot b_m \cdot R \cdot T}{P} - 3 \cdot b_m^2 \\
& c_3 \leftarrow b_m - \frac{R \cdot T}{P} \\
& c_4 \leftarrow 1 \\
& v \leftarrow \mathrm{polyroots}(c) \\
& v_L \leftarrow \mathrm{if}\left(\left|\mathrm{Im}(v_1)\right| < 10^{-15}, v_1, v_3\right) \quad \text{if } x_N = 1 \\
& v_L \leftarrow v_1 \quad \text{otherwise} \\
& v_L
\end{aligned}
$$

Function to Calculate the Fugacity Coefficient of the Vapor Phase:

$$
\begin{aligned}
\mathrm{Calc\_}\phi_V(T,P,y,k) := \;& \text{for } i \in 1..N \\
& \quad a\alpha_i \leftarrow a_i \cdot \alpha_T(T,i) \\
& a\alpha_m \leftarrow a\alpha_{rm}(a\alpha,y,k) \\
& b_m \leftarrow b_{rm}(b,y) \\
& v \leftarrow \mathrm{Calc\_v}_V(T,P,y,k) \\
& Z \leftarrow \frac{P \cdot v}{R \cdot T} \\
& \text{for } i \in 1..N \\
& \quad \phi term \leftarrow \ln\left[\frac{v + \left(1+\sqrt{2}\right)\cdot b_m}{v + \left(1-\sqrt{2}\right)\cdot b_m}\right] \\
& \quad \phi_i \leftarrow \exp\left[\frac{b_i}{b_m}\cdot(Z-1) - \ln\left[Z\cdot\left(1-\frac{b_m}{v}\right)\right] \ldots \right. \\
& \qquad \left. + \frac{1}{2\cdot\sqrt{2}\cdot b_m \cdot R\cdot T}\cdot\left[\frac{a\alpha_m \cdot b_i}{b_m} - 2\cdot\sum_{j=1}^{N} y_j\cdot\left(1-k_{i,j}\right)\cdot\sqrt{a\alpha_i \cdot a\alpha_j}\right]\cdot\phi term\right] \\
& \phi
\end{aligned}
$$

Function to Calculate the Fugacity Coefficient of the Liquid Phase:

$$
\begin{aligned}
\mathrm{Calc\_}\phi_L(T,P,x,k) := \;& \text{for } i \in 1..N \\
& \quad a\alpha_i \leftarrow a_i \cdot \alpha_T(T,i) \\
& a\alpha_m \leftarrow a\alpha_{rm}(a\alpha,x,k) \\
& b_m \leftarrow b_{rm}(b,x) \\
& v \leftarrow \mathrm{Calc\_}v_L(T,P,x,k) \\
& Z \leftarrow \frac{P \cdot v}{R \cdot T} \\
& \text{for } i \in 1..N \\
& \quad \phi term \leftarrow \ln\left[\frac{v + \left(1+\sqrt{2}\right)\cdot b_m}{v + \left(1-\sqrt{2}\right)\cdot b_m}\right] \\
& \quad \phi_i \leftarrow \exp\left[\frac{b_i}{b_m}\cdot(Z-1) - \ln\left[Z\cdot\left(1-\frac{b_m}{v}\right)\right] \ldots \right. \\
& \qquad \left. + \frac{1}{2\cdot\sqrt{2}\cdot b_m \cdot R \cdot T}\cdot\left[\frac{a\alpha_m \cdot b_i}{b_m} - 2\cdot\sum_{j=1}^{N} x_j\cdot\left(1-k_{i,j}\right)\cdot\sqrt{a\alpha_i \cdot a\alpha_j}\right]\cdot\phi term\right] \\
& \phi
\end{aligned}
$$

Function to Calculate Fugacity of the Pure, Subcooled Liquid Solute:

$$x_{pure} := \begin{bmatrix} 0 \\ 1 \end{bmatrix} \qquad \mathrm{fug2\_L}(T,P,k) := P \cdot \mathrm{Calc\_}\phi_L\left(T,P,x_{pure},k\right)_2$$

Fugacity of the Subcooled Liquid Phase (kPa) --> $\mathrm{fug2\_L}(T,P,k) = 0.283$

Function to Calculate the Fugacity of the Pure Solute in the Solid Phase:

$$\mathrm{fug2\_S}(T,P,k) := \mathrm{fug2\_L}\left(T,P_{tp},k\right)\cdot\exp\left[\frac{\Delta H_{fus}}{R}\cdot\left(\frac{1}{T_{tp}} - \frac{1}{T}\right) + \frac{v2\_s\cdot\left(P - P_{tp}\right)}{R\cdot T} - \frac{\Delta C_p}{R}\cdot\left(\ln\left(\frac{T_{tp}}{T}\right) - \frac{T_{tp}}{T} + 1\right)\right]$$

Fugacity of the Solid Phase --> $\mathrm{fug2\_S}(T,P,k) = 0.175$

Function to Calculate the Composition of the Vapor Phase:

$$
\begin{aligned}
\mathrm{Calc\_y}\left(y_{guess}, T, P, k\right) := \;& y_2 \leftarrow y_{guess} \\
& e \leftarrow 1 \\
& \text{while } e > Tol \\
& \quad y_a \leftarrow y_2 \\
& \quad y_1 \leftarrow 1 - y_2 \\
& \quad \phi_V \leftarrow \mathrm{Calc\_}\phi_V(T, P, y, k) \\
& \quad y_2 \leftarrow \frac{\mathrm{fug2\_S}(T, P, k)}{P \cdot \phi_{V_2}} \\
& \quad e \leftarrow \left| \frac{y_2 - y_a}{y_2} \right| \\
& y
\end{aligned}
$$

Enter Literature or Experimental Data to Regress Binary Interaction Parameters:

Example of Pressure, Temperature & Vapor-Phase Composition Data:

$$P_0 := \begin{bmatrix} 8.68347\cdot10^{3} \\ 9.7271\cdot10^{3} \\ 1.06492\cdot10^{4} \\ 1.33038\cdot10^{4} \\ 1.69008\cdot10^{4} \\ 1.99507\cdot10^{4} \\ 2.22406\cdot10^{4} \\ 2.43076\cdot10^{4} \\ 2.55336\cdot10^{4} \\ 8.21738\cdot10^{3} \\ 9.23062\cdot10^{3} \\ 1.02337\cdot10^{4} \\ 1.09734\cdot10^{4} \\ 1.2169\cdot10^{4} \\ 1.33241\cdot10^{4} \\ 1.43677\cdot10^{4} \\ 1.60599\cdot10^{4} \\ 1.71643\cdot10^{4} \\ 1.74885\cdot10^{4} \\ 1.89577\cdot10^{4} \end{bmatrix} \qquad T_0 := \begin{bmatrix} 308.15 \\ 308.15 \\ 308.15 \\ 308.15 \\ 308.15 \\ 308.15 \\ 308.15 \\ 308.15 \\ 308.15 \\ 328.15 \\ 328.15 \\ 328.15 \\ 328.15 \\ 328.15 \\ 328.15 \\ 328.15 \\ 328.15 \\ 328.15 \\ 328.15 \\ 328.15 \end{bmatrix} \qquad y_0 := \begin{bmatrix} 0.0075 \\ 0.00975 \\ 0.01066 \\ 0.0141 \\ 0.01605 \\ 0.01709 \\ 0.0183 \\ 0.01908 \\ 0.01922 \\ 0.001313 \\ 0.001672 \\ 0.00292 \\ 0.005464 \\ 0.01229 \\ 0.02114 \\ 0.02544 \\ 0.03053 \\ 0.03387 \\ 0.03473 \\ 0.03928 \end{bmatrix}$$

Function to Calculate the Error Between the Model's Predictions with a Given k_{12} and Experimental Data:

$$\mathrm{Err}(k_{12}) := \left| \begin{array}{l} k \leftarrow \begin{bmatrix} 0 & k_{12} \\ k_{12} & 0 \end{bmatrix} \\ \mathrm{Err} \leftarrow 0 \\ \text{for } i \in 1 .. \mathrm{rows}(P_0) \\ \quad \left| \begin{array}{l} y \leftarrow \mathrm{Calc\_y}(y_{guess}, T_{0_i}, P_{0_i}, k) \\ \mathrm{Err} \leftarrow \mathrm{Err} + (y_{2,1} - y_{0_i})^2 \end{array} \right. \\ \dfrac{\mathrm{Err}}{\mathrm{rows}(P_0)} \end{array} \right.$$

Plot of Error vs k_{12} Value to Determine the k_{12} Corresponding to the Minimum Error:

$k12 := 0.0995, 0.0996 .. 0.1005$

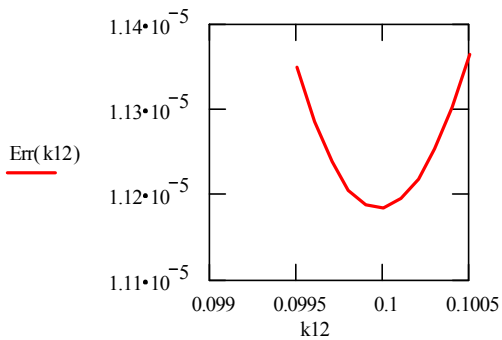

Provide an Array of Pressure Values (K) Over Which to Calculate Compositions at T:

$$P := \begin{bmatrix} 2000 \\ 4000 \\ 6000 \\ 8000 \\ 10000 \\ 12000 \\ 14000 \\ 16000 \\ 18000 \\ 20000 \\ 22000 \\ 24000 \\ 26000 \\ 28000 \\ 30000 \end{bmatrix}$$

Input the temperature of interest for each array:

$M := \mathrm{rows}(P) \qquad i := 1..M \qquad M = 15$

$Y_i := \mathrm{Calc\_y}\left(y_{guess}, 308.15, P_i, k\right)_2$

$Z_i := \mathrm{Calc\_y}\left(y_{guess}, 328.15, P_i, k\right)_2$

$$Y = \begin{bmatrix} 3.9479749 \cdot 10^{-5} \\ 5.2358477 \cdot 10^{-5} \\ 1.2025381 \cdot 10^{-4} \\ 2.9572259 \cdot 10^{-3} \\ 9.7156251 \cdot 10^{-3} \\ 0.0131675 \\ 0.0157444 \\ 0.0177951 \\ 0.0194675 \\ 0.0208446 \\ 0.0219812 \\ 0.0229165 \\ 0.0236808 \\ 0.0242982 \\ 0.0247887 \end{bmatrix} \qquad Z = \begin{bmatrix} 1.76825 \cdot 10^{-4} \\ 1.92197 \cdot 10^{-4} \\ 3.07572 \cdot 10^{-4} \\ 6.53201 \cdot 10^{-4} \\ 2.00918 \cdot 10^{-3} \\ 7.67749 \cdot 10^{-3} \\ 0.0167 \\ 0.02607 \\ 0.03593 \\ 0.04719 \\ 0.06326 \\ 0.40073 \\ 0.38801 \\ 0.37521 \\ 0.36227 \end{bmatrix}$$

Analyze Fit to Experimental Data

With k_{12} as Defined Under "System Parameters" Above:

$j := 1, 2..9$

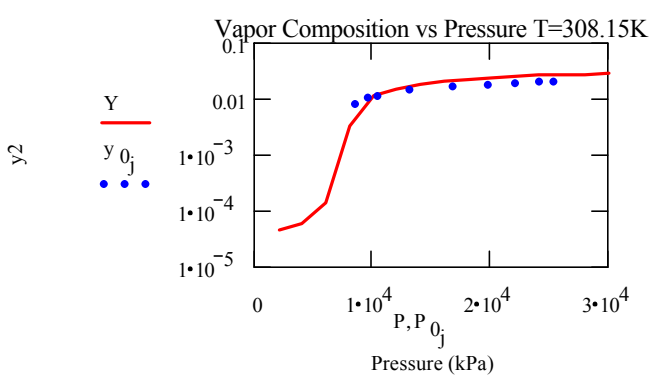

$q := 1, 2 .. 10 \qquad n := 10, 11 .. \mathrm{rows}(P_0)$

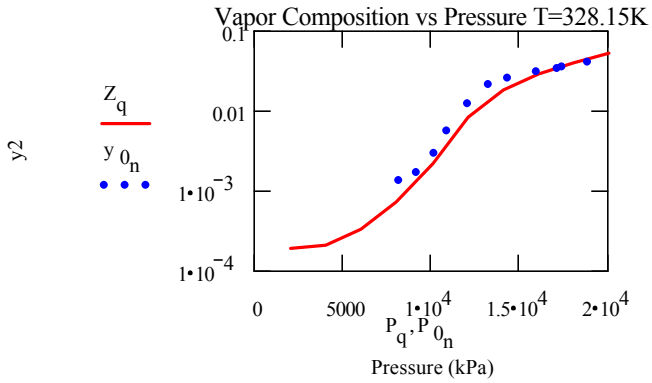

B.4 Solid-Vapor-Liquid Equilibrium Code

Define system:

Component #1: Carbon Dioxide (Anti-solvent)

Component #2: Toluene (Solvent)

Component #3: Naphthalene (Solid Solute)

Tolerance for code: $Tol := 0.00000000000001$

Number of components: $N := 3$

Counter: $i := 1..N$

Define Ideal Gas Constant (L kPa/mol K):

$R := 8.31451$

Required Inputs:

Temperature (K): $T := 298.15$

Pressure (bar): $P_{input} := 1.01325$

Calculations:

$P := P_{input} \cdot 100$

Pressure (kPa) --> $P = 101.325$

Input Component Parameters:

Critical Temperatures (K): $T_c := \begin{bmatrix} 304.2 \\ 591.7 \\ 748.35 \end{bmatrix}$

Critical Pressures (bar): $P_{cbar} := \begin{bmatrix} 73.8 \\ 41.1 \\ 39.7 \end{bmatrix}$

$P_c := 100 \cdot P_{cbar}$

Critical Pressure (kPa) --> $P_c = \begin{bmatrix} 7.38 \cdot 10^3 \\ 4.11 \cdot 10^3 \\ 3.97 \cdot 10^3 \end{bmatrix}$

Acentric factor: $\omega := \begin{bmatrix} 0.225 \\ 0.257 \\ 0.302 \end{bmatrix}$

Melting Temperature of Solid Solute (K): $T_m := 353.434$ $T_{tp} := T_m$

Triple Pt Temperature of Solute (K)--> $T_{tp} = 353.434$

Sublimation Pressure at Triple Pt (bar): $P_{tpbar} := 0.009752$ $P_{tp} := 100 \cdot P_{tpbar}$

Triple Pt Pressure of Solute (kPa) --> $P_{tp} = 0.9752$

Molar Volume of Solid Solute (L/mol): $v3\_s := 0.1119$

Heat of Fusion of the Solid Solute at Tm (J/mol): $\Delta H_{fus} := 19060$

Differential Heat Capacity of Solid Solute (J/mol K): $\Delta C_p := 53.7$

Initial Guess to Specify:

Guess for Pure Component Vapor Pressures at T (bar):

$$P_{guessbar} := \begin{bmatrix} 10 \\ 1 \\ 0.001 \end{bmatrix} \qquad P_{guess} := 100 \cdot P_{guessbar}$$

Guess for Pure Component Vapor Pressures at T (kPa) --> $P_{guess} = \begin{bmatrix} 1 \cdot 10^3 \\ 100 \\ 0.1 \end{bmatrix}$

Initial Guess for x_3: $x_{guess} := .1$

System Parameters to Specify:

Define Binary Interaction Parameters for Peng-Robinson EOS:

$$k := \begin{bmatrix} 0 & 0.09 & 0.094 \\ 0.09 & 0 & 0 \\ 0.094 & 0 & 0 \end{bmatrix} \qquad l := \begin{bmatrix} 0 & 0 & -0.024 \\ 0 & 0 & 0 \\ -0.024 & 0 & 0 \end{bmatrix}$$

Peng-Robinson Equation of State:

Calculate Pure Component Values:

$$\kappa_i := 0.37464 + 1.54226\cdot\omega_i - 0.26992\cdot\left(\omega_i\right)^2$$

$$\alpha_T(T,i) := \left[1 + \kappa_i\cdot\left(1 - \sqrt{\frac{T}{T_{c_i}}}\right)\right]^2$$

$$a_i := 0.457235528921382\cdot\frac{R^2\cdot\left(T_{c_i}\right)^2}{P_{c_i}}$$

$$b_i := 0.0777960739038884\cdot\frac{R\cdot T_{c_i}}{P_{c_i}}$$

Quadratic Mixing Rules:

$$a\alpha_{rm}(a\alpha,x,k) := \sum_{i=1}^{N}\sum_{j=1}^{N} x_i\cdot x_j\cdot\left(1 - k_{i,j}\right)\cdot\sqrt{a\alpha_i\cdot a\alpha_j}$$

$$b_{rm}(b,x) := \sum_{i=1}^{N}\sum_{j=1}^{N} \frac{\left[x_i\cdot x_j\cdot\left(1 - l_{i,j}\right)\cdot\left(b_i + b_j\right)\right]}{2}$$

Vapor Pressure Calculations -- Pure Component Form:

Function to Calculate the Compressibility Factor of the Vapor Phase:

$$\text{VP\_Calc\_Z}_V(T,P,A,B) := \left|\begin{array}{l} c_1 \leftarrow B^3 + B^2 - A\cdot B \\ c_2 \leftarrow A - 3\cdot B^2 - 2\cdot B \\ c_3 \leftarrow B - 1 \\ c_4 \leftarrow 1 \\ Z \leftarrow \text{polyroots}(c) \\ Z_V \leftarrow Z_3 \\ Z_V \end{array}\right.$$

Function to Calculate the Compressibility Factor of the Liquid Phase:

$$VP\_Calc\_Z_L(T,P,A,B) := \left| \begin{array}{l} c_1 \leftarrow B^3 + B^2 - A\cdot B \\ c_2 \leftarrow A - 3\cdot B^2 - 2\cdot B \\ c_3 \leftarrow B - 1 \\ c_4 \leftarrow 1 \\ Z \leftarrow \text{polyroots}(c) \\ Z_L \leftarrow Z_1 \\ Z_L \end{array} \right.$$

Function to Calculate the Fugacity Coefficient of the Vapor Phase:

$$VP\_Calc\_\phi_V(T,P,a,b) := \left| \begin{array}{l} A \leftarrow \dfrac{a\cdot P}{R^2\cdot T^2} \\ B \leftarrow \dfrac{b\cdot P}{R\cdot T} \\ Z_V \leftarrow VP\_Calc\_Z_V(T,P,A,B) \\ \phi_V \leftarrow \exp\left[\left(Z_V - 1\right) - \ln\left(Z_V - B\right) - \dfrac{A}{2\cdot\sqrt{2}\cdot B}\cdot\ln\left[\dfrac{Z_V + \left(1+\sqrt{2}\right)\cdot B}{Z_V + \left(1-\sqrt{2}\right)\cdot B}\right]\right] \\ \phi_V \end{array} \right.$$

Function to Calculate the Fugacity Coefficient of the Liquid Phase:

$$VP\_Calc\_\phi_L(T,P,a,b) := \left| \begin{array}{l} A \leftarrow \dfrac{a\cdot P}{R^2\cdot T^2} \\ B \leftarrow \dfrac{b\cdot P}{R\cdot T} \\ Z_L \leftarrow VP\_Calc\_Z_L(T,P,A,B) \\ \phi_L \leftarrow \exp\left[\left(Z_L - 1\right) - \ln\left(Z_L - B\right) - \dfrac{A}{2\cdot\sqrt{2}\cdot B}\cdot\ln\left[\dfrac{Z_L + \left(1+\sqrt{2}\right)\cdot B}{Z_L + \left(1-\sqrt{2}\right)\cdot B}\right]\right] \\ \phi_L \end{array} \right.$$

Function to Calculate the Vapor Pressure (bar) of Pure Components:

$$
\begin{aligned}
\mathrm{Calc\_P}_{sat}(T) := \;& \text{for } i \in 1..N \\
& \quad P_{vap_i} \leftarrow P_{guess_i} \\
& \quad a \leftarrow a_i \cdot \alpha_T(T, i) \\
& \quad b \leftarrow b_i \\
& \quad e \leftarrow 1 \\
& \quad \text{while } e > Tol \\
& \qquad \phi_V \leftarrow \mathrm{VP\_Calc\_}\phi_V\left(T, P_{vap_i}, a, b\right) \\
& \qquad \phi_L \leftarrow \mathrm{VP\_Calc\_}\phi_L\left(T, P_{vap_i}, a, b\right) \\
& \qquad P_{vap_i} \leftarrow P_{vap_i} \cdot \frac{\phi_L}{\phi_V} \\
& \qquad e \leftarrow \left| \left(\frac{\phi_L}{\phi_V}\right) - 1 \right| \\
& \quad P_{sat_i} \leftarrow P_{vap_i} \\
& P_{sat}
\end{aligned}
$$

Phase Equilibria Calculations -- Mixture Form

Function to Calculate the Molar Volume of the Vapor Phase:

$$
\begin{aligned}
\mathrm{Calc\_v}_V(T, P, y, k) := \;& \text{for } i \in 1..N \\
& \quad a\alpha_i \leftarrow a_i \cdot \alpha_T(T, i) \\
& a\alpha_m \leftarrow a\alpha_{rm}(a\alpha, y, k) \\
& b_m \leftarrow b_{rm}(b, y) \\
& c_1 \leftarrow b_m^3 + \frac{b_m^2 \cdot R \cdot T - a\alpha_m \cdot b_m}{P} \\
& c_2 \leftarrow \frac{a\alpha_m - 2 \cdot b_m \cdot R \cdot T}{P} - 3 \cdot b_m^2 \\
& c_3 \leftarrow b_m - \frac{R \cdot T}{P} \\
& c_4 \leftarrow 1 \\
& v \leftarrow \mathrm{polyroots}(c) \\
& v_V \leftarrow \mathrm{if}\left(\left|\mathrm{Im}(v_3)\right| < 10^{-15}, v_3, v_1\right) \\
& v_V
\end{aligned}
$$

"

Function to Calculate the Molar Volume of the Liquid Phase:

$$
\begin{aligned}
\mathrm{Calc\_v}_L(T,P,x,k) := \;& \text{for } i \in 1..N \\
& \quad a\alpha_i \leftarrow a_i \cdot \alpha_T(T,i) \\
& a\alpha_m \leftarrow a\alpha_{rm}(a\alpha,x,k) \\
& b_m \leftarrow b_{rm}(b,x) \\
& c_1 \leftarrow b_m^3 + \frac{b_m^2 \cdot R \cdot T - a\alpha_m \cdot b_m}{P} \\
& c_2 \leftarrow \frac{a\alpha_m - 2 \cdot b_m \cdot R \cdot T}{P} - 3 \cdot b_m^2 \\
& c_3 \leftarrow b_m - \frac{R \cdot T}{P} \\
& c_4 \leftarrow 1 \\
& v \leftarrow \mathrm{polyroots}(c) \\
& v_L \leftarrow \mathrm{if}\left(\left|\mathrm{Im}(v_1)\right| < 10^{-15}, v_1, v_3\right) \quad \text{if } x_N = 1 \\
& v_L \leftarrow v_1 \quad \text{otherwise} \\
& v_L
\end{aligned}
$$

Function to Calculate the Fugacity Coefficient of the Vapor Phase:

$$
\begin{aligned}
\mathrm{Calc\_}\phi_V(T,P,y,k) := \;& \text{for } i \in 1..N \\
& \quad a\alpha_i \leftarrow a_i \cdot \alpha_T(T,i) \\
& a\alpha_m \leftarrow a\alpha_{rm}(a\alpha,y,k) \\
& b_m \leftarrow b_{rm}(b,y) \\
& v \leftarrow \mathrm{Calc\_v}_V(T,P,y,k) \\
& Z \leftarrow \frac{P \cdot v}{R \cdot T} \\
& \text{for } i \in 1..N \\
& \quad \phi term \leftarrow \ln\left[\frac{v + \left(1+\sqrt{2}\right)\cdot b_m}{v + \left(1-\sqrt{2}\right)\cdot b_m}\right] \\
& \quad \phi_i \leftarrow \exp\left[\frac{b_i}{b_m}\cdot(Z-1) - \ln\left[Z\cdot\left(1-\frac{b_m}{v}\right)\right] \ldots \right. \\
& \qquad \left. + \frac{1}{2\cdot\sqrt{2}\cdot b_m \cdot R\cdot T}\cdot\left[\frac{a\alpha_m \cdot b_i}{b_m} - 2\cdot\sum_{j=1}^{N} y_j\cdot\left(1-k_{i,j}\right)\cdot\sqrt{a\alpha_i \cdot a\alpha_j}\right]\cdot\phi term\right] \\
& \phi
\end{aligned}
$$

Function to Calculate the Fugacity Coefficient of the Liquid Phase:

$$
\begin{aligned}
\mathrm{Calc\_}\phi_L(T,P,x,k) := \;& \text{for } i \in 1..N \\
& \quad a\alpha_i \leftarrow a_i \cdot \alpha_T(T,i) \\
& a\alpha_m \leftarrow a\alpha_{rm}(a\alpha,x,k) \\
& b_m \leftarrow b_{rm}(b,x) \\
& v \leftarrow \mathrm{Calc\_}v_L(T,P,x,k) \\
& Z \leftarrow \frac{P \cdot v}{R \cdot T} \\
& \text{for } i \in 1..N \\
& \quad \phi term \leftarrow \ln\left[\frac{v + \left(1+\sqrt{2}\right)\cdot b_m}{v + \left(1-\sqrt{2}\right)\cdot b_m}\right] \\
& \quad \phi_i \leftarrow \exp\left[\frac{b_i}{b_m}\cdot(Z-1) - \ln\left[Z\cdot\left(1-\frac{b_m}{v}\right)\right] \ldots \right. \\
& \qquad \left. + \frac{1}{2\cdot\sqrt{2}\cdot b_m \cdot R \cdot T}\cdot\left[\frac{a\alpha_m \cdot b_i}{b_m} - 2\cdot\sum_{j=1}^{N} x_j\cdot\left(1-k_{i,j}\right)\cdot\sqrt{a\alpha_i \cdot a\alpha_j}\right]\cdot\phi term\right] \\
& \phi
\end{aligned}
$$

Function to Calculate Fugacity of the Pure, Subcooled Liquid Solute:

$$x_{pure} := \begin{bmatrix} 0 \\ 0 \\ 1 \end{bmatrix} \qquad \mathrm{fug3\_L}(T,P,k) := P \cdot \mathrm{Calc\_}\phi_L\left(T,P,x_{pure},k\right)_3$$

Fugacity of the Subcooled Liquid Phase (kPa) --> $\mathrm{fug3\_L}(T,P,k) = 0.041$

Function to Calculate the Fugacity of the Pure Solute in the Solid Phase:

$$\mathrm{fug3\_S}(T,P,k) := \mathrm{fug3\_L}\left(T,P_{tp},k\right)\cdot\exp\left[\frac{\Delta H_{fus}}{R}\cdot\left(\frac{1}{T_{tp}} - \frac{1}{T}\right) + \frac{v3\_s\cdot\left(P - P_{tp}\right)}{R\cdot T} - \frac{\Delta C_p}{R}\cdot\left(\ln\left(\frac{T_{tp}}{T}\right) - \frac{T_{tp}}{T} + 1\right)\right]$$

Fugacity of the Solid Phase --> $\mathrm{fug3\_S}(T,P,k) = 0.014$

Function to Calculate the Compositions of the Liquid and Vapor Phases:

$$
\begin{aligned}
\mathrm{Calc\_xy}\left(x_{guess}, T, P, k\right) := \;& P_{vap} \leftarrow \mathrm{Calc\_P}_{sat}(T) \\
& K_1 \leftarrow \frac{P_{vap_1}}{P} \\
& K_2 \leftarrow \frac{P_{vap_2}}{P} \\
& K_3 \leftarrow \frac{P_{vap_3}}{P} \\
& e \leftarrow 1 \\
& x_3 \leftarrow x_{guess} \\
& \text{while } e > 10^{-5} \\
& \quad x_a \leftarrow x_3 \\
& \quad x_2 \leftarrow \frac{1 + \left(K_1 - K_3\right) \cdot x_3 - K_1}{K_2 - K_1} \\
& \quad x_1 \leftarrow 1 - x_3 - x_2 \\
& \quad y_1 \leftarrow K_1 \cdot x_1 \\
& \quad y_2 \leftarrow K_2 \cdot x_2 \\
& \quad y_3 \leftarrow K_3 \cdot x_3 \\
& \quad s \leftarrow \sum_{j=1}^{N} y_j \\
& \quad y_1 \leftarrow \frac{y_1}{s} \\
& \quad y_2 \leftarrow \frac{y_2}{s} \\
& \quad y_3 \leftarrow \frac{y_3}{s} \\
& \quad \phi_V \leftarrow \mathrm{Calc\_}\phi_V(T, P, y, k) \\
& \quad \phi_L \leftarrow \mathrm{Calc\_}\phi_L(T, P, x, k) \\
& \quad K_1 \leftarrow \frac{\phi_{L_1}}{\phi_{V_1}}
\end{aligned}
$$

$$K_2 \leftarrow \frac{\phi_{L_2}}{\phi_{V_2}}$$

$$K_3 \leftarrow \frac{\phi_{L_3}}{\phi_{V_3}}$$

$$x_3 \leftarrow \frac{fug3\_S(T,P,k)}{P \cdot \phi_{L_3}}$$

$$e \leftarrow \left| \frac{x_3 - x_a}{x_3} \right|$$

$$Sol^{<1>} \leftarrow x$$

$$Sol^{<2>} \leftarrow y$$

$$Sol$$

Calculate the Vapor and Liquid Compositions Over A Pressure Range:

$j := 1, 2 .. 60 \qquad P_j := 100 \cdot j$

$x1_j := Calc\_xy(x_{guess}, T, P_j, k)_{1,1} \qquad y1_j := Calc\_xy(x_{guess}, T, P_j, k)_{1,2}$

$x2_j := Calc\_xy(x_{guess}, T, P_j, k)_{2,1} \qquad y2_j := Calc\_xy(x_{guess}, T, P_j, k)_{2,2}$

$x3_j := Calc\_xy(x_{guess}, T, P_j, k)_{3,1} \qquad y3_j := Calc\_xy(x_{guess}, T, P_j, k)_{3,2}$

Enter Literature or Experimental Data:

Example of Pressure, Temperature, and Liquid Phase Composition Data:

$$P_0 := \begin{bmatrix} 3290 \\ 3670 \\ 4340 \\ 4990 \\ 5710 \\ 5770 \\ 6030 \end{bmatrix} \quad x1_0 := \begin{bmatrix} 0.334 \\ 0.373 \\ 0.456 \\ 0.591 \\ 0.907 \\ 0.928 \\ 0.969 \end{bmatrix} \quad x2_0 := \begin{bmatrix} 0.429 \\ 0.398 \\ 0.346 \\ 0.277 \\ 0.0689 \\ 0.051 \\ 0.0206 \end{bmatrix} \quad x3_0 := \begin{bmatrix} 0.237 \\ 0.229 \\ 0.198 \\ 0.132 \\ 0.0242 \\ 0.0209 \\ 0.0108 \end{bmatrix}$$

Analyze Fit to Experimental Data

Plot of Liquid Phase Composition As a Function of Pressure:

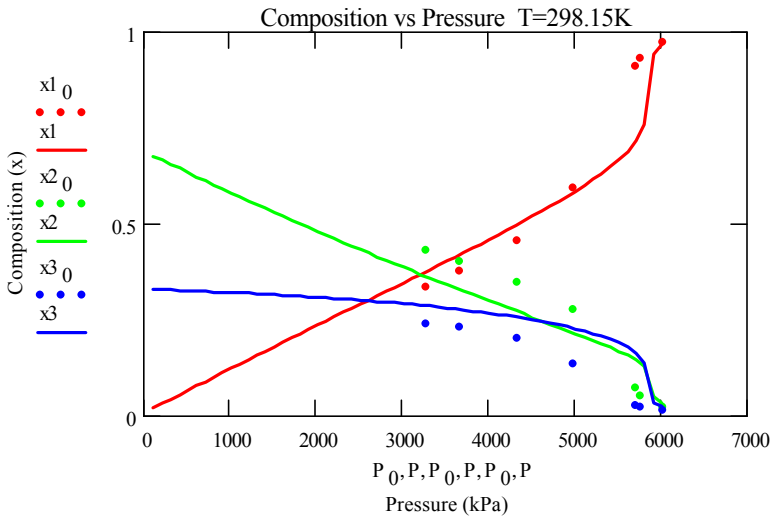

Plot of Predicted Vapor Phase Composition As a Function of Pressure: